2010

Dissolution of Chitosan in Ionic Liquids for Acylation Chemistry and Formation of Cellulose-Chitosan Blends

Cristina Stefanescu
Louisiana State University and Agricultural and Mechanical College, cmart56@lsu.edu

DISSOLUTION OF CHITOSAN IN IONIC LIQUIDS FOR ACYLATION CHEMISTRY AND FORMATION OF CELLULOSE-CHITOSAN BLENDS

A Dissertation

Submitted to the Graduate Faculty of the
Louisiana State University and
Agricultural and Mechanical College
in partial fulfillment of the
requirements for the degree of
Doctor of Philosophy

In

The Department of Chemistry

by
Cristina Stefanescu
B.S., Technical University of Iasi, Romania, 2004
M.S., Technical University of Iasi, Romania, 2005
December, 2010

ACKNOWLEDGEMENTS

I owe my deepest gratitude to my major professors Dr. William H. Daly and Dr. Ioan I. Negulescu for their support and supervision throughout all the stages of this project. I thank my graduate committee members Dr. Paul S. Russo, Dr. William E. Crowe, and Dr. Vincent L. Wilson for their resourceful contribution towards this dissertation.

I offer my regards and blessings to all of my colleagues and friends at the Louisiana State University who supported me in any respect during the completion of the project.

Special thanks go to my beloved husband, Eduard A. Stefanescu, for his support and motivation to pursue this dream. And last but not least, thanks to my mother, Angela, who made enormous sacrifices to give me an education.

TABLE OF CONTENTS

LIST OF TABLES

LIST OF FIGURES

LIST OF SCHEMES

LIST OF ABBREVIATIONS

AGU	Anhydroglucose Unit
BC	Benzoyl Chloride
BMIMAc	1-butyl-3-methylimidazolium acetate
BMIMCl	1-butyl-3-mehtylimidazolium chloride
DABCO	1,4-Diazobicyclo[2.2.2] Octane
DDA	Degree of Deacetylation
DMF	Dimethylformamide
DMSO	Dimethyl sulfoxide
DS	Degree of Substitution
DSC	Differential Scanning Calorimetry
DTG	Derivative Thermogravimetry
FT-IR	Fourier Transform Infrared Spectroscopy
K	Chitosan
KPATC	Chitosan reacted sequentially with phthalic anhydride and trityl chloride
KTCPA	Chitosan reacted sequentially with trityl chloride and phthalic anhydride
MTGA	Modulated Thermo-gravimetric Analysis
NBS	*N*-Bromosuccinimide
NMR	Nuclear Magnetic Resonance Spectroscopy
PA	Phthalic Anhydride
Py	Pyridine
SEM	Scanning Electron Microscopy
TC	Trityl Chloride

TGA	Thermo-gravimetric Analysis
XRD	X-Ray Diffraction

ABSTRACT

Dissolution of chitosan in ionic liquids was accomplished. It has been shown that 1-butyl-3-methylimidazolium acetate (BMIMAc) is a better solvent than 1-butyl-3-methylimidazolium chloride (BMIMCl). Dissolution of chitosan in BMIMCl required a prior regeneration of chitosan from 1% acetic acid solution. In the case of BMIMAc, both dried chitosan and regenerated chitosan from acetic acid solution have been dissolved in a relatively short amount of time. While concentrations up to 2 wt% of chitosan in BMIMCl could be obtained, concentrations of 10 wt % of chitosan in BMIMAc were realized.

Homogeneous phthalation and benzoylation of chitosan were achieved in these ionic liquids. According to FT-IR data both -OH and -NH_2 groups of chitosan reacted with benzoyl chloride and phthalic anhydride, respectively.

The reaction of chitosan with phthalic anhydride in the presence of a base or *N*-bromosuccinimide as catalyst and using ionic liquids as a solvent media was also studied. The presence of a base into system leads to an increase of the degree of substitution (DS = 0.41) of the functional groups of chitosan comparing with the reactions performed in the absence of a base (DS = 0.24), while the presence of a catalyst into system resulted in even higher increase of DS (0.85). The FT-IR data indicated that the hydroxyl groups of chitosan are being catalyzed to a greater extent than the amino groups. All the reactions products obtained in the presence of a catalyst were soluble in dimethyl sulfoxide and dimethylformamide.

Chitosan-cellulose blends were prepared using BMIMAc as common solvent. Rheological measurements of polymeric solutions indicated the formation of a complex between chitosan and cellulose molecules. Films prepared from polymeric solutions were investigated by means of FT-IR, TGA, XRD and SEM measurements. The shifting of the band corresponding to

–NH groups of chitosan from 1597 to 1565 cm^{-1} (FT-IR), the absence of diffraction peaks at 2θ = 10.7 and 14.9^{o} (XRD), the increased Ea for all polymeric blends (MTGA), and the presence of a homogeneous structure with no phase separation of the two polymers (SEM) serve as good evidence for the miscibility between chitosan and cellulose in the solid state.

CHAPTER 1 . INTRODUCTION AND LITERATURE REVIEW

1.1 Introduction of Polysaccharides

Polysaccharides, one of the most abundant and diverse families of biopolymers, are polymeric carbohydrate structures produced by microorganisms, by plants, by mammals and crustaceans. These biopolymers serve living organisms as storage materials, structural components, and protective substances. For example, macromolecules such as chitin and cellulose play an important role as links between other cell wall components and as structural molecules. Starch and glycogen are food reserves for plants and animals, respectively.(*1*) When the polysaccharides have in their structure only one type of monosaccharide, the polysaccharide is called homopolysaccharide (e.g. cellulose) while when more than one type of monosacchride is present they are called heteropolysaccharides (e.g. chitosan).

Polysaccharides provide the scientists with a broad spectrum of raw materials that exhibit biocompatibility, biodegradability, and versatility.

1.2 Properties of Chitin

Chitin, a polysaccharide, is found in the outer shell of insects, skeleton of shrimps, crabs, and other sea crustaceans, as well as in the internal structures of other intervetebrates (*2-4*) and cell walls of various fungi. Chitin, the most abundant polysaccharide containing amino groups and the second most abundant polysaccharide found in nature after cellulose, is composed of β(1-4) linked units of the amino sugar and N-acetyl-glucosamine randomly distributed throughout the polymer chain - depending on the processing method used to derive the biopolymer (Scheme 1.1). It took more than a century of study for chitin to have its structure identified and to be recognized as one of the most important natural biopolymers.(*5*) Chitin is a useful material in biomedical applications in wound

dressing. It was found to accelerate wound healing with the rationale that the abundantly present lysozyme enzyme in fresh and healing wounds acts to break down chitin powder to release the *N*-acetyl-glucosamine required for wound healing.(*6*) Due to the presence of acetamido groups present in its structure, strong intra- and intermolecular hydrogen bonding with the adjacent hydroxyl groups are formed within the chitin structure (Scheme 1.1). This accounts for the insolubility of chitin in most of organic solvents encumbering in this way its derivatization and commercial applications.

Scheme 1.1 Crystalline structure of chitin and chitosan. (*7*)

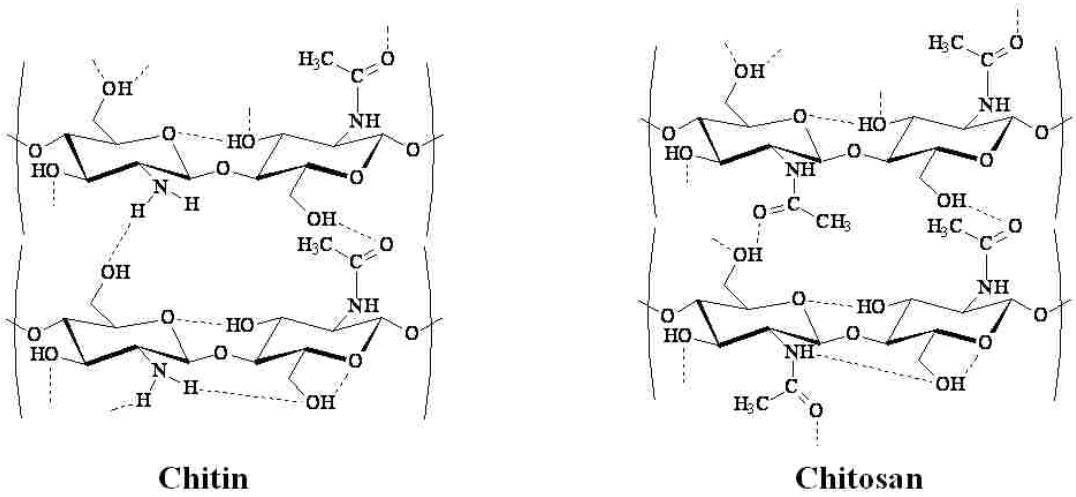

Chitin **Chitosan**

The primary biological function of crustacean chitin is to provide a structural scaffold to support the animal exoskeleton through an intimate link between the biopolymer with the biological system in which it is found. In the crustacean shells, chitin is closely related with proteins, where it provides bioadhesive properties between fiber beds of stacked laminas. According to Poulicek and coworkers,(*8*) the matrix in mollusk shell is composed of two structural units (Figure 1.1): 1) a mineralization matrix and 2) a high molecular weight chitinoproteic complex also called the protein carrier. The mineralization matrix consists of an acidic polypeptide fraction with strong affinity for Ca^{2+} ions, and as such, it is mostly soluble in decalcifying agents, like HCl. The protein carrier has

no affinity to calcium which is arranged in the form of sheets and layers. Chitin is trapped between mineralization matrices when $CaCO_3$ deposition takes place (Figure 1.1).

The isolation of chitin from the shell of mollusk is done via chemical procedures (Figure 1.2). The shells can be first treated with 30% HCl for demineralization of the crustacean shell followed by the removal of proteins by NaOH. The order of the procedure with acid and base can be reversed.

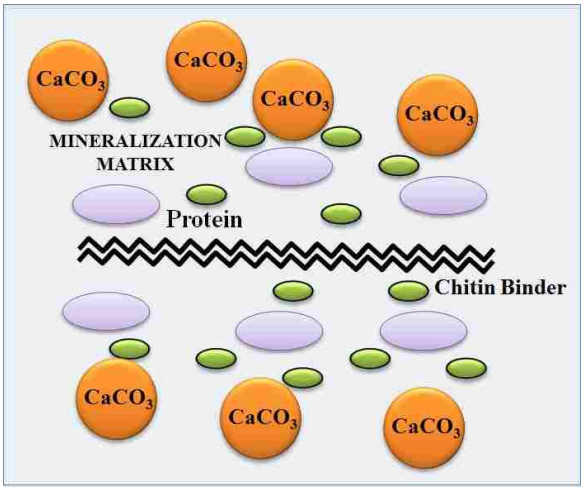

Figure 1.1 Schematic of the structure of the organic matrix in mollusk shells. Adapted from references. (*8-9*)

1.3 Synthesis and Structures of Chitosan

Chitosan is a linear polysaccharide obtained industrially through the alkaline *N*-deacetylation of the *N*-acetamido functional groups of chitin (Scheme 1.2). The N-deacetylation process is influenced by several factors: the source of chitin, NaOH concentration, reaction time, and reaction temperature.(*2, 7*) Chemically, chitosan is composed of randomly distributed β-(1-4)-linked deacetylated D-glucosamine units and N-acetyl-D-glucosamine units (Scheme 1.1). Typically, the degree of deacetylation in commercial chitosan is around 60% to 95%. Methacanon and coworkers(*2*) studied the *N*-deacetylation process of chitin and determined that at low NaOH concentrations there is not a significant change in the percent of deacetylation, not even at elevated

temperatures and times of reaction. However, an increase in the alkaline concentration, temperature, and time triggers a rapid increase in the deacetylation percent. Molecular weight and viscosity are affected as well by the different concentrations of NaOH and by different reaction of times. When 50% of NaOH was used for the deacetylation of chitin, a rapid decrease of molecular weight distribution was observed in the first hour but decreased subsequently. A 35% of alkali concentration in the deacetylation process showed that the decrease of viscosity and molecular weight distribution of the obtained chitosan was slowed.(*10*) In attempts to solve the problem involving the degradation of chitin main chain during the deacetylation process, it has been reported that the addition of $NaBH_4$,(*11*) thiophenol,(*12*) or N_2 gas(*13*) can minimize the chain scission.

Over the years, X-ray diffraction has been the most employed tool for the analysis of the molecular conformations of chitin and chitosan. Although the first X-ray study on a chitosan fiber was conducted as early as the middle of 1930s, chitosan's structure has been less studied than the one of chitin. Being a positively charged polymer, chitosan is soluble in acidic to neutral solutions. In acidic solutions chitosan behaves as a cationic polymer. Similar with the case of polyelectrolyte solutions, a surprising increase of the reduced viscosity (η_{sp}/C) of chitosan aqueous acid solutions is observed with a decrease in the concentration of solutions. This behavior can be attributed to an increase of the polymer volume following dilution, as a result of electrostatic repulsion in the chitosan chains. To prove this hypothesis researchers have screened these repulsions by addition of ionic salts to such solutions. For example, when NaCl is added to an aqueous acid chitosan solution, a typical linear relationship between reduced viscosity and solution concentration is obtained. Strong evidence correlated from multiple studies suggests that chitosan chains in solution are not very flexible and adopt a random coil extended conformation. In addition, the chain flexibility can be increased by elevating the ionic strength of solutions which disrupts the electrostatic interaction of the polysaccharide chains.

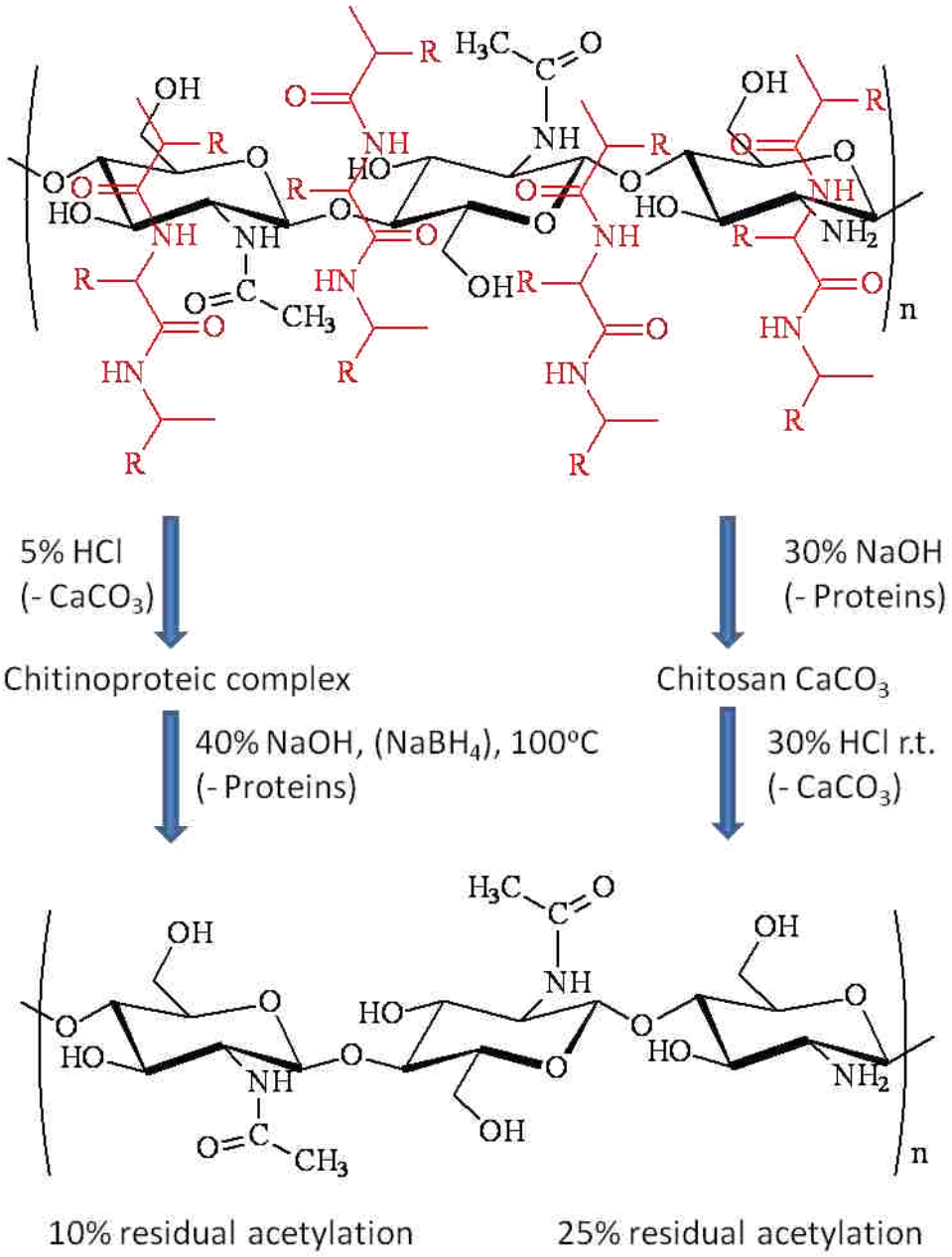

Figure 1.2 Isolation of chitosan from mollusk shell. (*8-9*)

1.4 Important Properties of Chitosan

As described in the previous section, the key factor that differentiates chitosan from chitin is represented by the degree of deacetylation. It is widely known that the deacetylation reaction can never be conducted to a complete conversion, and that the deacetylation degree in chitosan ranges typically from 70% to about 95%. One method yielding very high degrees of deacetylation (ca. 95%)

consists in reacting chitin with potassium hydroxide at 180°C for 30 minutes.(*14*) While some researchers have obtained chitosan by deacetylating the chitin from shrimp hulls or other crustaceans, other researchers have obtained it from fungi strains like absidia.(*15*) Since the nature of the manufacturing process preformed industrially often influences the characteristics of the final product, the quality and properties of the resultant chitosan products may vary from a company to another. The properties often affected by the manufacturing process include degree of deacetylation, purity, molecular weight, viscosity, polydispersity index, polymorphous structure etc.

Scheme 1.2 *N*-deacetylation of chitin. (*16*)

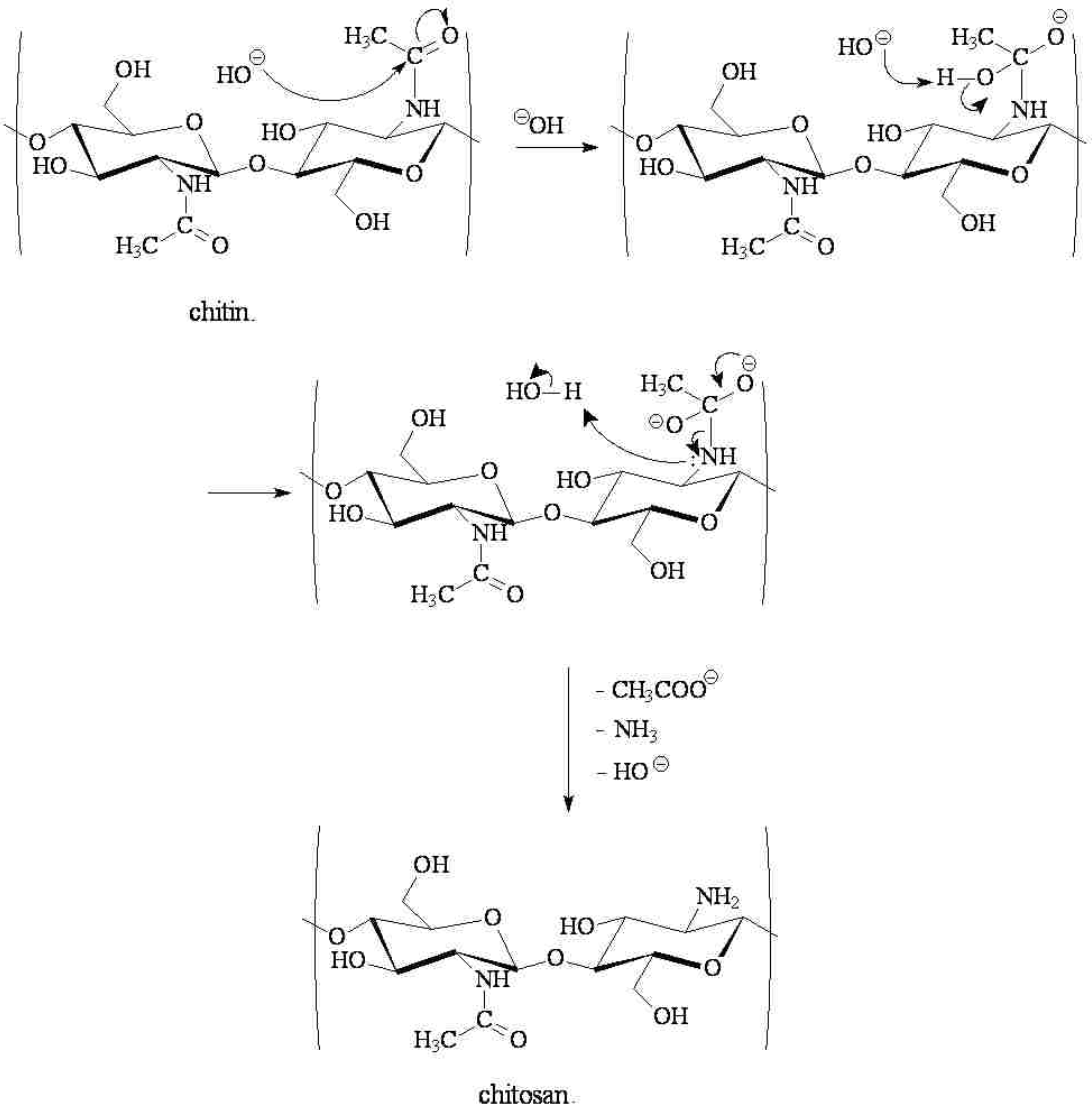

The degree of deacetylation is one of the most important properties of chitosan because it dictates the amount of free amino groups that can later play an important role in the polymer's ability to act as a chelating agent for many metal ions. Over the years several methods have been employed to determine the deacetylation degrees, including dye adsorption,(*17*) titration,(*18*) infrared spectroscopy,(*19*) NMR spectroscopy,(*20*) CHN elemental analysis,(*21*) high performance liquid chromatography (HPLC),(*22*) and enzymatic approaches.(*23*) For example, it was suggested that one of the best non-destructive ways to analyze the deacetylation degree in chitosan is the first derivative UV spectrophotometry at 199 nm.(*24-26*) Another proposed method was treating the amino groups in chitosan with sulfonic acid groups on dye ions, based on the 1:1 stoichiometry of interaction.(*27*)

Because of its high density of amino groups chitosan has very good coagulating properties, acting as a flocculant/coagulant in the presence of negatively charged polymers, proteins, dyes, etc. Additionally chitosan acts as a chelating agent for many metal ions. It was observed that chitosan's amino groups perform much better as a metal chelating agent than the acetyl groups in chitin.(*5*) Although this finding would imply that a higher amino group content is equivalent with higher metal adsorption rates, other studies have shown that the metal chelating ability of chitosan also depends on other parameters, such as crystallinity and affinity for water.(*28*)

Just like any other polymer, molecular weight, M, is another characteristic of interest in chitosan. While the M of chitin is typically above 10^6 g/mol, the M of chitosan is reduced through various degradation reactions that take place during the rough deacetylation treatment.(*5*) Commercial chitosan products have M usually in a range between 10^5 - 10^6 g/mol. The major factors that lead to the degradation of macromolecules during deacetylation include a combination of high temperatures, high shear forces imposed through mixing and dissolved oxygen. Typically, the thermal degradation of chitosan occurs at temperatures in excess of 280^{o}C. Even in the absence of

such harsh temperatures, dissolved oxygen has been shown to slowly degrade chitosan.(*5*) Among the methods that have been employed to determine the M of chitosan are viscometry,(*29*) chromatography,(*29-30*) and light scattering.(*31*)

Furthermore, an essential characteristic of chitosan solutions is viscosity. For a given set of environmental parameters (temperature, pressure, humidity etc), the viscosity of chitosan solutions has been observed to be influenced by factors like concentration, M, degree of deacetylation, pH and ionic strength.(*5*) Of course, if the environmental parameters are not fixed viscosity also varies with temperature and pressure. For example it was found that the intrinsic viscosity of dilute chitosan solutions decreases with an increase in the polymer's ionization or ionic strength.(*5*) In addition, the variation of viscosity with the pH has been observed to depend on the type of acid employed. If the pH is decreased with acetic acid the viscosity tends to increase, while for HCl a decrease in the pH triggers a decrease of viscosity.(*5*)

Regarding chitosan's solubility, the polysaccharide dissolves in nearly all solutions of organic acids at pH values below 6. In unmodified form it is, however, insoluble in organic solvents, water and alkaline solutions.(*5*) Perhaps the most frequently used organic acids to prepare chitosan solutions are acetic acid and formic acid. In addition, several dilute inorganic acid solutions (e.g. HNO_3, H_3PO_4, HCl, $HClO_4$) can be employed to dissolve chitosan. It has been also shown that a 3-to-1 mixture of dimethylformamide -to- dinitrogen tetroxide can dissolve chitosan very well.(*14*) Although chitosans with high degrees of deacetylation are water insoluble, it has been revealed that the polysaccharide with 50% deacetylation from homogeneous processing can be dissolved in water.(*32*) On the other hand, various chemical treatments of chitosan, like carboxymethylation for instance, can induce some water solubility of the biopolymer.(*17, 33-34*)

1.5 Applications of Chitosan

Among the many reasons behind the continuous search for new applications of chitosan are the polymer's biodegradability, non-toxicity and natural abundance. A comparison of the present trends in chitosan uses with the applications predominantly targeted 40 years ago reveals a broadening of the relevance spectrum. While in the 1970s chitosan was mostly utilized in sludge dewatering, food processing and metal ion chelation, today the industrial applications are focused on fabrication of high value products, such as feed additives, cosmetics, drug carriers, semi-permeable membranes, and pharmaceuticals.(*5*) The major factors that triggered the broadening of the applications spectrum are the improved quality and the reduced cost of the current chitosan grades, which can be attributed in great part to the superior industrial methods utilized today to synthesize the polymer.

One of the most important characteristic of chitosan consists in its ability to act as a binding agent for various chemicals such as those found in cholesterol, fats, proteins, metal ions, and even tumor cells. Water treatment, health care, as well as food and pharmaceutical industries are some of the main areas where chelation is regularly employed. For the treatment of waste waters, chelation focused mostly on the removal of harmful metal ions like copper, lead, mercury, uranium, etc. Early studies indicated that, when compared to other chelating polymers, chitosan had the best collection ability due to its high content of amino groups.(*14*) Other studies showed that chitosan can remove uranium from river and lake waters in amounts of 40% to 74%.(*35*) Additionally, it has been suggested that the chelating ability of chitosan can be supplementary enhanced through cross-linking,(*36*) homogeneous hydrolysis,(*28*) controlled N-acetylation,(*37*) and complexation with other polymers.(*38*) Owing to the high content of amino groups chitosan is a very good flocculant and coagulant, and is capable of interacting with negatively charged compounds, like proteins, dyes and various solids.(*5*) Some studies suggested that the coagulating efficiency of chitosan may

decrease with increasing the polymer molecular weight.(*39*) In line with the chelating applications of chitosan, Holme and Hall have synthesized a novel chelating chitosan derivative through the attachment of iminodiacetate moieties via a hydrophilic spacer group.(*40*) The synthetic steps employed in this work are presented in Figure 1.3. Starting from 1,2:3,4-di-O-isopropylidene galactose the authors prepared an epoxide through the reaction with epichlorohydrin. The product was further reacted with dimethyliminodiacetate to form a mixture of dimethyliminodiacetate and morpholone. The final chelating monosaccharide derivative was obtained through the base hydrolysis of the mixture followed by the acid treatment at 50^{o}C. The coupling to chitosan via reductive amination gave the resultant product which showed a strong binding capacity towards Cu (II) ions, and exhibited much better ion-exchange ability than the one of native chitosan.

Chitosan possesses excellent film forming characteristics, for which reason it is a valuable polymer in membrane fabrication. Chitosan membranes have been employed over the years in water purification, filtration, fruit coating, surgical dressings and drug encapsulation. In some water filtration studies chitosan-based membranes were showed to exhibit retention factors of 65-73% for sucrose, 54-57% for glucose and 3-6% for urea.(*41*) Most chitosan membranes are stable in both dilute acid and alkaline solutions. Cross-linked membranes with enhanced resistance to solvents may be prepared by addition of bifunctional chemicals to chitosan solutions.(*39*) Such bifunctional agents may include glutaraldehyde, carboxylic anhydrides and other various aldehydes. Additionally, the film forming ability of chitosan has been successfully employed in cell encapsulation for hormone delivery in medicine.(*42*) Owing to the semi-permeable nature of such membrane-films small molecules can diffuse from one side to the other of membranes, but cells and large molecules cannot. Besides cell encapsulation, chitosan has been shown to perform very well in applications related to controlled agrochemical release.(*43*)

Other areas where chitosan has found valuable applications include paper-making, food processing, pharmaceutics and biotechnology. Some of these applications are attributable to chitosan's ability to accelerate wound healing and plant germination and stimulate the immune system. Additionally, chitosan can also inhibit antifungal effects and tumor cells. In spite of the fact that chitosan has been found capable to complex with DNA and coagulate with red cells in blood, it should be recognized that further studies are needed to elucidate the interactions between living cells and the functional groups of cationic polymers, like chitosan.

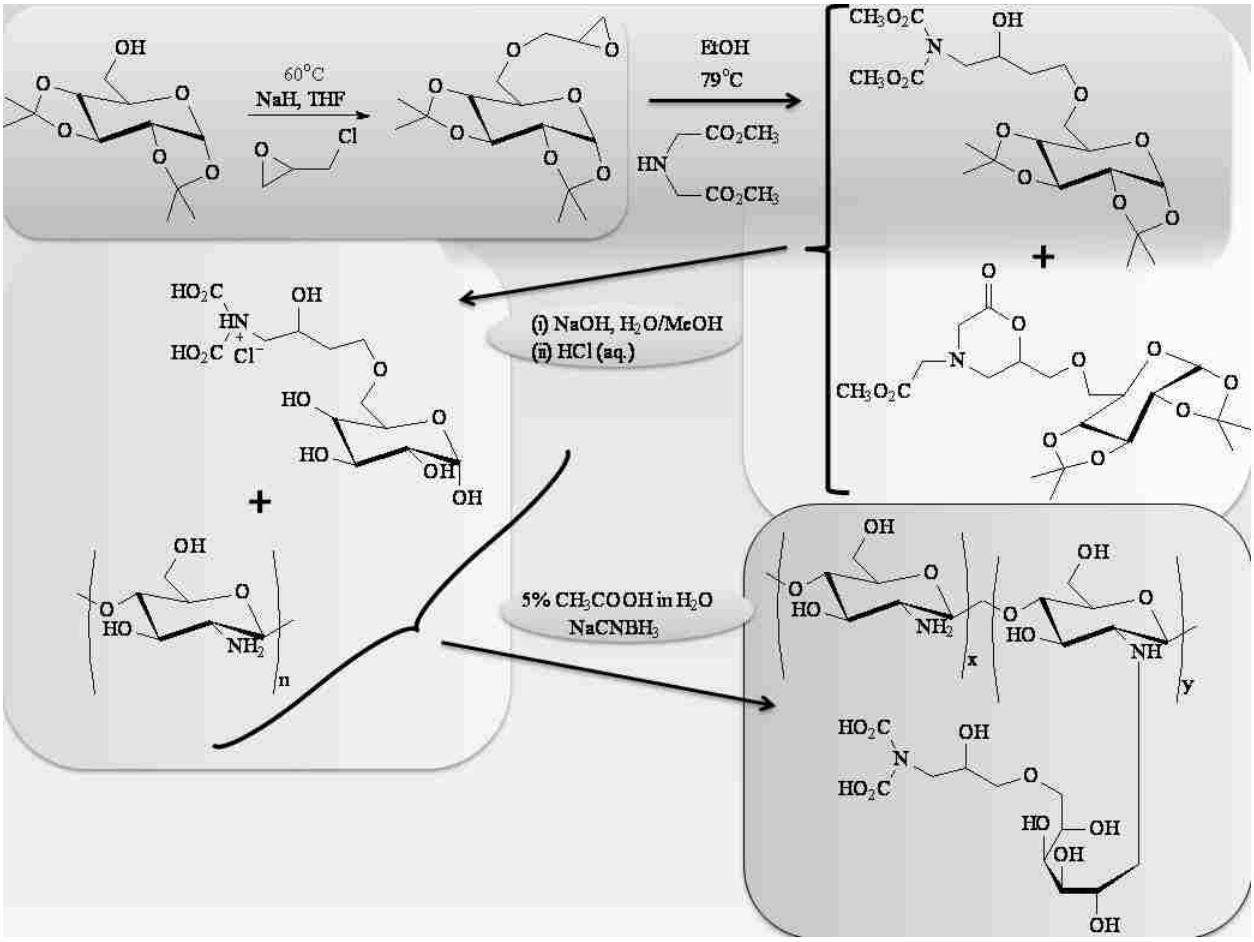

Figure 1.3 Schematic showing the synthetic steps used by Holme and Hall to obtain the Cu(II)-chelating chitosan derivative. Adapted from reference. (*40*)

1.6 Enzymes Involved in Chitosan Decomposition

Many living organisms, like insects, crustaceans, fungi and bacteria, regularly incorporate chitosan within various parts of their bodies. Because polysaccharide decomposition and synthesis plays an important role in the life style of such organisms, degrading and synthesizing enzymes are directly and actively involved in supporting and maintaining the metabolism and life of these beings.(*44*) For a long time it was believed that mammals did not possess enzymes involved in chitosan or chitin synthesis/degradation. Since this was the case, such enzymes were (and still are) targeted by researchers to control the growth and spreading of some insects, or some fungal and bacterial species that could interfere with the life style of human beings. In fact, such enzymes have been intensively studied for biotechnological applications. Cloning and sequencing are just two of the most utilized laboratory processes, frequently employed to better understand and describe the structure-function relationship of such enzymes in living organisms.

Chitinases represent a family of enzymes that have the ability of hydrolyzing the β-1,4-N-acetylglucosamide linkage in chitin and chitosan.(*45*) As a result of polysaccharides degradation, chitinases produce mainly disaccharides and a small amount of trisaccharides. More exactly, these enzymes can hydrolyze the bond between two consecutive N-acetylglucosamine units (here abbreviated GlcNAc: e.g. GlcNAc - GlcNAc) and the bond between a GlcNAc unit and a glucosamine one (abbreviated GlcN: e.g. GlcNAc - GlcN). Enzymes can discriminate the order of the linkages between consecutive units, for example GlcNAc - GlcN versus GlcN - GlcNAc. Besides hydrolyzing the GlcNAc – GlcN linkages, some enzymes were also found to hydrolyze the GlcN - GlcNAc ones. Chitinases were first detected in 1911 in orchid bulbs as part of the plant's defense system against fungi. Since their discovery, these enzymes were also isolated from other plants, as well as from bacteria, fungi, worms, insects and fishes. Recently, some chitinases were surprisingly found in the gastric juices of humans, and are believed to have digestive functions for catabolic

activity.(*46*) In addition to gastric juices, chitinases were also observed in the human blood(*47-48*) and cartilages.(*49*) The activity of human chitinases is related to several allergies and even asthma.(*50-52*)

On the other hand, chitosanases are the family of enzymes that attack chitosan, but do not attack chitin.(*45*) Just like chitinases, chitosanases decompose chitosan to the dimer and trimer saccharides. Chitosanases are defined by the Enzyme Commission as the enzyme family that can catalyze the endo hydrolysis of β-1,4-glycosidic linkages between GlcNAc and GlcN on chitosan polymers having degrees of acetylation in the range 30% - 60%. To date, however, the definition is still confusing and uncertain, suggesting that further information needs to be acquired about chitosanases to allow a better understanding of the enzymatic catalysis mechanisms. To provide an example of such an enzyme, in Figure 1.4 is presented a schematic of a crystal structure of family 46 chitosanase from *Streptomyces* sp. N174. As a side note, streptomyces represent the largest genus of actinobacteria, and are widely known for their antibiotic capabilities, being able to produce both antibacterials and antifungals. Knowing the pharmacological importance of streptomyces it is quite clear that the enzymes involved in the synthesis/degradation must be well studied and their catalyzing mechanisms must be thoroughly understood.

1.7 Cellulose and Cellulose Derivatives

Cellulose is one of the most researched and industrially employed polysaccharides on earth and is made of linear chains of β(1-4) linked D-glucose units (see Figure 1.5 for chemical structure).(*53*) It is a chiral and biodegradable, hydrophilic polymer insoluble in water and in most organic solvents. The β(1-4) linkages of the D-glucose units in cellulose are in contrast with the α(1-4) linkages of the D-glucose units observed in starch and other carbohydrates. These features allow cellulose to be a straight chain polymer, free of coils and branches, where the macromolecules adopt an extended, stiff, rod-like conformation.(*54*) Cellulose is essentially the most common organic

chemical on earth, being the structural component of the primary cell wall of green plants, algae and certain fungus-like microorganisms. For example, it was previously showed that the weight content of cellulose in wood and cotton is ca. 30% - 60% and 90%, respectively.(*53*)

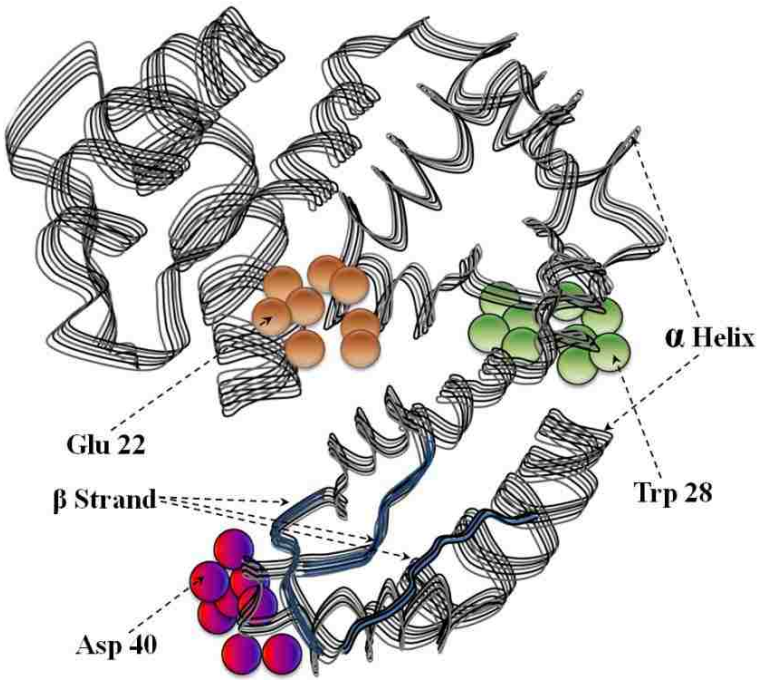

Figure 1.4 Schematic of a crystal structure of family 46 chitosanase from *Streptomyces* sp. N174. The catalytic crevice consists of two α helixes and three stranded β sheets. Glu22 and Asp40, indicated by brown and red beads, respectively, are catalytic residues. The green beads, symbolizing the tryptophan residueTrp28, are positioned between the upper and lower domains, acting like a hinge. (*44*)

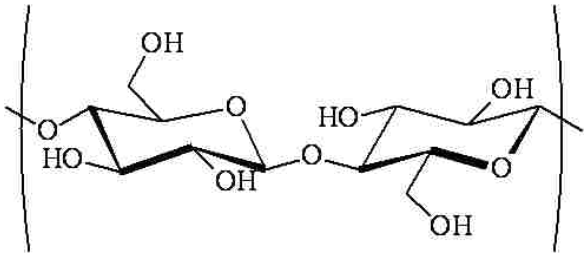

Figure 1.5 Chemical structure of cellulose.

Industrially, cellulose is an important component in the fabrication of paper, paperboard and card stock, and in the manufacturing of textiles, like those obtained from cotton and linen. Although cellulose has numerous uses in its native form, the conversion of cellulose to other derivatives

considerably broadens the spectrum of applications. Several useful cellulose derivatives can be obtained through the partial or full treatment of the hydroxyl groups of cellulose with various reagents. Among the most important commercial derivatives are *cellulose esters*, such as cellulose acetate and cellulose triacetate, and *cellulose ethers*, like ethylcellulose, methylcellulose, hydroxypropyl cellulose, carboxymethyl cellulose, hydroxypropyl methyl cellulose, hydroxyethyl methyl cellulose, etc.(*55*)

Regarding some of the characteristics and uses of certain *cellulose esters*, secondary cellulose acetate, which is obtained through the partial hydrolysis of the primary triacetate derivative, can be dissolved in relatively cheap and non-toxic solvents such as acetone. On the other hand, the primary cellulose triacetate only dissolves in more toxic solvents such as chloroform, nitrobenzene and epichlorohydrin.(*56*) The conversion of the triacetate derivative to the secondary diacetate derivative is very important in the development of practical fiber-making processes. Cellulose acetate derivatives are very good insulators and this characteristic is a major reason behind industrial fabrication of acetylated cotton. Furthermore, cellulose acetate fibers, with Y-shaped cross-sections, are commonly utilized to make cigarette filter tows.

In contrast to cellulose esters, *cellulose ethers* make significant contributions to the food and pharmaceutical industries.(*54*) For example, ethylcellulose, which is obtained by replacing some of the hydroxyl groups on the D-glucose units with ethyl ether groups, is utilized as a food additive and as an emulsifier. Figure 1.6 shows a SEM image of some spray-dried ethylcellulose microcapsules, commonly used to encapsulate fragrances, vitamins or pigments for food applications. Methyl cellulose, which is also used as an emulsifier and thickener in foods, is obtained by treating cellulose with a sodium hydroxide solution, followed by a treatment with methyl chloride. Hydroxypropyl cellulose results after replacing several hydroxyl groups on the D-glucose units of cellulose with hydroxypropyl groups, through a treatment with propylene oxide. Hydroxypropyl cellulose, along

with another derivative hydroxypropyl methylcellulose, is used in the pharmaceutical industry to make ophthalmic lubricants, like artificial tears. In foods, hydroxypropyl cellulose is utilized as thickener, emulsion stabilizer and low level binder. Carboxymethyl cellulose is synthesized by treating cellulose with chloroacetic acid in the presence of a base. It is used as a thickener and emulsion stabilizer in ice-cream, toothpaste, laxatives, diet pills, detergents, and others.

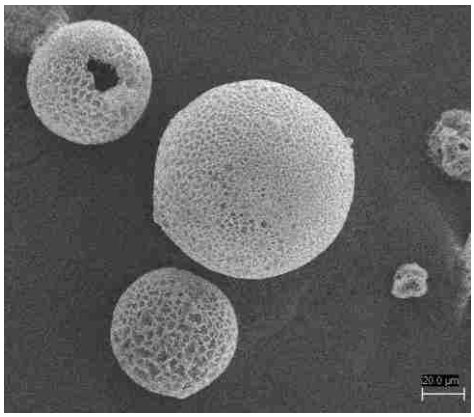

Figure 1.6 Typical spray-dried ethyl cellulose porous microcapsules used to encapsulate fragrances in foods. (*57*)

1.8 Ionic Liquids

Recently a rather new class of organic solvents, ionic liquids, has been found particularly useful in dissolution of polar organic materials, even polymers, which are otherwise difficult to dissolve.(*58*) Ionic liquids are organic salts that can be liquid even at temperatures as low as -96^{o}C; however, the term "ionic liquids" refers in the patent and academic literature to liquids composed entirely of ions that are fluid around or below 100^{o}C. Ionic liquids are generally benign solvents that can be used to a series of numbers of industrial processes resulting in improved yields, greater recyclability and an overall reduced environmental impact. These solvents have already found applications in commercial fields such as pharmaceuticals and fine chemicals,(*59-60*) nuclear industry,(*61-62*) and in mainstream petrochemical processes.(*63-64*) Some advantages that allowed ionic liquids to be called the green solvents of the future include their low vapor pressure over a

wide range of temperature, their excellent thermal stability, and the fact that they have good and tunable solubility properties and can be regenerated and used all over again in a process.

In order for an ionic liquid to be a good solvent it needs to have a low melting point so that no high temperature reaction to be required during a chemical process. The melting point of an ionic liquid is related to its lattice energy which is a measure of the strength of bonds in the ionic compound. The lattice energy can be calculated using Kapustinskii equation(*65*) (equation 1.8.1) which shows that by using anionic or cationic components with larger ionic radii it is possible to lower the lattice energy and therefore reduce the melting point of the ionic liquid. From the Kapustinskii equation it also can be observed that by increasing the ionic charge the lattice energy will tend to increase. However, according to Fajans' rules an increasing charge also results in increasing the covalent character particularly for small cations and large anions and thus reducing the melting point of the salt.(*66*)

$$U = (287.2\ v\ Z^{+}Z^{-}/r_o)(1 - 0.345/r_o) \qquad (1.8.1)$$

where: U = lattice energy, v = number of ions per molecule, r_o = sum of ionic radii, Z^{+}, Z^{-} = charge of ionic species.

The effect of anions on the melting point of 1-ethyl methylimidazolium cations is shown in Table 1.1.(*66*) It can be seen that increasing the ionic radii of the anions results in a decreased melting point of the corresponding ionic liquids. To further decrease the lattice energy of the ionic liquids, an increase of the length of the alkyl group of the imidazolium cations can be applied.

When choosing an ionic liquid as solvent, one has to take into consideration the processability of the solvent. Viscosity is one of the most important physical properties for determining the processability. A fluid is best to have a viscosity as low as possible and to have only small changes in viscosity through the normal operating temperature range. It was observed that in respect to the cation structure the viscosity of the ionic liquid increases with alkyl chain length(*67*)

and with the reduction of freedom of rotation (e.g. from butyl to isobutyl).(*68*) Published data on the viscosity of ionic liquids is almost nonexistent and even the few data existent in the literature are often neither comparable nor reproducible due to the highly dependence of viscosity on the measuring technique used and the purity of the sample.(*66*) More work needs to be done in order to rationalize different trends and to establish a correlation for model prediction that affects the viscosity of ionic liquids.

Table 1.1 Melting points for various 1-ethyl methylimidazolium salts.

Salt	Melting point, °C
[1-ethyl methylimidazolium] Cl^{35}	84
[1-ethyl methylimidazolium] $Br^{36,37}$	81
[1-ethyl methylimidazolium] $I^{36,37}$	79-81
[1-ethyl methylimidazolium] $[PF_6]^{38}$	62
[1-ethyl methylimidazolium] $[GaCl_4]^{40}$	47

Ionic liquids have an established ability to be used as replacements for volatile organic and dipolar aprotic solvents because most of their physical properties are close to those of the organic solvents. Also, ionic liquids have been found to dissolve rigid chain cellulose (*69-72*) and chitosan (*73-75*) under suitable conditions by disrupting the hydrogen bonds. The ionic liquids should have low melting points and low viscosities and need to be inert during conversion so that they can be suitable for the homogeneous modification of cellulose or chitosan.

One of the most important and common impurities in ionic liquids is water. Cellulose, for example, dissolved in pure 1-butyl-3-methylimidazolium chloride ionic liquid to an extent of up to 10%.(*76*) However, the presence of water content exceeding 1% in the ionic liquid inhibits the dissolution of cellulose.(*69*) If the water content is 0.1 to 1%, aggregation of the polymer chains take

place which will decrease the viscosity of the solution, the accessibility of the polymer and thereby the reactivity.(*77*)

Ionic liquids with ammonium cations, pyridinium cations, and imidazolium cations have been shown to dissolve cellulose (Figure 1.7). However, there is no basic understanding regarding the interaction between cellulose and the ionic liquids. Moulthrop(*78*) and Remsing(*72*) concluded by using ^{13}C and $^{35/37}Cl$-NMR experiments that Cl^- anion from 1-butyl-3-methylimidazolium chloride ionic liquid is much more involved in the disruption of the hydrogen bond existent in cellulose structure than the cation. The acetate counter-ion dissolves cellulose much better than the Cl^- counter-ion, but no measurements are known for this type of ionic liquids that would explain the interaction with the polymer.

There are a couple of reports regarding the dissolution of chitosan in 1-butyl-3-methylimidazolium chloride ionic liquid.(*73, 79*) However, the chitosan is not fully soluble and still shows some crystallinity in the solutions.

1.9 Chemical Modification of Cellulose in Ionic Liquids

Several studies have reported the ionic liquids as a media for the functionalization of cellulose for producing products with desired properties, such as: acetylation,(*80-81*) esterification,(*82-83*) etherification,(*84*) and carboxymethylation.(*80*) Cellulose, a polysaccharide with a structure similar to that of chitosan, has three hydroxyl groups in its repeating unit while chitosan has two hydroxyl groups (carbon 3 and 6) and an amino group at carbon 2. Due to the presence of three hydroxyl groups in its structure, cellulose has intermolecular and intramolecular hydrogen bonding which makes its dissolution impossible in most of the organic solvents. Cellulose is soluble in very polar organic N-oxides, such as the monohydrate of N-methyl morpholine N-oxide, NMMO, which is now the industrial solvent of choice to manufacture lyocell fibers. (*85-86*)

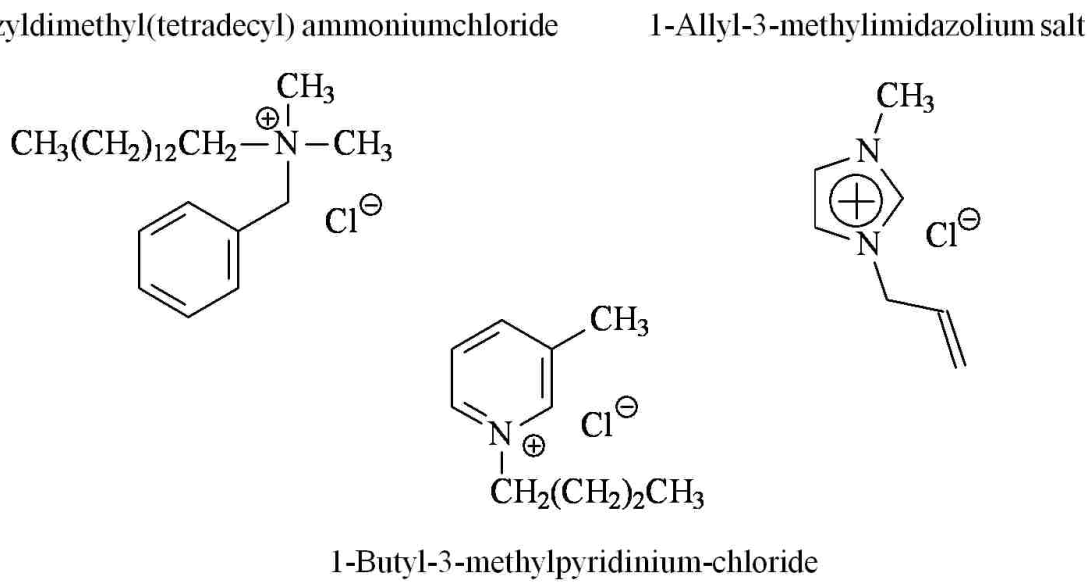

Figure 1.7 Examples of ionic liquids suitable for the dissolution of cellulose.

Acetylation of cellulose (Scheme 1.3) in 1-butyl-3-methylimidazolium chloride using acetyl chloride(*80*) or acetic acid anhydride(*87*) in the presence of pyridine at 80^{o}C for 2 hours yielded soluble products of controlled degree of substitution. However, when succinic anhydride was reacted with cellulose in 1-butyl-3-methylimidazolium chloride at different temperatures, reaction times, and different molar ratios of succinic anhydride/AGU of 1:1 to 14:1, respectively, the resulting products had very low degree of substitution with values varying from 0.04 to 0.53.(*88*) This inefficient esterification remains unclear.

Erdmender synthesized trityl cellulose by performing the reaction of trityl chloride with cellulose in 1-butyl-3-methylimidazolium chloride as solvent.(*84*) The addition of a base is necessary to prevent the degradation of cellulose by capturing the hydrogen chloride formed during the reaction. A degree of substitution of 1 can be obtained using a six-fold excess of trityl chloride and a reaction time of 3 hours. Surprisingly, when the same treatment of cellulose with trityl chloride was performed in different ionic liquid, 1-ethyl-3-methylimidazolium acetate, cellulose acetate was obtained instead of trityl cellulose. This behavior was explained by the formation of reactive trityl

acetic acid esters as intermediate which will undergo a transesterification reaction with cellulose to give cellulose acetate as final product.(*89*)

Scheme 1.3 Acetylation of cellulose.

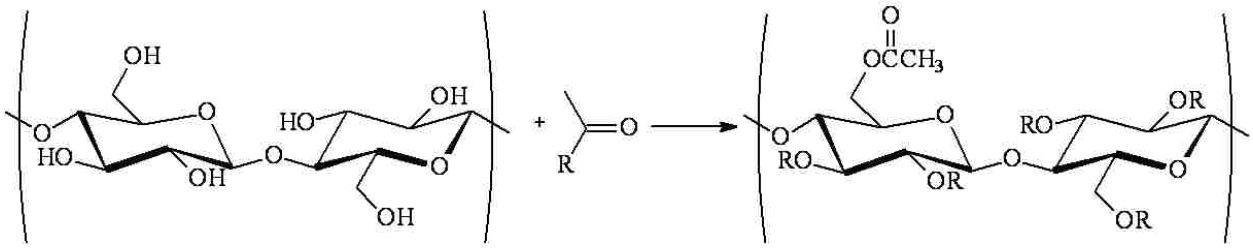

where R: H or -$COCH_3$

Reaction of cellulose with phenyl isocyanate in 1-butyl-3-methylimidazolium chloride has also been reported.(*76, 87*) Products soluble in DMSO, DMF, and THF were obtained for phenyl isocyanate/AGU ratios of 3:1 to10:1, respectively.

The homogeneous chemical modification of cellulose with phthalic anhydride in the presence of 1-allyl-3-methylimidazolium chloride and in the absence of catalyst has been reported by Liu and coworkers.(*82*) The phthalated cellulosic derivatives obtained showed a degree of substitution ranging from 0.10 to 0.73. The degree of substitution was observed to increase with the increment of reaction temperature, reaction time, and molar ratio of phthalic anhydride/AGU of cellulose. The phthalation reaction took place at C-6, C-3, and C-2 positions according to FT-IR and solid-state CP/MAS ^{13}C NMR spectroscopy. Upon chemical modification, the thermal stability of phthalated cellulose had been decreased. When the same reaction of cellulose with phthalic anhydride was performed in a different ionic liquid, 1-butyl-3-methylimidazolium chloride, higher degree of substitution ranging from 0.12 to 2.54 were obtained depending on the reaction temperature, molar ratio of phthalic anhydride/AGU of cellulose and reaction time.(*83*) We have extended the work to chitosan and observed significant differences in the nature of the products formed.

CHAPTER 2 . METHODS AND PRINCIPLES

2.1 Fourier Transform Infrared (FT-IR) Spectroscopy

FT-IR provides information about the types of functional groups present in an organic molecule by measuring the characteristic frequencies associated with bond stretching and bending vibration. A stretching vibration (symmetric or assymmetric) is the movement along the bond axis while bending consists of a change in the bond angle between bonds such as twisting, rocking, scissoring, and torsional vibrations. Usually, symmetric stretching vibrations occur at lower frequencies than asymmetric stretching vibrations while the stretching vibrations arise at higher frequencies than bending vibrations. A necessary condition for IR absorption is that a rhythmical change in the dipole moment of the molecule must take place during vibration. Thus, the alternating electric field generated by vibration couples the molecule vibration with the oscillating electric field of the incoming electromagnetic radiation.(*90-91*) The above mentioned vibrations are called fundamental absorptions and they develop from excitation from ground state to the lowest-energy excited state.

The vibrational frequencies are affected by the mass of the vibrating atoms and by the strength of the bonds. Bonds between atoms of lighter mass vibrate at higher frequencies than bonds between heavier atoms. Stronger bonds, which correspond to large force constants, vibrate at higher frequencies than weaker bonds.

For this research, formation of carboxylic, ester, amide, and imide groups was determined by FT-IR spectroscopy. The stretch of C=O in carboxylic acids appears at 1760-1710 cm^{-1}. A band at 1750-1735 cm^{-1} is evidence for the presence of carbonyl ester groups. The C=O stretch in amides is present in the spectra at approximately 1690-1630 cm^{-1}. An absorption at 1772 cm^{-1} corresponds to the imide carbonyl.

2.2 Nuclear Magnetic Resonance (NMR) Spectroscopy

Nuclear magnetic resonance (NMR) spectroscopy is a form of absorption spectrometry that studies the energy levels of distinct atomic nuclei of molecules when under appropriate conditions in a magnetic field.(*92*) In a magnetic field, the nuclei absorb electromagnetic radiation in the region of frequencies governed by the characteristics of the sample being analyzed.(*93*) The NMR works by supplying energy to the nuclei to force them to change their spin orientation with respect to that of the applied field. In the presence of an applied magnetic field the spin states are not equivalent because each nucleus is a charged particle with a magnetic field of its own called magnetic moment, μ. Hence, the spin states will have different energies and transitions between states become possible.

2.2.1 ^{1}H NMR Spectroscopy

^{1}H NMR gives information about the number of each of the distinct types of hydrogen being studied as well as acquires information about the chemical environment of the protons.(*91*) Under an applied magnetic field a molecule absorbs electromagnetic radiation that will cause a transition between spin states: the ground state and the excited state. The ground state decreases in energy and the excited state increases in energy when in the presence of an applied field. Because the absorption of energy is a quantized process, the energy absorbed must be related to the energy difference between the two states. This energy difference is a function of the strength of the applied magnetic field and it is influenced by a number of factors such as: the electron density surrounding the proton, the presence of nearby π-bonds, and the presence of neighboring protons. In a ^{1}H NMR spectrum the integration of the peaks gives information about the number of protons in a molecule, the chemical shifts indicate the type of proton environment, and the splitting patters tells about the adjacent protons/connectivity.

2.2.2 ^{13}C NMR Spectroscopy

^{13}C NMR is an important technique for determining the structures of organic molecules. A complete structure of an unknown compound can be identified when ^{13}C NMR is used together with ^{1}H NMR and IR spectroscopy. If in the ^{1}H NMR spectrum the information are obtained from the splitting patterns or integration, in a ^{13}C NMR spectrum the information about chemical structures are gained from the number of signals and the chemical shifts. The number of signals reveals the number of inequivalent carbons while the chemical shifts inform about the environment of each carbon.

Even if some of the principles of ^{1}H NMR apply to the study of ^{13}C NMR, there are aspects of ^{13}C NMR that differ from that of ^{1}H NMR: larger chemical shift range for ^{13}C peaks in comparison with the ^{1}H range; the intensities of the ^{13}C peaks do not correlate with the number of carbon atoms in a molecule; larger samples and longer times are required for ^{13}C NMR because the ^{13}C nuclei are much less abundant and much less sensitive than ^{1}H; the peaks of the ^{13}C spectrum are singlets.(*93*)

2.3 Rheology

Rheology is the study of the deformation and flow of materials.(*94-95*) Although the term is mainly applicable to liquids, it can also refer to soft solids or solids under conditions in which they flow rather than deform elastically. The word rheology derives from the Greek verbs rhei, to flow, and logos, to study. The ability of a system to store deformation energy, under the action of an external force, and to regain the initial shape after being deformed is called *elasticity*. The ability of a material to resist flow and to dissipate deformational energy is measured through the property called *viscosity*.(*95*)

The main relationship between force and deformation in solids is best described by the relation termed Hooke's law,(*96*) which states that the deformation is proportional to the applied force:

$$\tau = E\,\gamma \qquad (2.3.1)$$

In relation (2.3.1) τ represents the force per unit area, also called *stress*, γ represents the relative length change, also called *strain*, and E is the constant of proportionality known as *elastic modulus*. E is an intrinsic characteristic of a solid material. The equivalent relation for liquids is known as Newton's law of viscosity,(*94*) which states that the stress, τ, is proportional to the rate of straining, $d\gamma/dt$:

$$\tau = \eta\, d\gamma/dt \qquad (2.3.2)$$

The rate of straining is often symbolized as $\dot{\gamma} = d\gamma/dt$. While several real life materials obey these ideal laws for solids and liquids, many of them exhibit behaviors that lie in between the ideal elastic solid and the ideal viscous fluid. Some examples of such materials may include blood, paints, foods, toothpastes, polymers etc. An example of a material exhibiting a behavior in between the ideal elastic solid and the ideal viscous fluid is a rubber ball, like the one in the schematic shown in Figure 2.1. It can be seen that if the rubber ball is dropped on a hard surface from a certain altitude the ball does not return to that same altitude, but to a lower one. The difference in between the two altitudes was symbolized E", which depending on the bouncing cycle could be E_1", E_2" etc. In rheology this E" is known as loss modulus. The height that the rubber ball recovered after bouncing from the hard surface is known as the storage modulus, and is typically indicated with E'. The storage and loss modulus are linked through the complex modulus, E* following the relation:

$$(E^*)^2 = (E')^2 + (iE'')^2 \text{, where } i = \sqrt{-1} \qquad (2.3.4)$$

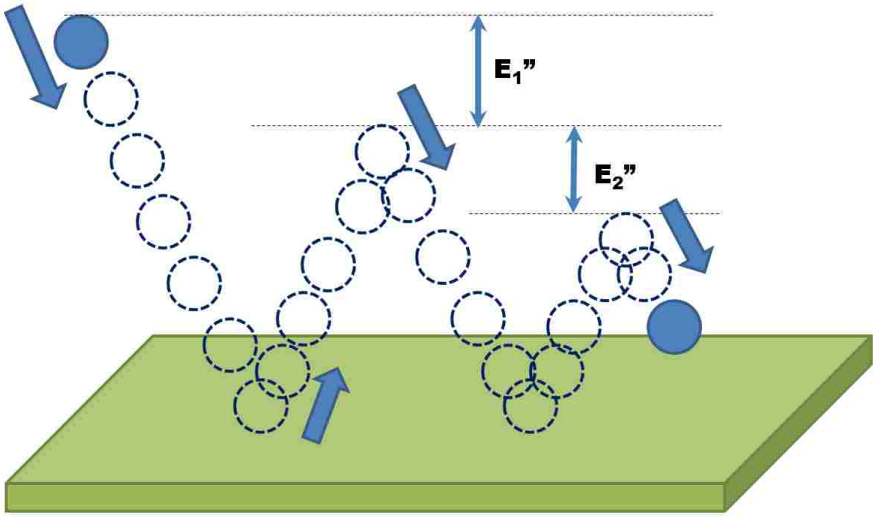

Figure 2.1 Schematic showing a rubber ball bouncing from a hard surface.

For practical purposes, the rheological behavior of various viscous systems is studied to identify the relationship existing between composition and performance under shear, as well as to observe the variation of viscosity, storage and loss moduli as a function of several parameters in the system. Identifying these properties and relationships is, more often than not, critical for achieving a fundamental understanding of materials' processability. For example, industrial processes require detailed studies of the interactions that occur among colloidal particles, polymers, surfactants and electrolyte salts. Although in complicated multi-component systems is difficult to formulate conclusions if too many parameters are varied, the reality is that the functionality of each component is often altered by addition of another. In order to obtain a more complete picture of how a system behaves in a real environment, all the constituents must be considered at once. The performance of polymer fluids in constrained environments can vary significantly from the one in bulk, especially when the molecules are confined to dimensions comparable to their sizes.

In Figure 2.2 are presented two of the most utilized rheological geometries for analysis of polymer solutions and composites. Both geometries are used for analysis of small quantities of material. While the parallel-disks geometry is usually preferred for the systems of higher viscosities,

the cone-and-plate geometry is typically utilized for systems of moderate viscosities, and involves a smaller gap between the upper and lower tools. The main advantage of the cone-and-plate over the parallel-disks is that the former device eliminates the problem with the radial dependence of the shear rate and shear strain,(*94*) providing a homogeneous flow of the material independent of the position between the upper and lower tools.(*96*) For systems of even smaller viscosities (e.g. water) a couette geometry is typically utilized for rheological analysis, where the liquid is placed in a barrel-like bottom tool in which a tubular upper tool spins around a centered axis.

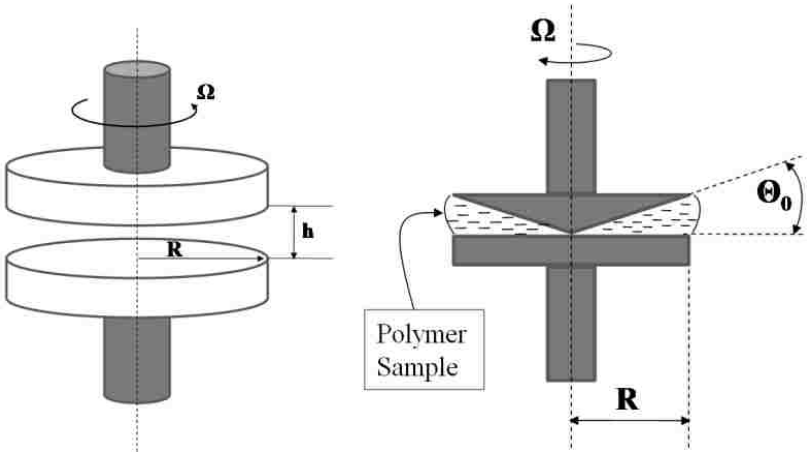

Figure 2.2 Schematic representation of the parallel-disk (left) and cone-and-plate (right) geometries. The parameters are: h is the distance between the plates, Ω is the constant angular velocity of the plate or cone in rotation, θ is the angular displacement, R is the radius of the plate and/or cone. (*97*)

2.4 Differential Scanning Calorimetry (DSC)

Differential Scanning Calorimetry (DSC) is one of the most extensively utilized thermal analysis techniques, in which the difference in the amount of heat needed to elevate the temperature of a sample and reference are measured as a function of temperature.(*98*) Duplicate matching sensors are employed for measuring the thermal changes of the sample and a reference, with the sample and reference being maintained at nearly the same temperature throughout the entire experiment. The important characteristic of this technique is highlighted by the word “differential” as the concept behind each measurement is to obtain information on the thermal changes in the

sample by heating or cooling it next to the inert reference.(*99*) Due to this differential attribute the resultant signal corresponds exclusively to the thermal variation to be studied, as any potentially unwanted thermal effects impact both sensors in the same way.(*98*) A schematic representation of the main DSC instrument components is presented in Figure 2.3. The sample and reference pans are enclosed in the DSC cell, which incorporates also the temperature sensors and the heating devices. As indicated in the schematic, a computer is employed to control the parameters of the system, to capture the data and to analyze it.

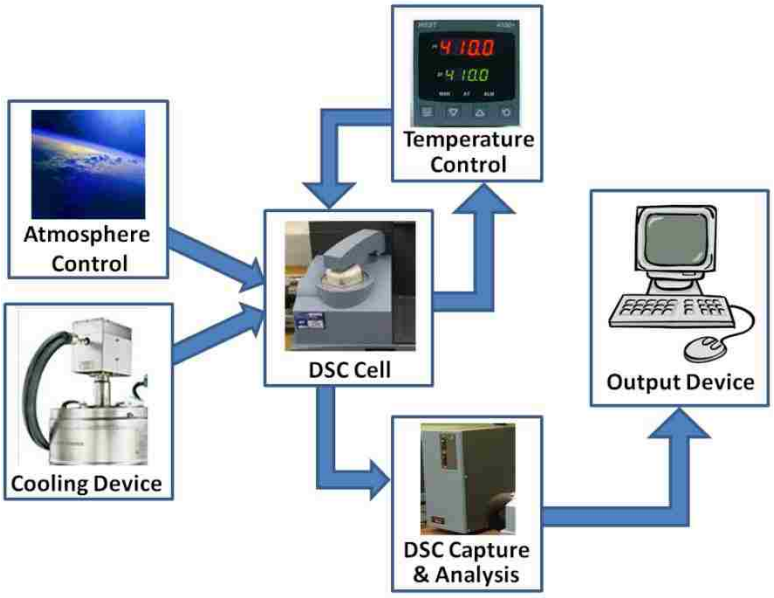

Figure 2.3 Schematic representation of the main DSC instrument components. Adapted from website. (*100*)

Another thermal technique related to DSC is Differential Thermal Analysis (DTA) in which a sample and an inert reference are subjected identical thermal cycles, while recording any temperature difference between sample and reference. The major difference between DSC and DTA is represented by the nature of signal produced with the two techniques. While for DSC the signal is proportional to the difference in thermal power between the sample and the reference ($d\Delta q/dt$), for DTA the signal is proportional to the temperature difference between the sample and the inert reference.(*99*) Owing to the DSC's quantitative calorimetric advantages that DTA measurements do

not provide, the more recent DSC instruments have gradually replaced the older DTA instruments on the market.(*98*)

2.5 Thermogravimetry (TG)

Thermogravimetry (TGA or TG) is an experimental procedure in which changes in weight of a specimen are recorded as the specimen is heated either in air, or in a controlled atmosphere such as nitrogen, under a rigorously controlled temperature programme.(*98, 101*) In short, a sample of the material of interest is placed into an aluminum, platinum or alumina basket that is supported on, or suspended from an analytical balance located outside of a furnace chamber. Prior to the measurement the balance is tarred, and the sample basket is heated according to the predetermined thermal cycle. When the sample undergoes thermal degradation, volatile components are lost during the TGA experiment and the mass loss can be observed and recorded. Additionally, materials can lose weight from a simple physical process such as drying. The balance sends the weight signal to the computer for storage, along with the sample temperature and the elapsed time. The TGA curve plots the TGA signal, converted to percent weight change on the Y-axis against the reference material temperature on the X-axis. For example, in Figure 2.4a is presented a TGA curve (blue curve) for an HCl-doped polyaniline sample. Representations of percent weight change versus time (t) may be also encountered especially when isothermal decompositions are performed, such as the one presented in Figure 2.4b.

The weight loss process emerges as a step in the TGA curve. Although most of the sample's mass is lost around one specific temperature the shape of the curve appears sigmoid, because some reactions start before and/or end after the main reaction temperature. Additionally, because a reaction in the solid state is relatively slow compared to gas or solution reactions, a thermogravimetric trace of such a transformation may be seen to occupy a wide span of temperature. Although other factors may be involved in some cases, the rate of reaction is often controlled by the

rate of heat transfer to or from the reaction interface.(*98*) Since the reaction evolves in time and the temperature always increases with respect to time, graphical representations show the reaction covering a spread of temperature. Because of this spread of reaction over time a careful definition of decomposition temperature must be formulated before comparing results.(*101*)

An alternate and very useful way to represent thermogravimetric results is to plot the temperature-derivative curve of the original data as a function of temperature (time-derivative curves are also possible). The resultant derivative thermogravimetry (DTGA) plot provides critical information about overlapping reactions or about slow reactions concurrent with fast reactions that may take place during the heating cycle. An example of a DTGA curve is presented in Figure 2.4a (red curve). The curve clearly exhibits several peaks, indicative of several decomposition processes.

Typical TG experiments are performed raising the temperature at a constant rate. Such experiments are known as non-isothermal or scanning. The less encountered isothermal measurements, like the one presented in Figure 2.4b, are carried-on at a constant temperature and are often used in kinetic studies.(*101*)

TGA *Kinetics.* Flynn and Wall developed a constant heating rate method to obtain simple kinetic information.(*102*)

$$d\alpha/dt = Z \exp(-Ea/RT)(1-\alpha)^n$$

where: α = fraction of decomposition

t = time (seconds)

Z = pre-exponential factor (1/seconds)

Ea = activation energy (J/mole)

R = gas constant (8.314 J/mole K)

N = reaction order (dimensionless)

In order to determine Ea, Flynn and Wall rearranged the above mentioned equation to get the following:

$$Ea = (-R/b)\, d(\ln\beta)/d(T^{-1})$$

where: b = constant assuming n = 1

β = heating rate (^{o}C/minute)

T = temperature of weight loss (^{o}C)

The activation energy (Ea) and the pre-exponential factor (Z) are calculated using the slope obtained from (lnβ) versus (1/T) plot.

Modulated Thermogravimetric Analysis (MTGA).(*103*) This technique superimposes a sinusoidal temperature modulation on the traditional underlying heating profile. This sinusoidal temperature program produces a change in the rate of weight loss. The use of discrete Fourier transformation allows kinetic parameters to be calculated on a continuous basis.

2.6 Important Thermal Parameters in Polymers

It is generally accepted that the thermal properties of polymers depend not only on the type of monomeric unit(s) comprising them, but also on their secondary and tertiary structures, like for instance stereochemistry, molecular weight, polydispersity index, their ability to crystallize or remain amorphous, etc. In real life applications polymers must be stable and maintain their structure and morphology when exposed to various temperatures and other environmental conditions. In line with this idea, the present section provides general information about some critical thermal parameters of polymers, such as glass transition temperature, melting/crystallization temperature and decomposition temperature.

The glass transition temperature, *Tg*, is the temperature at which the amorphous regions of a polymer begin behaving like glassy state materials.(*104-105*) From this definition it results that when a polymer is exposed to temperatures below the *Tg*, the polymer becomes very rigid and

brittle, because the long-range chain motions disappear. However, if the system exposed to temperatures below *Tg* is again heated to temperatures above *Tg*, the polymer segments slowly start moving and a transition from the glassy state to a rubbery-like state takes place.(*106*) This important transition in polymers is influenced by certain factors, such as chain flexibility, molecular structure, molar mass, branching and cross-linking. Low *Tg* materials exhibit high chain mobility and low rigidity. Low secondary forces promote mobility of the amorphous polymer leading to low *Tg* values.(*105*) Along with changes in hardness and elasticity, variations can also be observed in the specific volume, the modulus, the heat capacity, and the refractive index of a polymer when a transition from the glassy state to a rubbery-like state occurs.(*107*) The easiest way to determine the *Tg* of polymers is through a DSC measurement, where the sample is cooled below its *Tg* and then heated up. The *Tg* of a polymer is dependent on the heating rate utilized, for which reason the heating rate always needs to be specified. In Figure 2.5 is presented the *Tg* of a poly(methyl methacrylate) (PMMA) sample, as resulted from a DSC measurement. A step-like transition is clearly distinguishable.

Another very important thermal characteristic of polymers is the melting temperature, *Tm*. The *Tm* of a polymer is the temperature at which the macromolecular chains forming the crystalline domains lose their periodicity and order. The size of crystallites, as well as the presence or absence of defects in the crystallite, influence considerably the range of temperatures that typically accompany the melting of a polymer.(*104-105*) This range of temperatures is a useful indication on the sample crystallinity. In theory, polymers that are 100% crystalline should show only a *Tm* transition, while polymers that are 100% amorphous should exhibit only a *Tg* transition. In reality, however, 100% crystalline polymers are never possible due to crystallization defects and varying sizes of the crystallites. As a result of such defects, polymers are most of the times semicrystalline and contain crystalline and amorphous domains, thus exhibiting both *Tm* and *Tg*. Around *Tm* the

segmental motion of chains is elevated and does not permit the formation of stable nuclei. However, if the temperature is decreased below *Tm* the translational, rotational, and vibrational energies and the diffusion rate of the polymeric chains decrease, allowing for the formation of crystallization nuclei.(*104*)

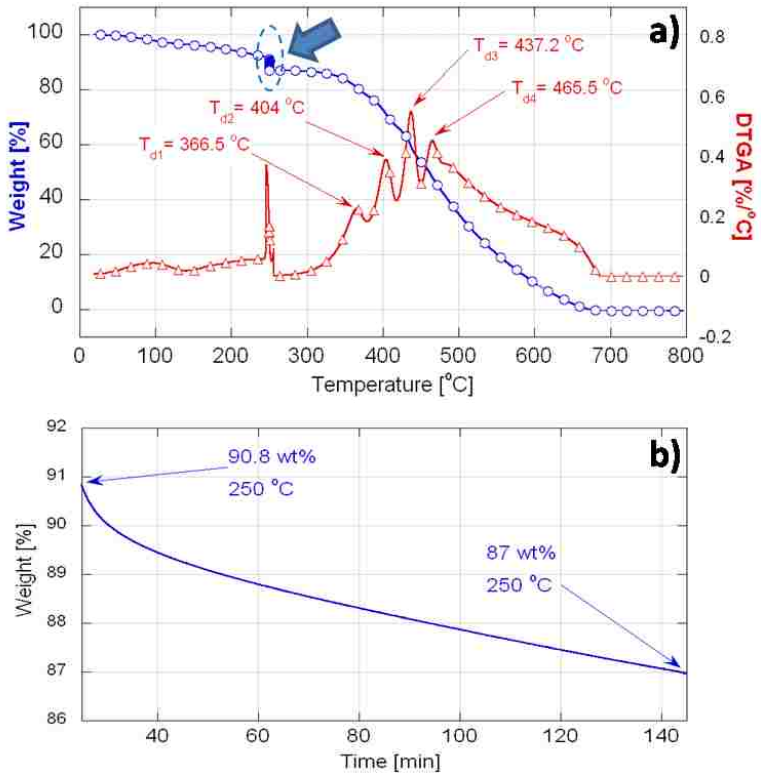

Figure 2.4 (a) Typical thermogravimetric results as a function of temperature obtained from an HCl-doped polyaniline sample: TG curve - blue, DTGA curve – red. The isothermal weigh loss indicated in (a) with the blue thick arrow is presented in (b) as a function of time. (*57*)

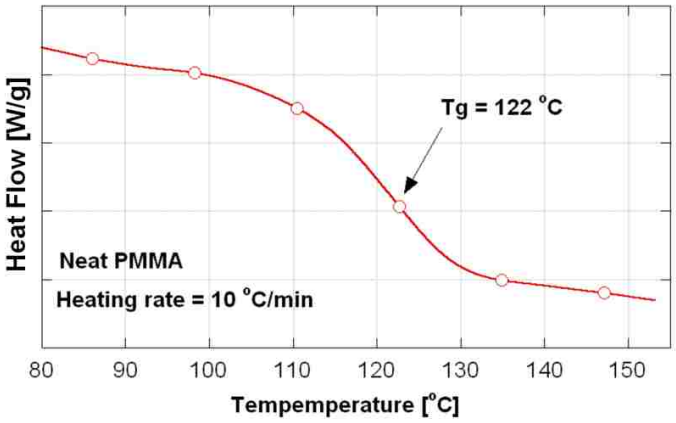

Figure 2.5 *Tg* of a PMMA sample as resulted from a DSC measurement performed with a heating rate of 10 °C/min. (*57*)

The temperature of crystallization is also commonly referred to as freezing temperature T_f. Since crystallization is a complex development that involves formation of crystallites and the expansion of crystalline areas, the freezing temperature is also an interval of temperatures, much like *Tm*. Just like with the determination of T_g, a very common way to determine the relative crystallinity of polymers is to perform DSC measurements, as the one presented in Figure 2.6. The enthalpy variation ΔH resulted from the DSC measurements is directly proportional to the amount of crystalline polymer in the sample. When various samples are considered the ΔH values are typically used to compare their crystallinity with respect to each other. For comparison purposes, the lowest point in the DSC dip is generally regarded as the *Tm* of the sample.

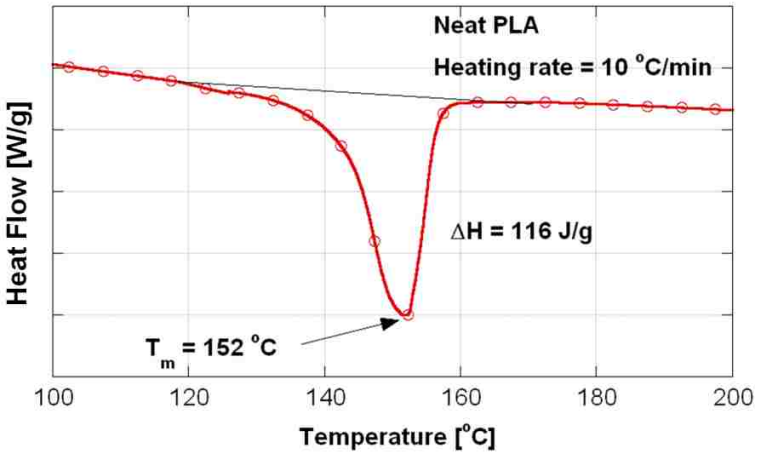

Figure 2.6 *Tm* and ΔH of a PLA sample as resulted from a DSC measurement performed with a heating rate of 10 °C/min. (*57*)

Finally, another important thermal characteristic of polymers is the decomposition temperature, T_d. Thermal decomposition of a chemical, also known as thermolysis, is an endothermic process in which the chemical is divided into at least two other new chemicals upon heating.(*98, 101*) Polymers will typically break up into more than just two chemicals because the macromolecular chains are long and they can be fragmented at any segmental bond in the chain. For this reason, while small molecules have a rather well defined T_d, in the case of polymers T_d is in fact a broad range of temperatures. For practical purposes, the T_d of a polymer is generally obtained

through thermogravimetric (TGA) measurements, like the one presented in Figure 2.4 in the chapter "Thermogravimetry". In this figure the broad range of decomposition temperatures of polyaniline is illustrating a large step loss in the weight vs temperature plot. To allow comparison of T_d for various polymers or polymer composites, researchers typically report the peak temperature of a DTGA curve as the T_d of a polymeric system. Many times it is possible for a polymer to undergo several concomitant decomposition processes, as is the case of the doped polyaniline presented in Figure 2.4.

2.7 Scanning Electron Microscopy (SEM)

Scanning Electron Microscopy (SEM) is a robust and very popular technique that offers researchers the possibility of obtaining greatly detailed three-dimensional-like images from a wide variety of heterogeneous organic and inorganic materials from the nanometer (nm) to the micrometer (μm) scale.(*108*) A tungsten filament is typically employed in SEM to provide a beam of electrons that is finely focused on the area or volume of the sample to be examined.(*109*) The electron beam may be either static or swept in a raster across the area of the sample to give information about a certain point or to generate an image, respectively. In high vacuum SEM the sample to be analyzed must be either conductive or must be coated with one or several of the metals from the category gold, palladium, iridium, etc.(*110*)

The interaction between the electron beam and the sample generates several types of signals, including secondary electrons, backscattered electrons, characteristic X-rays and photons of various natures.(*108-109*) Depending on the signal analyzed, a large spectrum of information may be obtained about the surface topography, crystallography and the composition of the sample. Secondary electrons are generated as ionization products as a result of the sample irradiation with the primary electron beam. The energy of the primary electrons dictates the amount of secondary electrons produced, where higher energies (up to a certain limit) result in larger amounts of secondary electrons. Through the use of secondary electrons SEM is able to reveal sample details of

less than 1 – 5 nm and to provide a wide range of magnifications from cca 10 times to about 500,000 times.

On the other hand, backscattered electrons are the electrons reflected from the sample through elastic scattering, and are typically used in analytical SEM together with the characteristic X-rays. Backscattered electrons are characterized by higher energies than secondary electrons, for which reason they typically cannot be collected by a secondary electron detector. Images obtained with backscattered electrons generally provide useful information about the distribution of different elements in heterogeneous samples, since the intensity of the backscattered electrons signal is strongly related to the atomic number of the specimen. In order to assure a good contrast of images obtained using backscattered electrons, the elements from a sample subjected to analysis should have a difference in the atomic number of at least three.

Finally, characteristic X-rays are generated as a result of the electron beam removing an inner shell electron from the sample, which causes a higher energy electron to fill the shell and release energy.(*108*) The characteristic X-rays are used to identify the composition and measure the abundance of elements in the sample by equipping the SEM instrument with either *energy-dispersive X-ray spectroscopy* or *wavelength dispersive X-ray spectroscopy* components.

The size of the electron spot in SEM, which is affected by the wavelength of the electrons and the electron-optical system that produces the scanning beam, determines the final resolution of the resultant images. Other factors affecting the resolution may include the size of the interaction volume and the extent to which the material interacts with the electron beam. The SEM cannot reach resolutions to allow imaging of individual atoms because the spot size and the interaction volume are both large compared to the distances between atoms. SEM can analyze bulk samples, not only thin films or foils. Furthermore, when compared to the optical microscope the typical scanning electron microscope has a magnification limit about 250 times higher than the one of the best light

microscope. Besides a much better resolution and the possibility to achieve higher magnifications, another great advantage of the SEM over classical optical microscopy is the much improved depth of focus. The difference in the depth of focus obtained with the two techniques is evidenced in Figure 2.7.

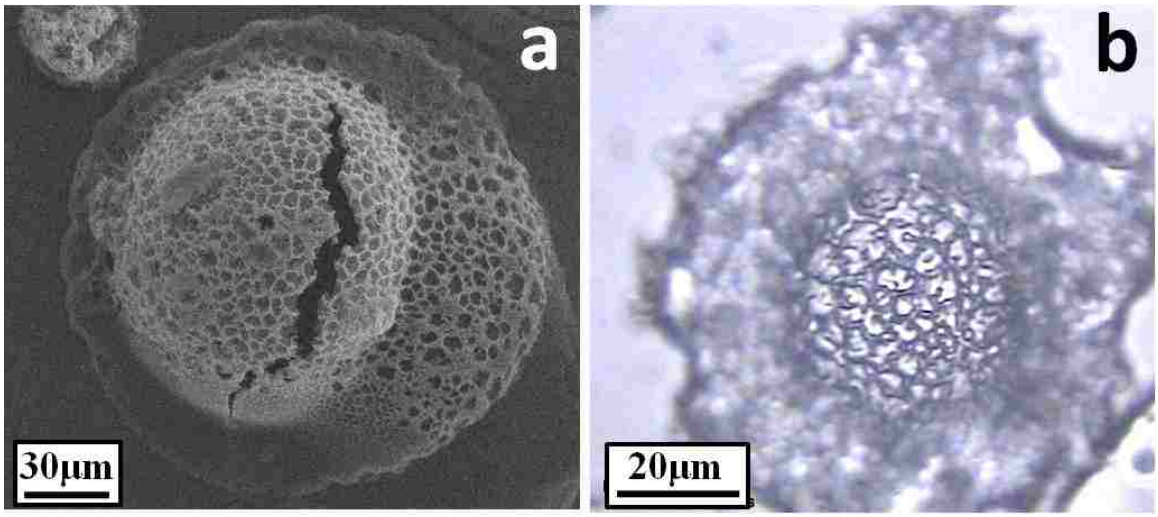

Figure 2.7 An SEM image (a) showing a damaged spray-dried ethylcellulose microcapsule is compared to an optical microscopy image (b) from a similar system. The difference in the depth of focus achieved with the two techniques is apparent. While in (a) both the elevated top of the capsule and the bottom film surrounding capsule are clearly visible, in (b) only the elevated top is distinguishable, but the bottom film appears completely fuzzy. (*111*)

2.8 X-Ray Diffraction (XRD)

X-ray diffraction is a powerful non-destructive technique capable of providing information on the averaged volume characteristics of a crystalline sample.(*112-113*) It is used predominantly in crystallography and it involves projecting an X-ray beam against a crystalline structure and analyzing the pattern produced by the diffraction of rays through the closely spaced grate of atoms. In Figure 2.8 is presented the schematic of a typical 4-circle X-ray diffractometer. The diffractometer consists of three basic elements, an X-ray tube, a sample holder, and an X-ray detector. The X-radiation is produced in the X-ray tube through the emission of electrons from a tungsten cathode. Following emission, electrons are accelerated in vacuum and forced to collide with

the metal anode, also called target. The detector records and processes this X-ray signal and converts the signal to a count rate which is afterwards output to a computer monitor. One type of resultant X-radiation is known as the "white or continuous radiation", and is characterized by a broad, continuous spectrum of wavelengths. On the other hand, the "characteristic radiation" is a set of X-rays described by very sharp peaks of discrete wavelengths that are characteristic to the analyzed crystal.(*114*)

Because X-rays belong to the electromagnetic spectrum, they exhibit the characteristics of both waves and particles.(*112*) This means that when X-ray beam strikes an atom the beam's energy will be partly diffracted and partly adsorbed. Although the X-rays were discovered in 1895 by the German physicist W. Roentgen, it was the English physicists Sir W.H. Bragg and his son Sir W.L. Bragg, in 1913, who explained why the X-ray beams were reflected at angles of certain degrees of incidence by the faces of the crystals, when irradiated.(*113*) The explanation provided by the two Bragg physicists resulted in a law, widely accepted today as the Bragg's law of diffraction, which states that when the X-rays strike an atom they force the electronic cloud to travel and re-radiate waves with essentially the same frequency.(*113*) The equation describing Bragg's law is the following:

$$n\lambda = 2d\,sin\theta \qquad (2.8.1)$$

In equation (2.8.1) λ is the wavelength of the incident X-ray beam, θ is the angle of incidence, n represents an integer, and d is the distance between atomic layers in the analyzed crystal. When several waves superimpose as a result of diffraction, a new wave is created, which depends on the frequency, amplitude and relative phase of the initial waves.(*113*) The interference of waves can be constructive, when the two rays are in phase, or destructive when the two waves are out of phase.

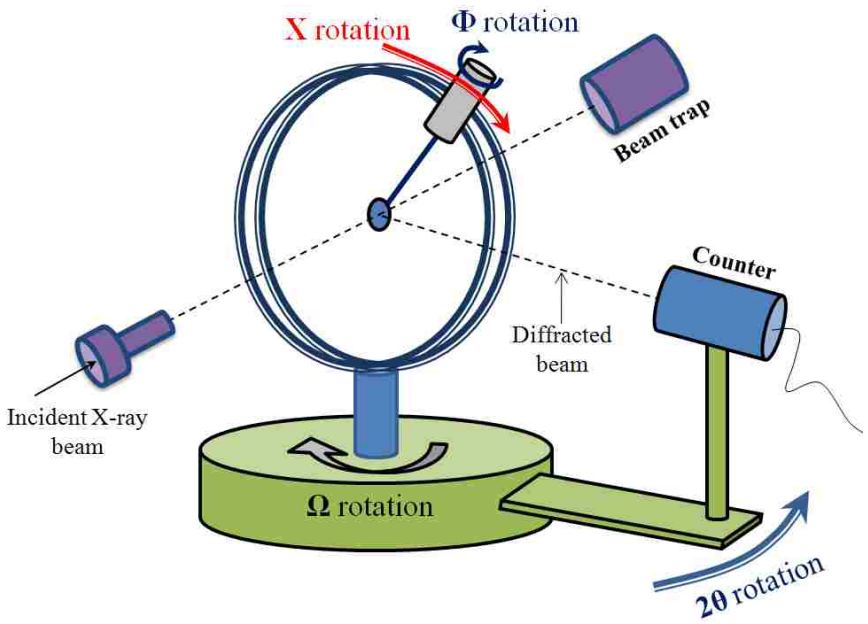

Figure 2.8 Schematic of 4-circle diffractometer also indicating the angles between the incident ray, the detector and the sample. Adapted from reference. (*115*)

CHAPTER 3 . HOMOGENEOUS MODIFICATION OF CHITOSAN IN 1-BUTYL-3-METHYLIMIDAZOLIUM ACETATE

3.1 Objective of Study

Chitosan is a very rigid polymer due to the intra and intermolecular hydrogen bonding present in its structure (Scheme 3.1) and its solubility is decreased in most of the organic solvents. By modifying the chitosan with different reagents, new desired chemical and physical properties can be induced which will enlarge the field of the potential applications. However, difficulties for the modification of chitosan are generally encountered owing to the lack of solubility and the reactions under heterogeneous conditions.

Recently a rather new class of organic solvents, ionic liquids, has been found particularly useful in dissolution of polar organic materials, even polymers, which are otherwise difficult to dissolve.(*58*) Ionic liquids are able to dissolve rigid chain cellulose(*69-70, 116-117*) and chitosan(*73*) under suitable conditions by disrupting the hydrogen bonds.

The removal of one to two hydrogens from the amino group of the chitosan structure and the replacement with hydrophobic groups has as a result the destruction of chitosan inherent crystalline structure and the improvement of solubility in general organic solvents. By modifying the chitosan with different reagents, new desired properties can be induced which will enlarge the field of the potential applications. Several studies have tried to accomplish regioselective and quantitative chemical modifications of chitosan using as a solvent dimethylformamide (DMF)(*118-119*), DMF containing 5% (v/v) water(*120*), DMF/ethanol(*121*), or acetic acid.(*122-123*) Chemical modification of the N-amino functional groups of chitosan using phthalic anhydride results in the formation of N-phthaloylated chitosan which is a particularly important and indispensible organosoluble precursor. Phthaloylation is ideal for protection as well for improving solubility.(*119*) However, partial O-substitution also takes place in addition to the N-phthaloylation creating an obstacle to regioselective

and quantitative substitution. In their work, Kurita et al.(*120*) reported both N,O-phthaloylation when using DMF as a solvent but the addition of hydroxyl-bearing cosolvents to the system leads to selective N- phthaloylation.

Nishimura et al.(*119*) and Kurita et al.(*121*) have used trityl chloride for the regioselective ether protection of primary hydroxyl groups of the N-phthaloyl chitosan. The resulting product has superiority in solubility in organic solvents to the starting N-phthaloyl chitosan. The most important characteristic of trityl chloride and phthalic anhydride (protecting groups) is that they can easily be removed so that further modifications could be realized in order to obtain new types of bioactive polysaccharides. The dephthaloylation is efficiently carried out by treatment with hydrazine monohydrate at 80^{o}C and the detritylation is easily done in the presence of dichloroacetic acid.

1-Allyl-3-methylimidazolium bromide, 1-ethyl-3-methylimidazolium thiocyanate, 1-ethyl-3-methylimidazolium aluminum tetrachloride, 1-ethyl-3methylimidazolium methanesulfonate, 1-butyl-3-mehtylimidazolium chloride (BMIMCl) and 1-butyl-3-methylimidazolium acetate (BMIMAc) ionic liquids have been tested for the dissolution of chitosan. Only BMIMCl and BMIMAc proved to be good solvents for its dissolution. While BMIMAc is able to form a homogeneous solution with concentrations of chitosan up to 10 wt%, BMIMCl is capable to dissolve chitosan only for concentrations up to 2-3 wt%.

Due to the scarcity of reports on functionalization of chitosan in homogeneous media, the aim of the present chapter is to investigate the reaction of chitosan in homogeneous 1-butyl-3-methylimidazolium acetate (BMIMAc) ionic liquid solutions (Figure 3.1). 1-Butyl-3-methylimidazolium acetate, an organic salt with a melting point below 100^{o}C, was found to completely dissolve chitosan under suitable conditions by disrupting the hydrogen bonds (Scheme 3.1). Homogeneous conditions for the chemical change of the polymer are needed in order to obtain a high extent of reaction and regioselective substitution.

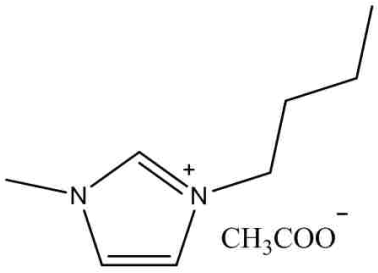

Figure 3.1 Chemical structure of 1-butyl-3-methylimidazolium acetate (BMIMAc).

Scheme 3.1 Dissolution of crystalline chitosan in BMIMAc ionic liquid.

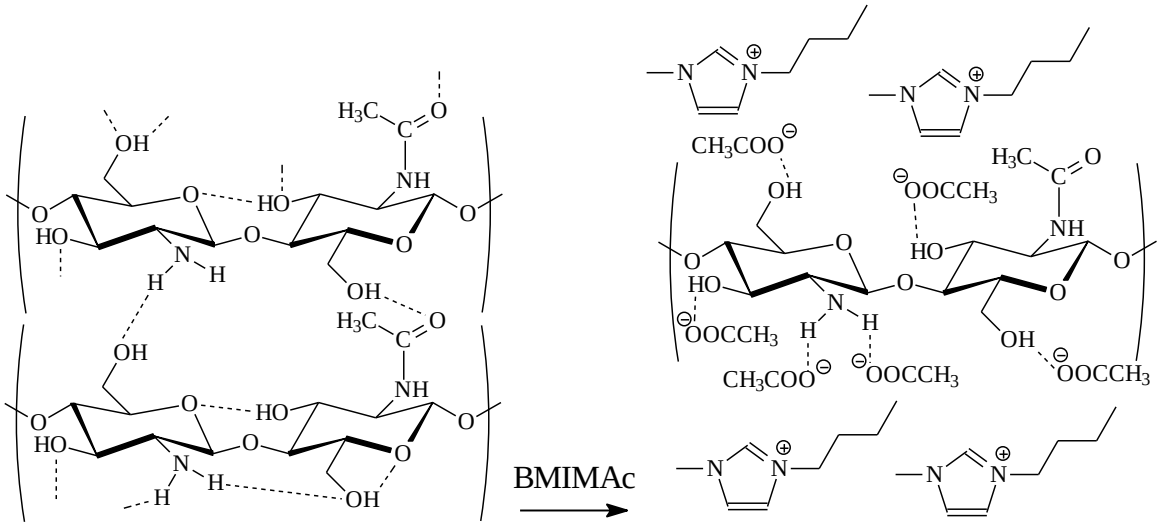

Chitosan

3.2 Overall Synthesis Performed in the Present Project

Chemical modification of chitosan in the presence of 1-butyl-3-methylimidazolium acetate as solvent was performed using phthalic anhydride and benzoyl chloride (Scheme 3.2). Chitosan with a Brookfield viscosity of 200K cps was dried and used for the dissolution in BMIMAc without further purification. The reaction of chitosan with benzoyl chloride was carried out at elevated temperatures in the presence of a base to capture the hydrogen chloride released during the reaction. The reaction of chitosan with the commercial phthalic anhydride was performed in the presence as well as in the absence of a base at elevated temperatures or in the presence of a catalyst. For all the reactions various molar ratios of the reagents and different temperatures were used. The homogeneous

conditions used for the chemical modification of chitosan should lead to a random distribution of the substituents along the polymeric chain.

Scheme 3.2 Reaction of chitosan with phthalic anhydride or benzoyl chloride.

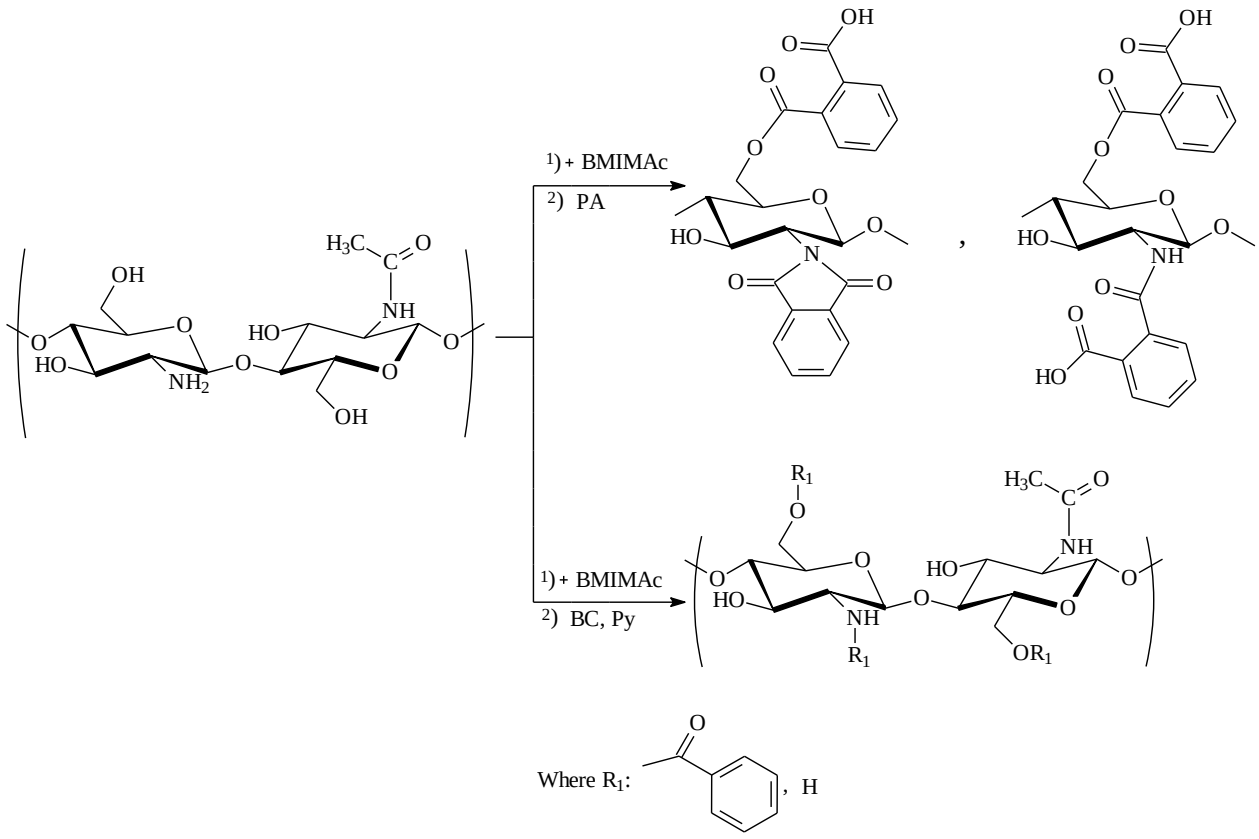

3.3 Dissolution of Chitosan in BMIMAc

The dissolution of chitosan in the ionic liquid solvent was achieved by adding the dried polymer (0.06g) and the BMIMAc (2.45g) to a vial under argon followed by magnetic stirring and heating it to 85-95^{o}C. A homogeneous, transparent, and viscous chitosan solution was obtained after the complete dissolution (Figure 3.2). The dissolution time varied with the percentage of polymer added to the ionic liquid. For a 2 wt% solution of chitosan, the dissolution time was approximatively 12h (as observed by naked eye) while for concentrations up to 6 wt%, 2-3 days are required to achieve a clear solution.

BMIMAc and chitosan before heating to 85-95^{0}C

BMIMAc and chitosan after heating to 85-95^{0}C (a homogeneous transparent solution)

Figure 3.2 Slurry of chitosan in BMIMAc before dissolution (left); polymeric solutions containing chitosan dissolved in BMIMAc (right).

3.4 Experimental

3.4.1 Materials

All chemicals were used as received, without any further purification. The ionic liquid solvent, 1-butyl-3-methylimidazolium acetate (BMIMAc), the catalyst, *N*-Bromosuccinimide (NBS), benzoyl chloride (BC), 1,4-diazobicyclo[2.2.2] octane (DABCO), pyridine, and chitosan (K) with a Brookfield viscosity of 200K cps, were purchased from Sigma Aldrich Chemical Company. The chitosan was dried over night at 90^{o}C and used without any further purification. Dimethyl sulfoxide, DMSO, was obtained from Fisher Scientific. Phthalic anhydride, PA, was acquired from Mallinckrodt.

3.4.2 Instrumentation

The ^{1}H NMR spectra were recorded with a Bruker AV-400 spectrometer operating at 400 MHz. For each spectrum thirthy two scans were accumulated at room temperature. The ^{13}C NMR spectra were recorded on a VNMRS-700 spectrometer with an acquisition time of 0.21 sec and a relaxation delay of 2 sec. 256 scans were accumulated for each spectra.

FT-IR spectra were recorded on a ThermoNicolet 300 Fourier Transform Infrared spectrometer using a KBr disc containing 1% of very fine ground samples. Thirty two scans were taken for each sample in the range of 4000-400 cm^{-1} at a resolution of 4 cm^{-1} in the transmission mode.

DSC measurements were performed using a TA 2920 MDSC instrument. Samples of 2-5 mg were subjected to analysis using a heating rate of 10^{o}C/min. Fresh and dried samples were used for a first heating run to 150^{o}C followed by cooling to 25^{o}C and a second heating run to 150^{o}C. The samples were placed in a covered aluminum sample holder while an empty pan was used as a reference. Dynamic thermogravimetric analysis was run in a nitrogen atmosphere using a TA thermobalance (Model 2950). The experiments were conducted at a heating rate of 10^{o}C/min until 600^{o}C. The thermogravimetric analysis was performed with 7-16 mg samples under nitrogen atmosphere. The integration and processing of the curves resulted from the DSC and TGA instruments were done by using TA Universal analysis software.

3.4.3 Syntheses

3.4.3.1 Representative Procedure for the Chemical Modification of Chitosan with Benzoyl Chloride (BC)

The reaction of the dissolved chitosan in BMIMAc with BC was realized by adding first 1.176 mL pyridine in a molar ratio of 5:1 (pyridine: AGU of chitosan) to a flask containing the amber homogeneous solution of the dissolved chitosan (0.47g). Upon the addition of pyridine the mixture became less viscous. Next, 1.695 mL BC was added in small amounts. After every addition of BC the flask was vigorously agitated. The addition of pyridine and BC was realized under argon atmosphere. Two hours were allowed for the reaction to proceed at 85-90^{o}C under magnetic stirring. After cooling the solution to room temperature, the polymer was precipitated, filtered and than washed with 800 mL mixture of CH_3OH and H_2O. The benzoylated chitosan collected was dried at

45°C for 24 hours followed by a further drying under vacuum at 50°C for 2 hours. The weight of the dry product was 0.619 g with a computed % yield of 80% if the theoretical yield is calculated for a degree of substitution of 1.

3.4.3.2 Representative Procedure for the Chemical Modification of Chitosan with Phthalic Anhydride (PA)

The dried chitosan (0.315g) and the BMIMAc (14.251g) were added to a round bottom flask under argon. The flask was heated to 100°C and the mixture was agitated using magnetic stirring. The dissolution time for the resultant 2.2 wt% amber solution of chitosan was approximatively 6 hours (observed by naked eye). To ensure a complete dissolution of chitosan, 30 more minutes were allowed for the reaction mixture to proceed at 100°C. The reaction with PA was performed in the absence of any base. The fine powder of PA (0.869g) was added in a molar ratio of 3:1 (PA: AGU of chitosan) to a round bottom flask containing the chitosan solution. The reaction mixture was heated in oil bath at 100°C for 2 hours and 4 hours, respectively. After cooling the solution to room temperature, the polymer was precipitated in methanol, filtered and then washed with 800 mL mixture of CH_3OH and H_2O. The phthalated chitosan collected was dried at 45°C for 24 hours followed by a further drying under vacuum at 50°C for 2 hours. The weight of the dry product was 0.445 g with a computed % yield of 78% if the theoretical yield is calculated for a degree of substitution of 1.

3.4.3.3 Representative Procedure for the Chemical Modification of Chitosan with Phthalic Anhydride (PA) in the Presence of Pyridine or 1,4-Diazobicyclo[2.2.2] Octane (DABCO) as Base

The reaction of chitosan (0.038g) with PA (0.174g) was performed by adding PA and a base (0.079g) (pyridine or DABCO) at room temperature to the chitosan solution in BMIMAc. The reaction was allowed to proceed at 100°C for 4 hours. After cooling the solution to room temperature, the polymer was precipitated in methanol, filtered and then washed with 800 mL

mixture of CH_3OH and H_2O. The phthalated chitosan collected was dried at 45^oC for 24 hours followed by a further drying under vacuum at 50^oC for 2 hours. The weight of the dry product was 0.045 g with a computed % yield of 65% if the theoretical yield is calculated for a degree of substitution of 1.

3.4.3.4 Representative Procedure for the Chemical Modification of Chitosan with Phthalic Anhydride (PA) in the Presence of N-Bromosuccinimide (NBS) as Catalyst

The reaction of chitosan with PA in BMIMAc in the presence of a catalyst proceeded homogeneously. It was performed as follow: PA (0.165g) and NBS (0.198g) were first dissolved in DMSO (2mL) before addition of the solution at room temperature to the chitosan solution. The DMSO was also used to reduce the viscosity of the solution. The reaction was allowed to proceed at 100°C for 4 hours under magnetic stirring. After cooling the solution to room temperature, the polymer was precipitated in methanol (200mL), filtered and then washed thoroughly with methanol (400mL). The phthalated chitosan collected was dried first at 45°C for 24 hours and then under vacuum at 50°C for 2 hours for a complete removal of methanol. The weight of the dry product was 0.098 g with a computed % yield of 91% if the theoretical yield is calculated for a degree of substitution of 1. While the molar ratio of PA to anhydroglucose unit of chitosan was kept constant to 3:1, 5:1, or 7:1 the molar ratios of NBS to the anhydroglucose unit of chitosan was 3:1, 7:1, and 10:1, respectively.

3.5 Results/Discussion

3.5.1 Chitosan Characterization

FT-IR Analysis of Chitosan

FT-IR spectroscopy is a powerful tool used to identify chemicals that are either organic or inorganic in the form of solids, liquids, and gases. FT-IR gives information about the functional groups in a molecule by identifying the frequencies of the molecular bonds vibrations. There are

several specific frequencies for any given bond at which it can vibrate so that species can be determined. For a molecule to vibrate it needs to be excited by having it absorb light energy. For this research, formation of the carbonyl groups from esters, amides, and imides was determined by FT-IR. The presence of aromatic rings in the products was also established.

The degree of acetylation of chitosan (15%) was determined by using the method of Miya, Iwamoto, Yashikawa, and Mima.(*124*) The following formula was used for the calculation of the % of acetyl content:

$$(A_{1658}cm^{-1}/A_{3435}cm^{-1})*100/1.33 \qquad (3.6.1)$$

where the $A_{3435}cm^{-1}$ of the –OH band was used as a reference. The areas were calculated by drawing a baseline for the absorbances.

Figure 3.3 shows the FT-IR spectra of commercial chitosan. A characteristic absorption band between 1650-1590 cm^{-1} represents the free amino group positioned at C_2 of the anhydroglucose units of chitosan. The peaks at 1658 cm^{-1} and 1596 cm^{-1} correspond to amide I and amide II indicating that the chitosan used in this research is not fully deacetylated. The absorption band at 1658 cm^{-1} represents the C=O stretch while the 1596 cm^{-1} peak is indicative of N-H bending for secondary amides (this band overlaps with the N-H bend in primary amines). Usually, the absorption band for carbonyl groups takes place at frequencies around 1700 cm^{-1}. Though, the absorption was shifted to a lower frequency due to the conjugation with the amine group. This conjugation results in an increased single bond character between the carbon and the oxygen and thus lowering the frequency of the C=O. Another characteristic is the broad O-H stretching absorption band between 3200 cm^{-1} and 3600 cm^{-1} which overlaps with the N-H stretch of amides and primary amines. The aliphatic C-H stretch takes place at 2878 cm^{-1} while the C-O-C bridge symmetric stretching occurs at 1075 cm^{-1}.

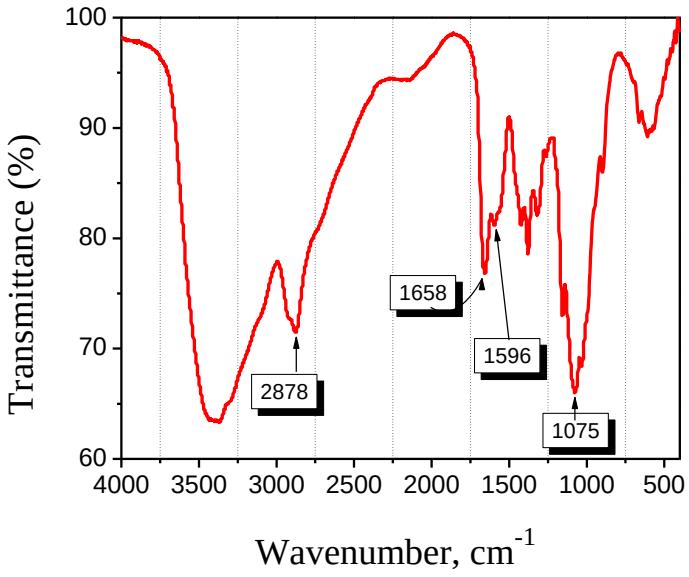

Figure 3.3 FT-IR spectra of commercial chitosan.

^{1}H NMR Characterization of Chitosan

The ^{1}H NMR of chitosan was first determined by Domard and coworkers.(*125*) The authors also established the ^{1}H-^{1}H and ^{13}C-^{1}H correlations which allowed them the determination of the degree of deacetylation of chitosan. Using the same technique, Rinaudo and coworkers were able to assign the chemical shifts of ^{1}H and ^{13}C NMR signals for chitosan.(*126*)

The ^{1}H NMR spectrum of chitosan is presented in Figure 3.4 D_2O/d_4-CD_3COOD was used as internal standard for assigning the chemical shifts of the protons. In the ^{1}H NMR spectrum the chemical shift at 4.69 ppm corresponds to the internal standard. The N-acetyl peak appears at 1.9 ppm, while the acetal proton of the glucosamine and the –C<u>H</u>-NH_2 proton appear at 4.4 ppm and 3.01 ppm respectively. The remaining hydrogens –C<u>H</u>-OH, -C<u>H_2</u>-OH, -C<u>H</u>-CH_2-OH, and HO-CH-C<u>H</u>-CH-CH_2 appear as clustered signal between 3.4 ppm and 4.1 ppm. The calculation of residual N-acetyl groups is achieved by dividing the integral of the N-acetyl signal at 1.906 ppm by 3 (3 hydrogens per N-acetyl group), and the result of this calculation is divided by the integral of glucosamine protons and multiplied by the number of glucosamine protons (Equation 3.6.1).(*127*)

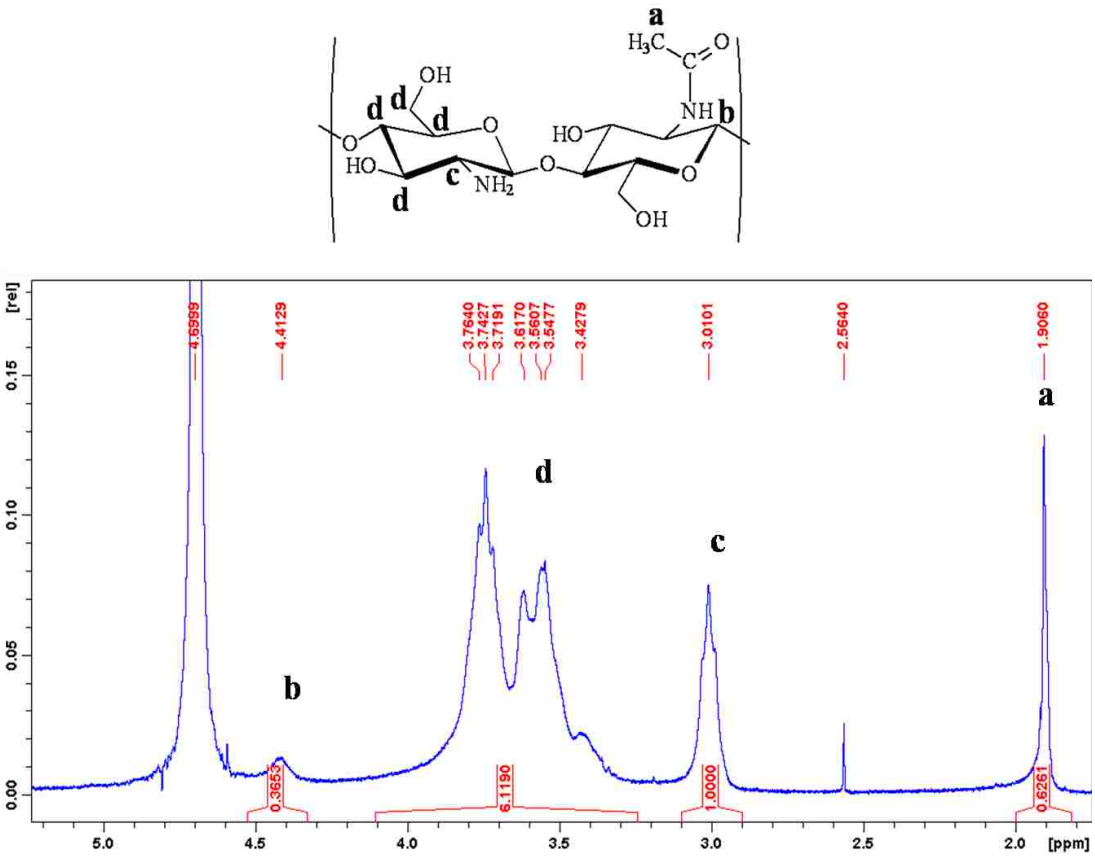

Figure 3.4 ^{1}H NMR of commercial chitosan (82% DDA) in D_2O/d_4-CD_3COOD.

Equation 3.6.1:

$$\% \text{ N-acetyl} = (I_{1.906}/3)(5/I_{\text{glucosamine protons}})*100$$

$$\% \text{ Deacetylation} = 100 - \% \text{ N-acetyl}$$

The degree of deacetylation (DDA) of commercial chitosan was computed as 82% by ^{1}H NMR.

3.5.2 Benzoylation of Chitosan in BMIMAc Ionic Liquid

The reaction of chitosan with BC using BMIMAc ionic liquid as solvent is accompanied by *N*-benzoylation and O-benzoylation. The nucleophilic *N*-amino groups of chitosan undergo addition at the carbonyl groups of the BC, followed by the elimination of the chloride ion leaving group. The mechanistic route towards the formation of the end product via this reaction is presented in Scheme 3.3.

Scheme 3.3 Mechanistic route towards the synthesis of benzoylated chitosan.

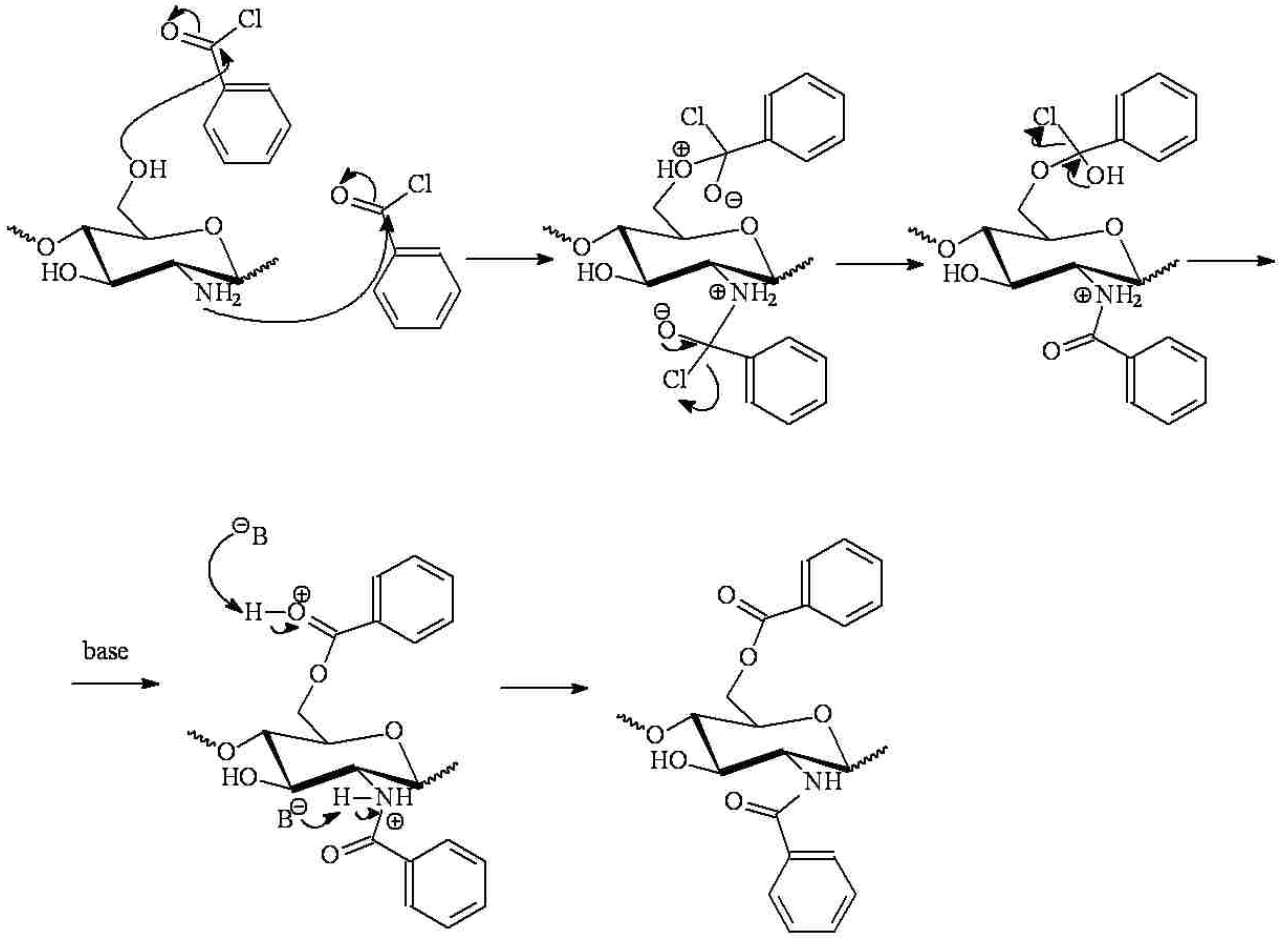

3.5.2.1 FT-IR Characterization of Benzoylated Chitosan in BMIMAc Ionic Liquid

In the FT-IR spectra of chitosan reacted with BC, the appearance of new peaks at 3091, 1745, 1661, 1556, 1376, and 1240 cm^{-1} are indicative of the presence of substituted AGU (Figure 3.5). The absorption peak at 3091 cm^{-1} is attributed to the sp^2 C-H stretch in the aromatic ring. The C-O stretch absorption in esters is evidenced by two strong peaks at 1376 and 1240 cm^{-1} while the strong peak at 1745 cm^{-1} corresponds to C=O stretch vibration in esters. The absorption bands at 1661 cm^{-1} and 1556 cm^{-1} are indicative of carbonyl stretch and N-H bending in amides, respectively. The presence of these new peaks shows that benzoyl chloride indeed reacted with both the -OH and -NH_2 groups of the AGU of chitosan as shown in Scheme 3.3.

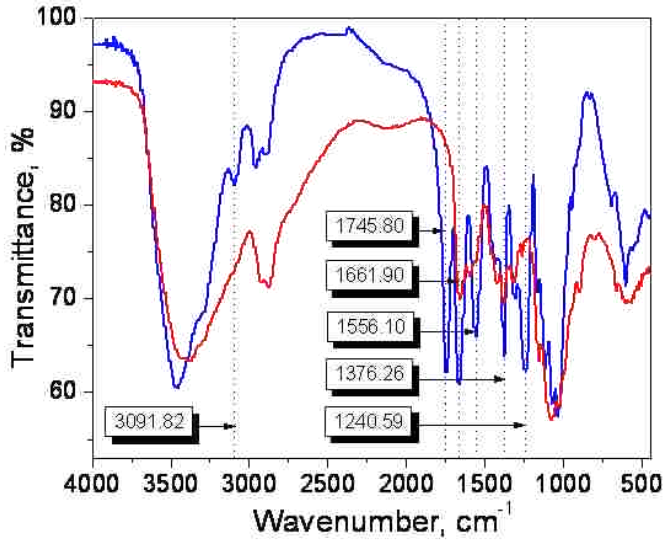

Figure 3.5 FT-IR spectra of chitosan (red line) and chitosan reacted with benzoyl chloride (blue line) using BMIMAc as solvent.

3.5.2.2 Solid State ^{13}C NMR Characterization of Benzoylated Chitosan in BMIMAc Ionic Liquid

The reaction of chitosan with BC was also studied by solid state ^{13}C NMR spectroscopy, and the spectra of benzoylated chitosan and unmodified chitosan are presented in Figure 3.7 and Figure 3.6, respectively. According to solid state ^{13}C NMR, the reaction of chitosan with BC in BMIMAc did not take place to a significant extent. The new signal at 173.6 ppm and the chemical shifts between 14.8 ppm and 23.9 ppm are attributed to traces of BMIMAc solvent still present in the final product.

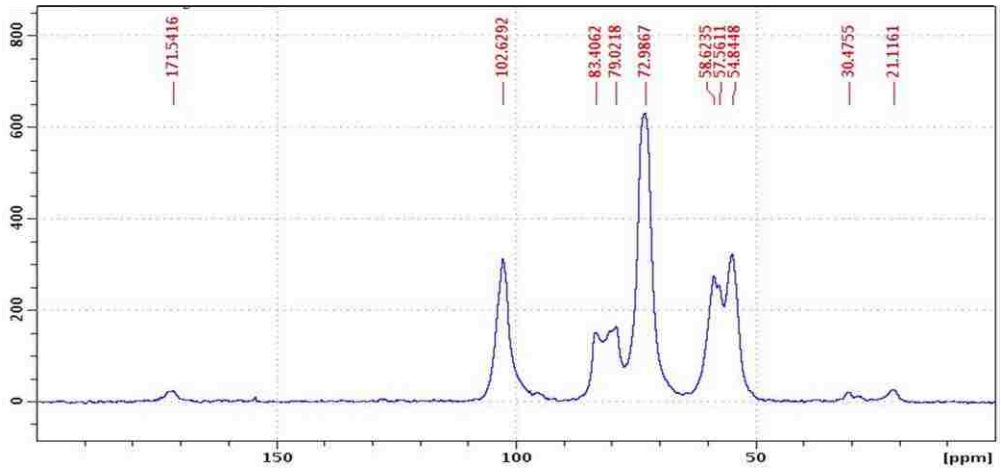

Figure 3.6 Solid-state ^{13}C NMR spectrum of chitosan powder.

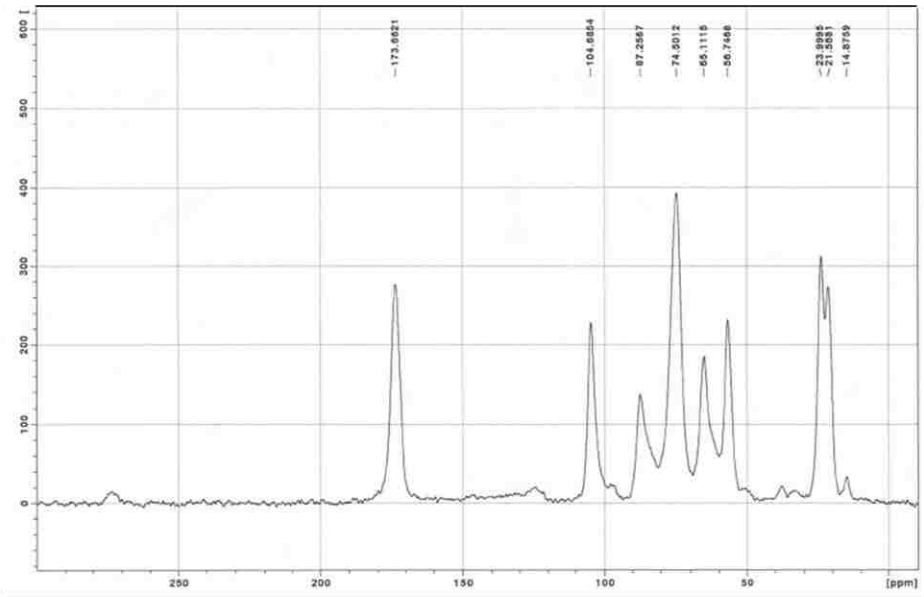

Figure 3.7 Solid-state ^{13}C NMR spectrum of chitosan reacted with benzoyl chloride.

3.5.3 Phthaloylation of Chitosan in BMIMAc Ionic Liquid

N-phthaloylation of chitosan with PA is an efficient way for the protection of the amine groups of the polymer as well as for improving solubility. The first step in this type of reaction is the attack of the nucleophilic *N*-amino groups of chitosan at the carbonyl carbons of the PA. The intermediates formed are called tetrahedral intermediates because the carbonyl carbons have been changed to a tetrahedral geometry and sp^3 hybridization. The rate determining step of the *N*-phthaloylation of chitosan is the expulsion of the carboxylate (-O-COR) leaving group from the thetrahedral intermediate.(*128*) The reaction of chitosan with PA is also accompanied by partial O-phthaloylation. The mechanistic route towards the formation of the end product via this reaction is summarized in Scheme 3.4.

3.5.3.1 FT-IR Analysis of Phthalated Chitosan

FT-IR Spectra confirms that the reaction of chitosan (dissolved in BMIMAc) with PA resulted in product containing carboxylic, ester, amide, and imide groups.

In the FT-IR spectra of chitosan reacted with PA the presence of the new peaks at 1774, 1716, 1652, 1564, and 1378 cm^{-1} (Figure 3.8) indicates that the reaction proceeded as described above (Scheme 3.4). The band at 1716 cm^{-1} is evidence for the presence of carbonyl ester groups in anhydroglucose repeating units (AGU) of substituted chitosan. Usually the stretch of the carbonyl bonds occurs in the range 1750-1735 cm^{-1} for normal esters, but the absorption was shifted to a lower frequency due to the conjugation of the carbonyl group with the aromatic ring attached to it. The absorption at 1652 cm^{-1} is attributed to an overlapping of carbonyl groups from carboxylic acid and the amide functions. The stretch of C=O in carboxylic acids appears at 1730-1700 cm^{-1}. However, due to the conjugation present in the system and intermolecular hydrogen bonding the carbonyl peak appears to a much lower frequency. The C=O stretch is present in spectra of amides at approximately 1680-1630 cm^{-1}. In spectra of phthalated chitosan it is overlapped with the carboxyl absorption and consequently one peak can be seen at 1652 cm^{-1}. The C-O stretch absorption in esters is evidentiated by the peak at 1378 cm^{-1}. The band at 1564 cm^{-1} is indicative of N-H bending for secondary amides. The absorption at 1774 cm^{-1} corresponds to the imide carbonyl. The imide group is a result of the cyclization shown in Scheme 3.4. None of the aromatic anhydride carbonyl bond absorptions (around 1850 cm^{-1} and 1790 cm^{-1}) were observed in spectra of the reaction products purified by washing with methanol, confirming thus that the products were free of unreacted phthalic anhydride. From the graph (Figure 3.8) it can be seen that the intensity peaks of the phthalated chitosan reacted for 2 hours are lower than the peaks of the phthalated chitosan reacted for 4 hours indicating that the increase of the reaction time favors the degree of substitution. The intensity of the newly formed peaks in the phthalated chitosan was compared in the absorption mode (after baseline correction) of the FT-IR spectra relative to the intensity of the C-O-C stretch of the acetal peak in the polymer backbone (1076 cm^{-1}).

Scheme 3.4 Mechanistic route towards the synthesis of phthalated chitosan.

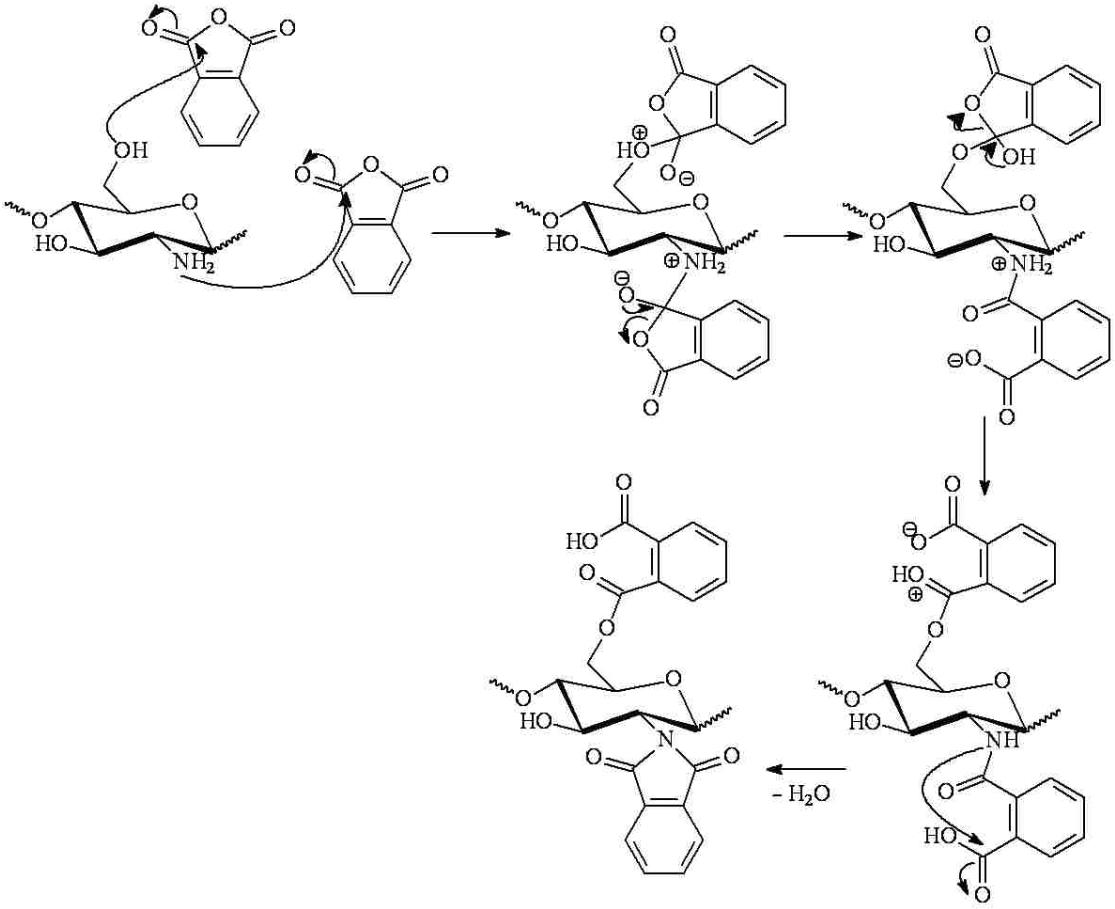

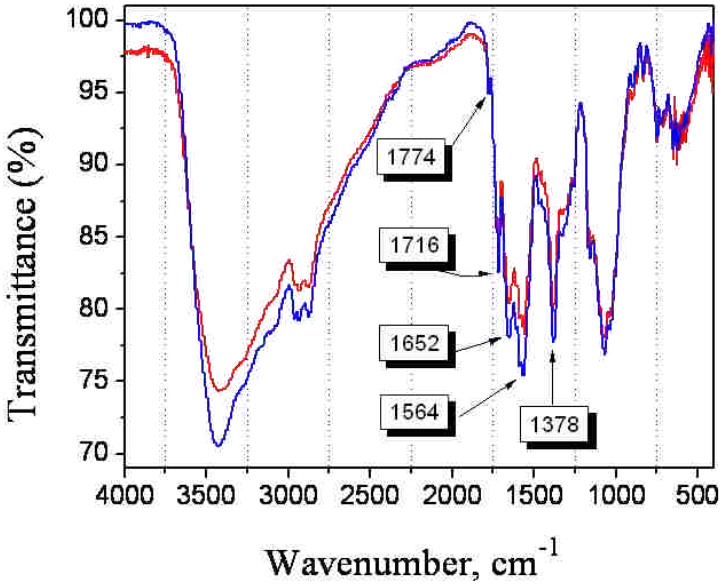

Figure 3.8 FT-IR spectra of chitosan reacted with phthalic anhydride for 2 hours (red line) and phthalated chitosan for 4 hours (blue line).

3.5.3.2 FT-IR Analysis of Pthalated Chitosan Performed in the Presence of Pyridine or 1,4-Diazobicyclo[2.2.2] Octane (DABCO) as Base

The new peaks in the FT-IR spectra of the phthalated chitosan in the presence of a base, (BMIMAc used as solvent) indicate that the reaction proceeded as described in Scheme 3.4. The absorption band at 723 cm^{-1} is a characteristic for ortho-disubstituted aromatic rings, suggesting that the PA reacted with the chitosan (Figure 3.9). The characteristic absorptions due to phthalimido groups at 1778 cm^{-1} and 1716 cm^{-1} were observed in the IR spectrum indicating the amino groups of chitosan has been reacted. The imide group is a result of the cyclization as shown in Scheme 3.4. The absorption band at 1654 cm^{-1} is attributed to the carbonyl stretch in carboxylic acids and carbonyl stretch in amides. Typically the carbonyl stretch for carboxylic acids takes place at a higher frequency but the conjugation of the carbonyl group with the aromatic ring attached to it and the presence of intermolecular hydrogen bonding shifts the band to a lower frequency, 1654 cm^{-1}. The N-H bending for amide can be identified at 1561 cm^{-1}. The presence of all these peaks confirms that both -OH and $-NH_2$ of the chitosan anhydroglucose unit reacted with PA.

When the films used for the FT-IR were heated to 200^{o}C for 2 hours and spectra were again recorded, an increase in the intensity peaks corresponding to imide and ortho-disubstituted aromatic rings and a decrease in the intensity peaks for carbonyl stretch and N-H bending for amides is observed (Figure 3.10, Table 3.4 and Table 3.5). This behavior is a result of cyclization with the formation of imide groups (Scheme 3.4).

When the reactions of chitosan with PA in the presence of pyridine or DABCO (Figure 3.11) using BMIMAc as a solvent are compared, it can be observed that in the presence of DABCO the absorption intensities are greater than those observed using pyridine (Table 3.1 and Table 3.2).

The highest absorption intensities for the reaction of chitosan with PA in the presence of pyridine was obtained when the temperature of the reaction was 100°C. Temperatures of 80°C or 120°C resulted in lower absorption intensities (Table 3.3).

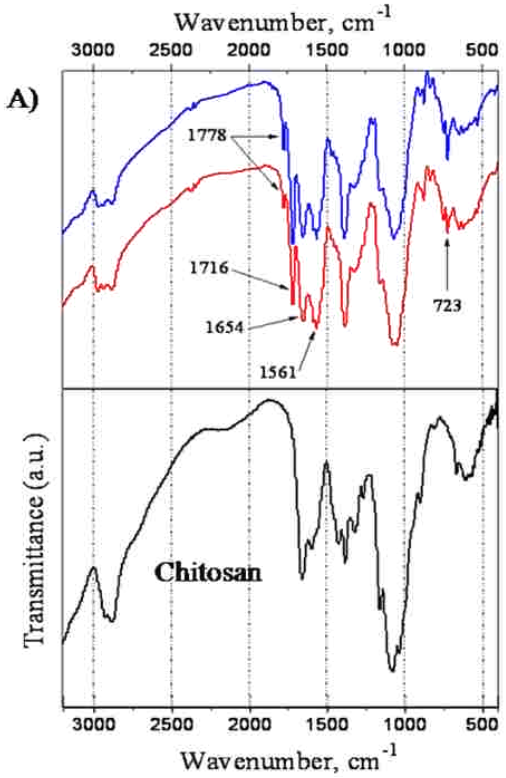

Figure 3.9 FT-IR Spectra of chitosan reacted with PA (with molar ratio of PA to chitosan being 5:1) in: A) BMIMAc using pyridine (red spectrum) and DABCO (blue spectrum) as a base.

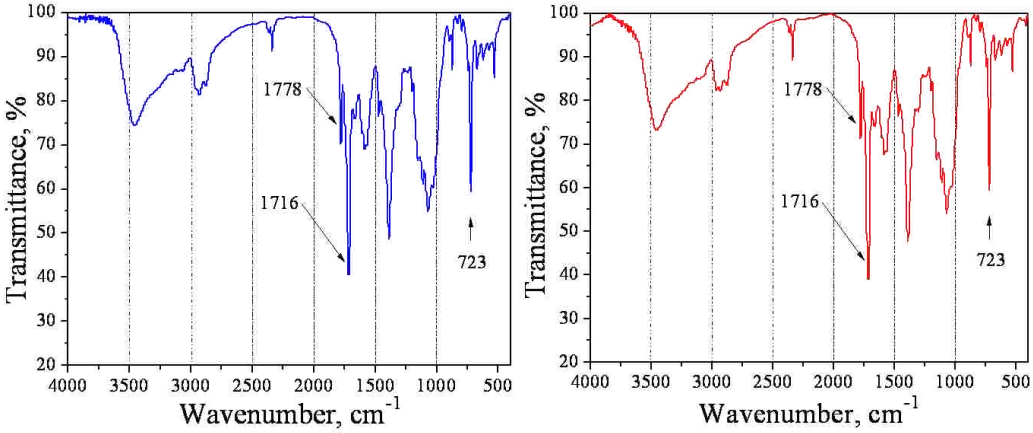

Figure 3.10 FT-IR FT-IR Spectra of chitosan reacted with PA (with molar ratio of PA to chitosan being 5:1) in BMIMAc using DABCO (blue spectrum) as a base and using pyridine (red spectrum) as a base after heating the KBr pellets containing the sample to 200°C for 2 hours.

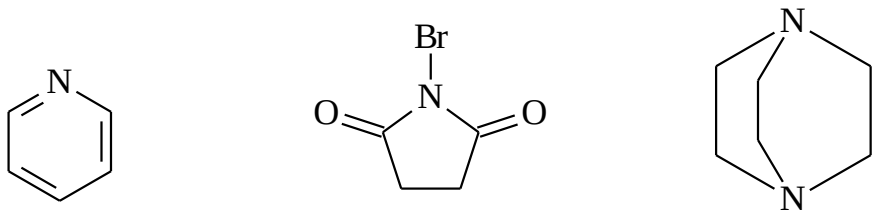

a b c

Figure 3.11 Chemical structures of pyridine (a), *N*-Bromosuccinimide (NBS) (b), and 1,4-Diazobicyclo[2.2.2] Octane (DABCO) (c).

Table 3.1 Ratio of the newly formed absorption peaks in the phthalated K to the C-O-C bridge symmetric stretching (1076 cm^{-1}); the molar ratio of pyridine:K was 3:1, 5:1, and 10:1, respectively, while the molar ratio of PA:K was constant (5:1).

Experiment 4h 100°C	imide/CO	Ester/CO	carbox acid/CO	amideII/CO	1380/CO
Exp 116 KPA+Py 5:1 3:1, AcIL	0.05	0.29	0.68	0.72	0.69
Exp 117 KPA+Py 5:1 5:1, AcIL	0.15	0.53	1.00	0.99	0.84
Exp 78 KPA+Py 5:1 10:1, AcIL	0.18	0.68	0.82	0.94	0.91

Table 3.2 Ratio of the newly formed absorption peaks in the phthalated K to the C-O-C bridge symmetric stretching (1076 cm^{-1}); the molar ratio of DABCO:K was 3:1, 5:1, and 10:1, respectively, while the molar ratio of PA:K was constant (5:1).

Experiment 4h 100°C	imide/CO	Ester/CO	carbox acid/CO	amideII/CO	1380/CO
Exp 122KPA+DABCO 5:1 3:1, AcIL	0.09	0.49	0.92	0.94	0.86
Exp 123KPA+DABCO 5:1 5:1, AcIL	0.13	0.57	0.94	0.99	0.89
Exp 77 KPA+DABCO 5:1 10:1, AcIL	0.28	0.94	0.85	0.90	0.94

The DS of the reaction products were calculated using two calibration curves (Figure 3.12) obtained with the help of FT-IR spectra. Physical mixtures of either mono methyl phthalate or N-

methyl phthalimide with chitosan were employed to obtain calibration curves that will be used to calculate the DS's for the imide and ester groups, respectively, of the reacted chitosan. Six samples containing mono methyl phthalate-to-chitosan or N-methyl phthalimide-to-chitosan weight percent ratios of 5:95, 10:90, 15:85, 20:80, 25:75, and 30:70, respectively were prepared by mixing the 2 compounds. Next, the ratio of the absorption peaks from FT-IR spectra corresponding to ester groups or imide groups to the C-O-C stretch of the acetal peak in the chitosan backbone was plotted against the percent content of mono methyl phthalate or N-methyl phthalimide from the physical mixture. The intercept corresponding to the mono methyl phthalate plot doesn't go to zero because the absorption peak of the carbonyl stretch in ester groups is overlapped with the absorption peak of the carbonyl stretch in amide groups present in chitosan. The calculated DS's for the reacted chitosan in the presence of DABCO or pyridine are presented in Table 3.6. Based upon this analysis, the presence of DABCO in the reaction system increases the DS of the reaction products when compared with those in the presence of pyridine.

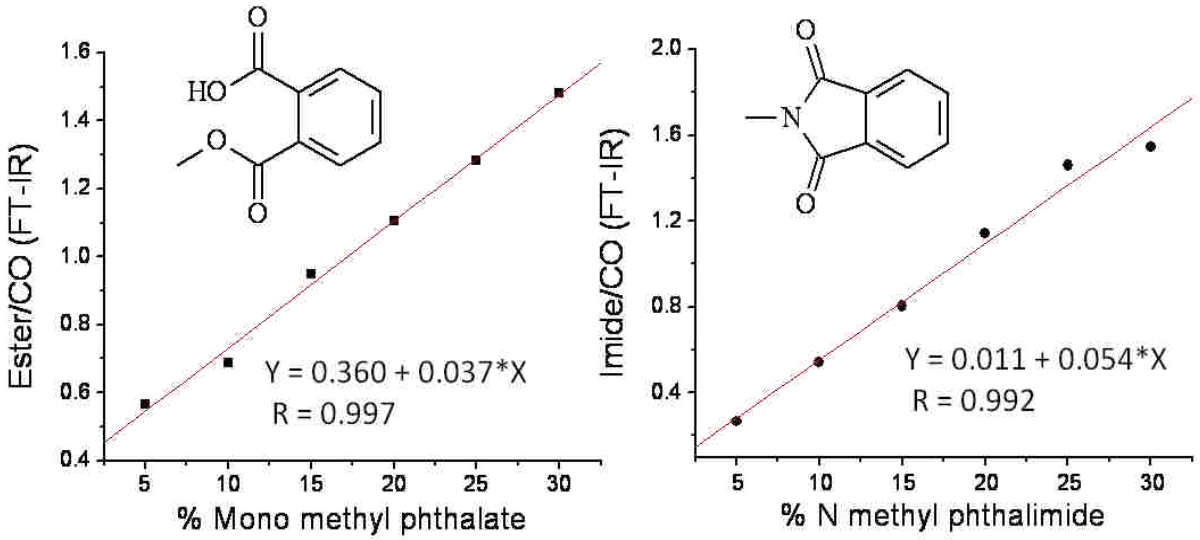

Figure 3.12 Calibration curves obtained for different physical mixtures of either mono methyl phthalate or N-methyl phthalimide with chitosan using FT-IR.

Table 3.3 Ratio of the newly formed absorption peaks in the phthalated K to the C-O-C bridge symmetric stretching (1076 cm^{-1}); the molar ratio of both pyridine:K and PA:K was 5:1; temperatures of 80°C, 100°C and 120°C were used for reactions.

Experiment 4h	imide/CO	Ester/CO	carbox acid/CO	amideII/CO	1380/CO
Exp 124 KPA+Py 5:1 5:1, 80°C AcIL	0.11	0.49	0.80	0.91	0.83
Exp 117 KPA+Py 5:1 5:1, 100°C AcIL	0.15	0.53	1.00	0.99	0.84
Exp 125 KPA+Py 5:1 5:1, 120°C AcIL	0.13	0.51	0.86	0.87	0.82

Table 3.4 Ratio of the newly formed absorption peaks in the phthalated K to the C-O-C bridge symmetric stretching (1076 cm^{-1}) after heating the KBr pellets containing the sample to 200°C for 2 hours; the molar ratio of pyridine:K was 3:1, 5:1, and 10:1, respectively, while the molar ratio of PA:K was constant (5:1).

Experiment after heating to 200°C	imide/CO	Ester/CO	carbox acid/CO	amideII/CO	1380/CO
Exp 116 KPA+Py 5:1 3:1, AcIL	0.28	0.96	0.38	0.25	0.75
Exp 117 KPA+Py 5:1 5:1, AcIL	0.43	0.95	0.53	0.42	0.84
Exp 78 KPA+Py 5:1 10:1, AcIL	0.54	1.46	0.48	0.63	1.17

Table 3.5 Ratio of the newly formed absorption peaks in the phthalated K to the C-O-C bridge symmetric stretching (1076 cm^{-1}) after heating the KBr pellets containing the sample to 200°C for 2 hours; the molar ratio of DABCO:K was 3:1, 5:1, and 10:1, respectively, while the molar ratio of PA:K was constant (5:1).

Experiment after heating to 200°C	imide/CO	Ester/CO	carbox acid/CO	amideII/CO	1380/CO
Exp 122KPA+DABCO 5:1 3:1, AcIL	0.43	1.07	0.47	0.32	0.91
Exp 123KPA+DABCO 5:1 5:1, AcIL	0.48	1.03	0.45	0.33	0.91
Exp 77 KPA+DABCO 5:1 10:1, AcIL	0.59	1.50	0.46	0.59	1.95

Table 3.6 Degree of substitution (DS) of phthalated chitosan in the presence of DABCO or pyridine as base (calculated from FT-IR calibration curves).

Experiment after heating to 200^{0}C	DS	Experiment after heating to 200^{0}C	DS
Exp 116 KPA+Py 5:1 3:1, AcIL	0.41	Exp 122KPA+DABCO 5:1 3:1, AcIL	0.52
Exp 117 KPA+Py 5:1 5:1, AcIL	0.45	Exp 123KPA+DABCO 5:1 5:1, AcIL	0.51
Exp 78 KPA+Py 5:1 10:1, AcIL	0.77	Exp 77 KPA+DABCO 5:1 10:1, AcIL	0.8

3.5.3.3 FT-IR Analysis of Phthalated Chitosan Performed in the Presence of N-Bromosuccinimide (NBS) as Catalyst

N-Bromosuccinimde (Figure 3.11) showed to be a highly effective catalyst for the phthaloylation of chitosan at both functional groups (–OH and $–NH_2$). The role of NBS is not clear but a possible explanation is that it acts as a source for Br^+, which in turn activates the carbonyl groups of PA to produce highly reactive acylating agent, as shown in Scheme 3.5. The acylating agent reacts with hydroxyl and amino groups of chitosan, which upon elimination of NBS produces phthaloylated chitosan.(*129-132*) This hypothesis, however, needs further investigation to determine exactly the actual role of the NBS reagent.

When the reaction of chitosan with PA was carried in the presence of NBS as catalyst significantly increased intensities of the carbonyl bands between 1720 and 1640 cm^{-1} were observed when compared with the reactions in the presence or absence of a base (Figure 3.12, Figure 3.9, and Figure 3.8). As a result, enough substitution took place at the functional groups of chitosan to disrupt the strong hydrogen bonding existent in its structure so that the product resulting from phthaloylation was soluble in DMSO and DMF.

Increasing the amount of catalyst in the reaction system led to an increase of the intensity peaks in the FT-IR spectra corresponding to imide (1777 cm^{-1}), carboxyl (1716 cm^{-1}), ester (1655 cm^{-1}) groups, and ortho-disubstituted aromatic rings (723 cm^{-1}). The cyclization reaction with the formation of imide groups took place to a greater extent when higher amounts of catalyst were present (Table 3.7 and Table 3.8). Changing the molar ratio of PA to AGU of chitosan from 3:1 to 5:1 didn't have much of an impact on the intensity peaks of FT-IR spectra, but a molar ratio of 7:1 (PA:AGU) increased the intensity peaks corresponding to imide and ester groups (Table 3.9).

Heating the films used for the FT-IR measurements to 200^{o}C for 2 hours and recording the spectra again, led to an increase in the intensity peaks corresponding to imide (1777 cm^{-1} and 1716 cm^{-1}) and ortho-disubstituted aromatic rings (723 cm^{-1}) and a decrease in the intensity peaks for carbonyl stretch (1655 cm^{-1}) and N-H bending (1560 cm^{-1}) for amides (Figure 3.13, Table 3.10, and Table 3.11). This behavior is a result of amic acid cyclization leading to the formation of imide groups (Scheme 3.4).

The calculated DS using the calibration curves from Figure 3.12 are compared in Table 3.12. Based upon this analysis, higher DS values are obtained with the increase of both PA and NBS added to the system.

Table 3.7 Ratio of the newly formed absorption peaks in the phthalated K to the C-O-C bridge symmetric stretching (1076 cm^{-1}); the molar ratio of NBS:K was 3:1, 7:1, and 10:1, respectively, while the molar ratio of PA:K was constant (3:1).

Experiment (4h at 100^{o}C)	imide/CO	ester/CO	carbox. acid/CO	amide II/CO
Exp 161 KPA+NBS 3:1 3:1, BMIMAc	0.33	0.92	0.96	0.98
Exp 162 KPA+NBS 3:1 7:1, BMIMAc	0.47	1.55	0.61	0.48
Exp 163 KPA+NBS 3:1 10:1, BMIMAc	0.63	1.59	0.48	0.29

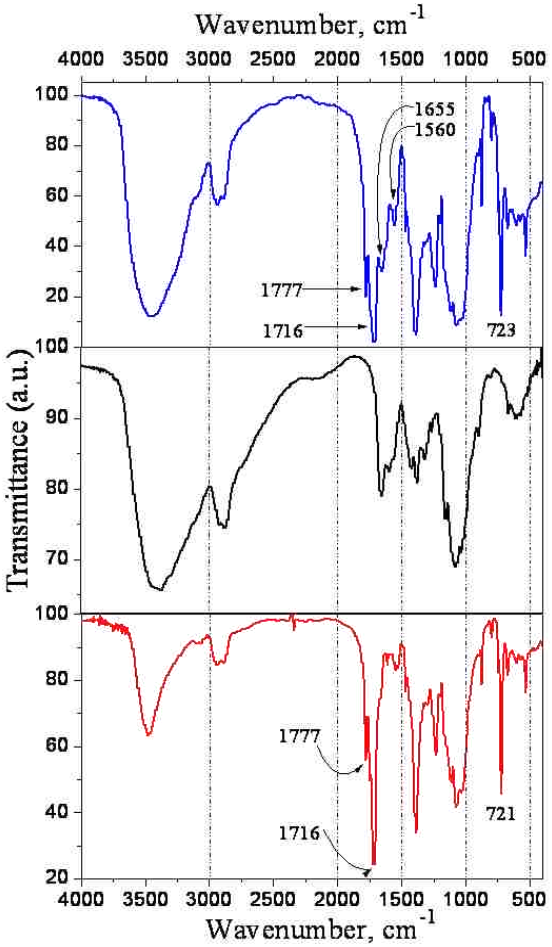

Figure 3.13 FT-IR spectra of chitosan reacted with PA in the presence of NBS (the molar ratio of PA to chitosan and NBS to chitosan being 3:1 and 10:1, respectively) in BMIMAc (blue spectra). The red spectrum represents the phthalated chitosan heated to 200°C for 2 hours. The black line shows the spectrum of original chitosan.

Table 3.8 Ratio of the newly formed absorption peaks in the phthalated K to the C-O-C bridge symmetric stretching (1076 cm^{-1}); the molar ratio of NBS:K was 3:1, 7:1, and 10:1, respectively, while the molar ratio of PA:K was constant (5:1).

Experiment (4h at 100°C)	imide/CO	ester/CO	carbox. acid/CO	amide II/CO
Exp 155 KPA+NBS 5:1 3:1, AcIL	0.3	1.14	0.7	0.68
Exp 154 KPA+NBS 5:1 7:1, AcIL	0.41	1.17	0.76	0.87
Exp 148 KPA+NBS 5:1 10:1, AcIL	0.39	1.25	0.76	0.74

Table 3.9 Ratio of the newly formed absorption peaks in the phthalated K to the C-O-C bridge symmetric stretching (1076 cm^{-1}); the molar ratio of PA:K was 3:1, 5:1, and 7:1, respectively, while the molar ratio of NBS:K was constant (3:1).

Experiment (4h at 100°C)	imide/CO	ester/CO	carbox. acid/CO	amide II/CO
Exp 161 KPA+NBS 3:1 3:1, AcIL	0.33	0.92	0.96	0.98
Exp 155 KPA+NBS 5:1 3:1, AcIL	0.3	1.14	0.7	0.68
Exp 164 KPA+NBS 7:1 3:1, AcIL	0.44	1.36	0.68	0.56

Table 3.10 Ratio of the newly formed absorption peaks in the phthalated K to the C-O-C bridge symmetric stretching (1076 cm^{-1}) after heating the KBr pellets containing the sample to 200°C for 2 hours; the molar ratio of NBS:K was 3:1, 7:1, and 10:1, respectively, while the molar ratio of PA:K was constant (3:1).

Experiment after heating to 200°C	imide/CO	ester/CO	carbox. acid/CO	amide II/CO
Exp 161 KPA+NBS 3:1 3:1, BMIMAc	0.55	1.28	0.58	0.64
Exp 162 KPA+NBS 3:1 7:1, BMIMAc	0.58	1.76	0.39	0.3
Exp 163 KPA+NBS 3:1 10:1, BMIMAc	0.67	1.61	0.37	0.22

Table 3.11 Ratio of the newly formed absorption peaks in the phthalated K to the C-O-C bridge symmetric stretching (1076 cm^{-1}) after heating the KBr pellets containing the sample to 200°C for 2 hours; the molar ratio of NBS:K was 3:1, 7:1, and 10:1, respectively, while the molar ratio of PA:K was constant (5:1).

Experiment after heating to 200°C	imide/CO	ester/CO	carbox. acid/CO	amide II/CO
Exp 155 KPA+NBS 5:1 3:1, AcIL	0.5	1.65	0.41	0.47
Exp 154 KPA+NBS 5:1 7:1, AcIL	0.53	1.4	0.4	0.69
Exp 148 KPA+NBS 5:1 10:1, AcIL	0.57	1.61	0.45	0.52

Table 3.12 Degree of substitution (DS) of phthalated chitosan in the presence of NBS as catalyst (calculated from FT-IR calibration curves).

Experiment after heating to 200^{0}C	DS	Experiment after heating to 200^{0}C	DS	Experiment after heating to 200^{0}C	DS
Exp 161 KPA+NBS 3:1 3:1, AcIL (DMSO)	0.65	Exp 164 KPA+NBS 7:1 3:1, AcIL (DMSO)	1.15	Exp 155 KPA+NBS 5:1 3:1, AcIL (DMSO)	0.85
Exp 162 KPA+NBS 3:1 7:1, AcIL (DMSO)	0.93	Exp 165 KPA+NBS 7:1 7:1, AcIL (DMSO)	0.95	Exp 154 KPA+NBS 5:1 7:1, AcIL (DMSO)	0.73
Exp 163 KPA+NBS 3:1 10:1, AcIL (DMSO)	0.88	Exp 166 KPA+NBS 7:1 10:1, AcIL (DMSO)	1.75	Exp 148 KPA+NBS 5:1 10:1, AcIL (DMSO)	0.85

Scheme 3.5 Mechanism of phthaloylation of chitosan using NBS as a catalyst.

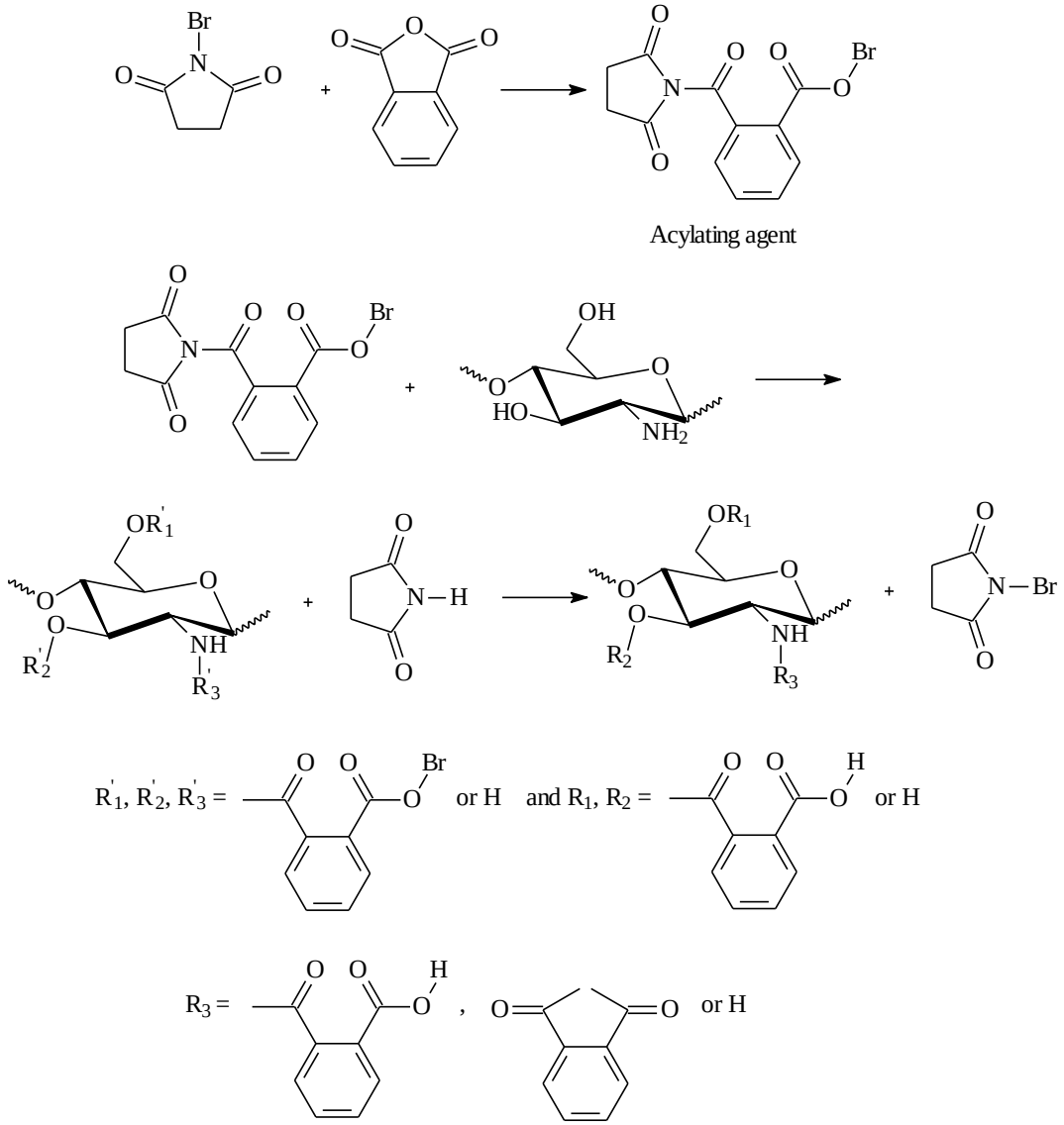

3.5.3.4 ^{1}H NMR Measurements

The ^{1}H NMR spectrum of phthaloylchitosan is shown in Figure 3.14. Mainly, two sets of broad peaks can be observed: one set consisting of four peaks centering at 7.31, 7.45, 7.49, and 7.83 ppm assigned to the phthaloyl groups (the peaks at 7.68 and 7.75 ppm correspond to residual BMIMAc ionic liquid) and the other between 1.1 and 5.0 ppm belong to the chitosan backbone hydrogen (associated with DMSO-d_6 at 2.5 ppm and unremoved BMIMAc ionic liquid at 0.98, 1.36, 3.83, and 4.15 ppm). The peak at 9.15 ppm is attributed to the proton in carboxylic acids.

The ^{1}H NMR (400 MHz; CD_3OD) signals for BMIMAc ionic liquid are: δ_H: 0.98 (3H, t, $N(CH_2)_3)C\underline{H}_3$); 1.36 (2H, m, $N(CH_2)_2C\underline{H}_2CH_3$): 1.86 (2H, m, $NCH_2C\underline{H}_2CH_2CH_3$); 1.88 (3H, s, CH_3COO^-); 3.92 (3H, s, NCH_3); 4.21 (2H, t, $NC\underline{H}_2(CH_2)_2CH_3$); 7.57 (1H, d, $CH_3NC\underline{H}CHN$); 7.63 (1H, d, $CH_3NCHC\underline{H}N$); 10.33 (1H, s, $NC\underline{H}N$). These results are in agreement with those obtained by Wu and coworkers.(*133*)

The degree of substitution (DS) of phthalated chitosan was determined by ^{1}H NMR spectroscopy using the integral of peaks of the chitosan backbone at 2.8 – 5.3 ppm and integral of peaks due to aromatic protons at 7.0 – 8.0 ppm (equation 3.1). Because traces of the BMIMAc ionic liquid are still present in the final products, the calculation of DS was performed according to the equation 3.1 only after the area corresponding to the ionic liquid peaks was subtracted. To find out what is the area of the ionic liquid peaks that is overlapping with either the area of the chitosan backbone or the area of the aromatic protons needed for the calculation of the DS, the integral of the peaks corresponding to the 3 protons at 0.84 - 0.93 ppm of the methyl group from BMIMAc was calculated. With the obtained value, the integral peak of a single proton was obtained by dividing by 3 (the number of protons present in the methyl group). In the region between 7.0 – 8.0 ppm of the aromatic protons, two protons from the ionic liquid are overlapped while in the region between 2.8-5.3 ppm of the chitosan backbone five protons from the BMIMAc are overlapped. The integral of the

peaks corresponding to the solvent still present in the products was subtracted before using the equation 3.1 for the calculation of DS.

$$DS = 7*I_{arom}/4*I_{AGU} \quad (3.1)$$

The calculated DS's are compared in Table 3.13 and Table 3.14. Based upon this analysis, the maximum DS achieved was 0.28. These results do not seem to be reliable since the products are soluble in DMSO. The modified chitosan must have a higher degree of substitution in order to become soluble. On the other hand, the DS's obtained from the calibration curves of the FT-IR spectra (Table 3.12) are more accurate with much bigger values that are close to a DS=1.

Table 3.13 Degree of substitution (DS) of phthalated chitosan; the molar ratio of NBS:K was 3:1, 7:1, and 10:1, respectively, while the molar ratio of PA:K was constant (3:1).

Experiment (4h at 100°C)	DS
Exp 161 KPA+NBS 3:1 3:1, AcIL	0.16
Exp 162 KPA+NBS 3:1 7:1, AcIL	0.23
Exp 163 KPA+NBS 3:1 10:1, AcIL	0.25

Table 3.14 Degree of substitution (DS) of phthalated chitosan; the molar ratio of NBS:K was 3:1, 7:1, and 10:1, respectively, while the molar ratio of PA:K was constant (5:1).

Experiment (4h at 100°C)	DS
Exp 155 KPA+NBS 5:1 3:1, AcIL	0.27
Exp 154 KPA+NBS 5:1 7:1, AcIL	0.28
Exp 148 KPA+NBS 5:1 10:1, AcIL	0.22

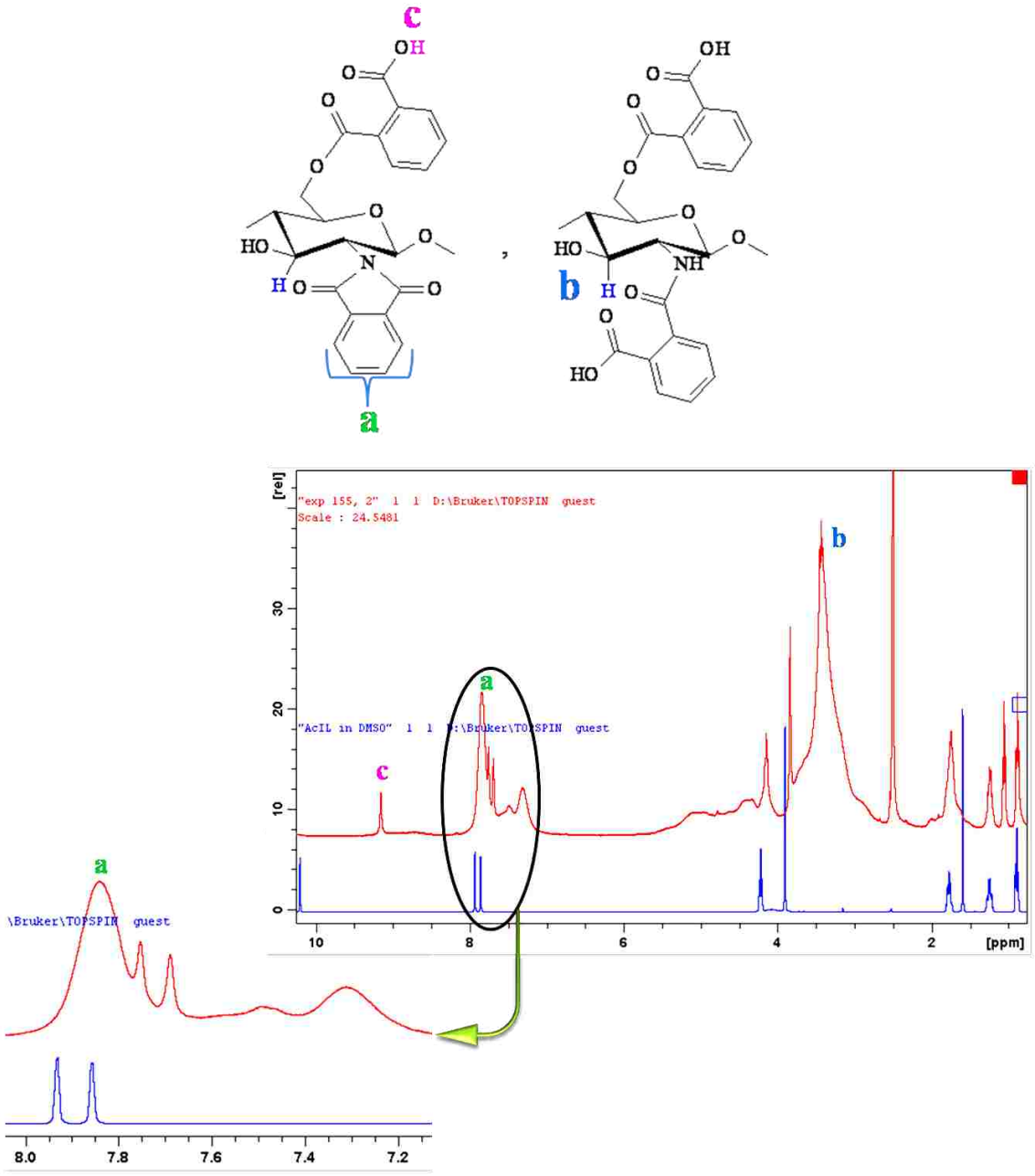

Figure 3.14 ^{1}H NMR spectra of BMIMAc (blue line) and chitosan reacted with PA in the presence of NBS (the molar ration of K to PA and K to NBS being 5:1 and 3:1, respectively).

3.5.3.5 TGA/DSC Measurements

The reaction of chitosan with phthalic anhydride reduced the thermal stability of the reaction product (Figure 3.15). The onset temperatures of degradation were 275^{o}C (chitosan), 226^{o}C (phthalated chitosan 4h) and 238^{o}C (phthalated chitosan 2h), with maximum rates (DTG) at 90^{o}C

and 300°C (chitosan), 93°C and 245°C (phthalated chitosan 4h), and 93°C and 253°C (phthalated chitosan 2h). The maximum rates at 90°C and 93°C are assigned to the water loss. The maximum rates at 253°C and 245°C of the phthalated chitosan are attributed to the degradation of polymer backbone as well as the degradation of amide and imide substituted species. At 50 % weight loss, the decomposition temperature of chitosan (330°C) is higher than those of phthalated chitosan samples prepared with reaction time of 2h (320°C) and 4h (312°C), respectively. The same trend was observed for the thermal stability: at 667°C chitosan lost 69% of its weight, phthalated chitosan from 2h and 4h runs lost 71% and 73% of their initial weight, respectively.

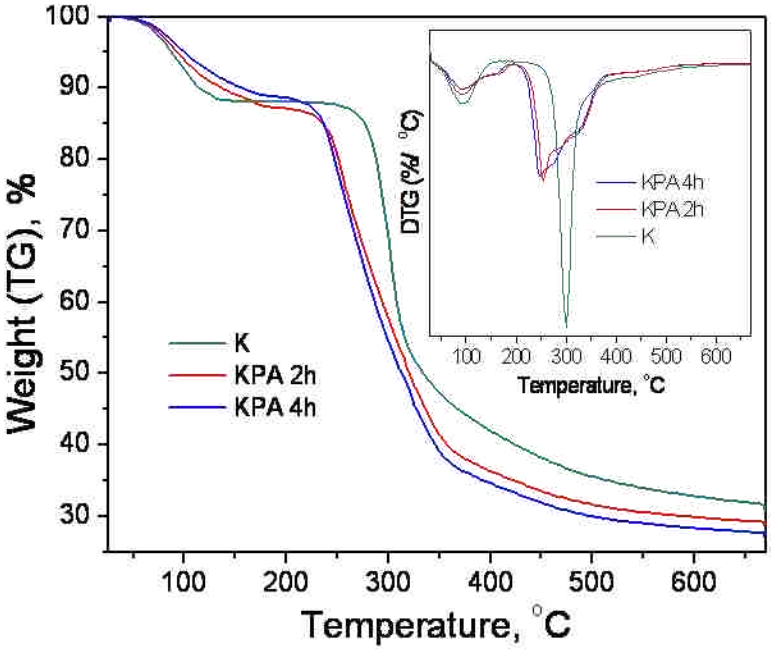

Figure 3.15 Thermogravimetric traces (TG) and corresponding derivatives for chitosan (green lines), phthalated chitosan 2h (red lines), and phthalated chitosan 4h (blue lines).

Figure 3.16 illustrates the TGA thermograms of unmodified chitosan and reacted chitosan in the presence of a base. The TGA curves give an initial decrease below 150°C due to loss of moisture (Figure 3.16 left). After that, the native chitosan starts to decompose at 280°C, whereas the phthalated chitosan samples obtained in the presence of DABCO or pyridine begin to decompose at 250°C and 253°C, respectively (Figure 3.16 right). At 50% weight loss, the decomposition

temperature occurs at 456°C for native chitosan and 360°C and 361°C for the phthalated chitosan samples obtained in the presence of DABCO and pyridine, respectively. This decreasing trend of decomposition temperature indicated that the thermal stability of the phthalated chitosan is lower than that of the native chitosan. However, when the thermal stability is compared to that of the regenerated chitosan from the BMIMAc ionic liquid (Table 3.15 and Table 3.16) the phthalated chitosan samples showed an improved thermal stability up until 350^{o}C. As the temperature increased, the amounts of residual fractions seemed to come closer, i.e., at 600^{o}C regenerated chitosan lost 64% of its weight, phthalated chitosan lost about 63% of its initial weight. These results may indicate that not much substitution took place since the weight loss of both chitosan and reacted chitosan showed similar values. A higher substitution would have resulted in a higher weight loss for the reacted chitosan.

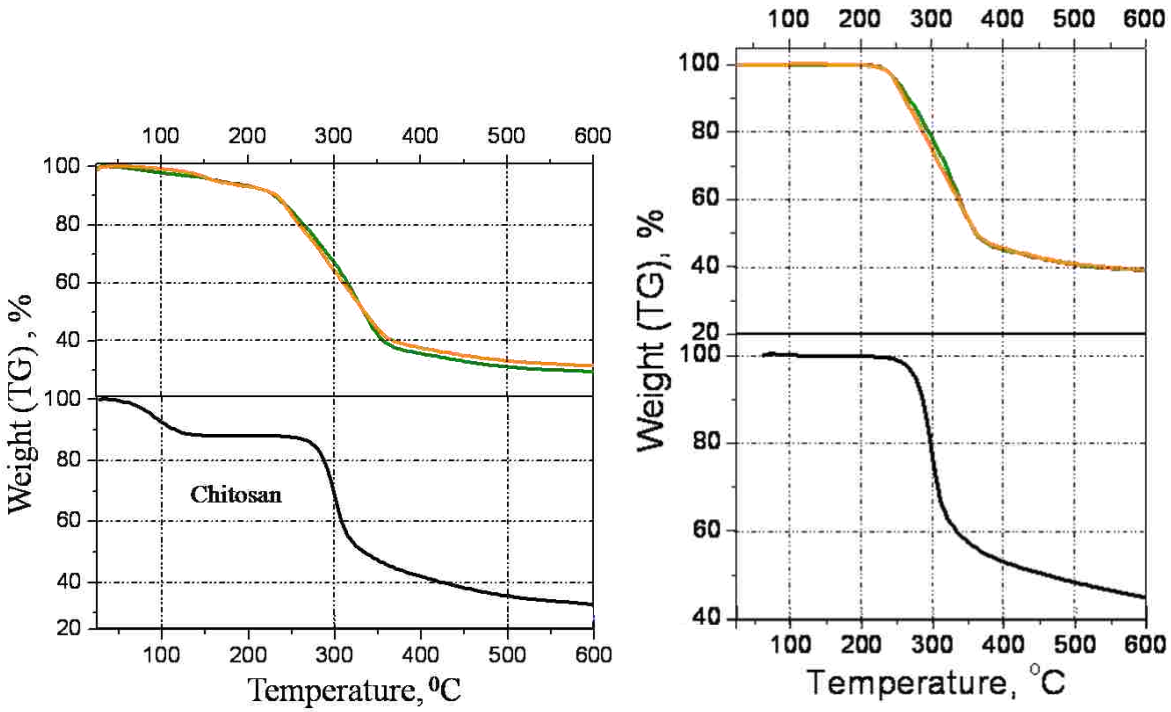

Figure 3.16 Thermogravimetric traces (TG) for chitosan reacted with PA (with molar ratio of PA to chitosan being 5:1) in BMIMAc using pyridine (orange spectrum) and DABCO (green spectrum) as a base (left); Thermogravimetric traces (TG) of the samples with the thermograms corresponding to the second heating scan to 600^{o}C recorded imediately after the first run to 150^{o}C (right).

The weight loss up to 150°C of the reaction products is attributed to the loss of water as a result of cyclization and formation of imide groups as confirmed by the FT-IR studies.

Table 3.15 indicates that the thermal stability of the phthalated chitosan obtained in the presence of DABCO as base increases with the increase of the base added to the system. In the case of the phthalated chitosan synthesized in the presence of pyridine as base (Table 3.16), the thermal stability decreases with the amount of base used for the reaction.

The thermal behavior of chitosan and phthalated chitosan obtained in the presence of NBS as catalyst are presented in Figure 3.17. Table 3.17 and Table 3.18 indicate that an increase for the onset temperatures of degradation when compared to that of regenerated chitosan and even of pure chitosan is observed for the reaction products when the amount of PA was kept constant (PA:AGU chitosan = 3:1 or 7:1) and the molar ration of NBS:AGU of chitosan is varied from 3:1 to 7:1 and 10:1. The same trend is observed for the thermal stability of the reaction products up until 350°C (Table 3.17 and Table 3.18). If one compared the residual weights at 300°C and 350°C, respectively, the reacted chitosan from experiment 163 is more stable (87 % and 64 % respectively) but at 400°C the original chitosan sample has a higher weight loss (45%).

Table 3.15 Thermogravimetric data for chitosan and for reaction products with PA in the presence of DABCO as base; the molar ratio of DABCO:K was 3:1, 5:1, and 10:1, respectively, while the molar ratio of PA:K was constant (5:1).

Sample 4h at 100°C	Onset temperature °C	300°C Residual weight%	325°C Residual weight%	350°C Residual weight%	400°C Residual weight%
Chitosan	280	71.6	51.8	47.5	42.1
Regenerated chitosan	225.31	56	51.4	47.8	43.6
Exp122 KPA+DABCO 5-1 3-1	250.29	72.6	60.3	52	42.3
Exp 123 KPA+DABCO 5-1 5-1	251.9	76.8	64.6	54.7	42.3
Exp 77 KPA+DABCO 5-1 10-1	236.39	78	66.6	54.5	45.2

Table 3.16 Thermogravimetric data for chitosan and for reaction products with PA in the presence of pyridine as base; the molar ratio of pyridine:K was 3:1, 5:1, and 10:1, respectively, while the molar ratio of PA:K was constant (5:1).

Sample 4h at 100°C	Onset temperature °C	300°C Residual weight%	325°C Residual weight%	350°C Residual weight%	400°C Residual weight%
Chitosan	280	71.6	51.8	47.5	42.1
Regenerated chitosan	225.31	56	51.4	47.8	43.6
Exp 116 KPA+Py 5:1 3:1	253.66	72.7	61.7	54	44.3
Exp 117 KPA+Py 5:1 5:1	245.16	70.9	60	52.3	42.2
Exp 78 KPA+Py 5:1 10:1	119.54 229.48	65.7	56.1	46.1	39.9

Table 3.17 Thermogravimetric data for chitosan and for reaction products with PA in the presence of NBS as catalyst; the molar ratio of NBS:K was 3:1, 7:1, and 10:1, respectively, while the molar ratio of PA:K was constant (3:1).

Sample 4h at 100°C	Onset temperature °C	300°C Residual weight%	325°C Residual weight%	350°C Residual weight%	400°C Residual weight%
Chitosan	280	71.6	51.8	47.5	42.1
Regenerated chitosan	225.31	56	51.4	47.8	43.6
Exp 161 KPA+NBS 3-1 3-1 AcIL	231	63.7	51.2	40.5	35.7
Exp 162 KPA+NBS 3-1 7-1	288	81.3	69.7	54.1	35.3
Exp 163 KPA+NBS 3-1 10-1	302	87.5	78.1	64	29.3

Table 3.19 shows the thermogravimetric data for regenerated chitosan and for reaction products with PA in the presence of NBS as catalyst when the molar ratio of PA:K was 3:1, 5:1, and 7:1, respectively, while the molar ratio of NBS:K was constant (3:1). From the table it can be seen that the increase of the amount of PA added to the system resulted in enhanced thermal stability of the reaction products up to 325°C. When the molar ratio of NBS:K is kept constant to 10:1 and the molar ratio of PA:K is varied from 5:1 to 7:1 (Table 3.20), respectively, a decrease of the thermal

stability of the phthalated chitosan is observed. However, at a molar ratio of PA:K of 3:1 the reaction product showed an increased thermal stability up until 350^{o}C when compared with both chitosan and regenerated chitosan. The residual weights at 400^{o}C for the reacted chitosan in the presence of NBS (Table 3.17- Table 3.20) showed much lower values than those of chitosan and regenerated chitosan. This may be attributed to the presence of a higher substitution in the reacted chitosan which will have as a result a higher weight loss at higher temperatures.

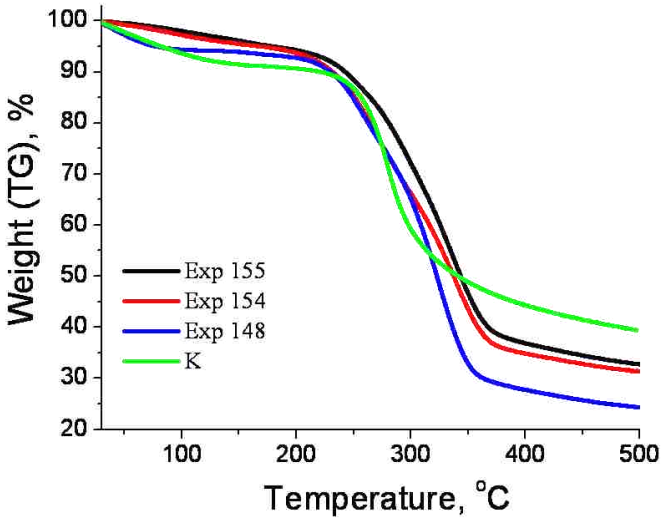

Figure 3.17 Thermogravimetric traces (TG) for K (green line) and K reacted with PA; the molar ratio of NBS: K was 3:1 (black line), 7:1 (red line), and 10:1 (blue line), respectively, while the molar ratio of PA:K was constant (5:1).

Table 3.18 Thermogravimetric data for chitosan and for reaction products with PA in the presence of NBS as catalyst; the molar ratio of NBS:K was 3:1, 7:1, and 10:1, respectively, while the molar ratio of PA:K was constant (7:1).

Sample 4h at 100°C	Onset temperature °C	300°C Residual weight%	325°C Residual weight%	350°C Residual weight%	400°C Residual weight%
Chitosan	280	71.6	51.8	47.5	42.1
Regenerated chitosan	225.31	56	51.4	47.8	43.6
Exp 164 KPA+NBS 7-1 3-1	276	75.5	63.8	48.6	35.7
Exp 165 KPA+NBS 7-1 7-1	319	84.9	77.9	65.5	29.3
Exp 166 KPA+NBS 7-1 10-1	206	54.6	47.7	38.3	28.3

Table 3.19 Thermogravimetric data for chitosan and for reaction products with PA in the presence of NBS as catalyst; the molar ratio of PA:K was 3:1, 5:1, and 7:1, respectively, while the molar ratio of NBS:K was constant (3:1).

Sample 4h at 100°C	Onset temperature °C	300°C Residual weight%	325°C Residual weight%	350°C Residual weight%	400°C Residual weight%
Chitosan	280	71.6	51.8	47.5	42.1
Regenerated chitosan	225.31	56	51.4	47.8	43.6
Exp 161 KPA+NBS 3-1 3-1	231	63.7	51.2	40.5	35.7
Exp 155 KPA+NBS 5-1 3-1	247	72	60	46	37
Exp 164 KPA+NBS 7-1 3-1	276	75.5	63.8	48.6	35.7

Table 3.20 Thermogravimetric data for chitosan and for reaction products with PA in the presence of NBS as catalyst; the molar ratio of PA:K was 3:1, 5:1, and 7:1, respectively, while the molar ratio of NBS:K was constant (10:1).

Sample 4h at 100°C	Onset temperature °C	300°C Residual weight%	325°C Residual weight%	350°C Residual weight%	400°C Residual weight%
Chitosan	280	71.6	51.8	47.5	42.1
Regenerated chitosan	225.31	56	51.4	47.8	43.6
Exp 163 KPA+NBS 3-1 10-1	302	87.5	78.1	64	29.3
Exp 148 KPA+NBS 5-1 10-1	227	65	47.8	32.5	28
Exp 166 KPA+NBS 7-1 10-1	206	54.6	47.7	38.3	28.3

The weight loss up to 150°C of the reaction products is attributed to the loss of water as a result of cyclization and formation of imide groups as confirmed by the FT-IR studies. Differential scanning calorimetry (DSC) measurements (Figure 3.18) were in agreement with this hypothesis. Fresh and dried samples were used for a first heating run to 150°C followed by cooling to 25°C and a

second heating run to 150°C. On the second heating run no endothermic peak was observed which suggests complete cyclization on the first heating run to 150°C which showed an endothermic peak around 80-85°C.

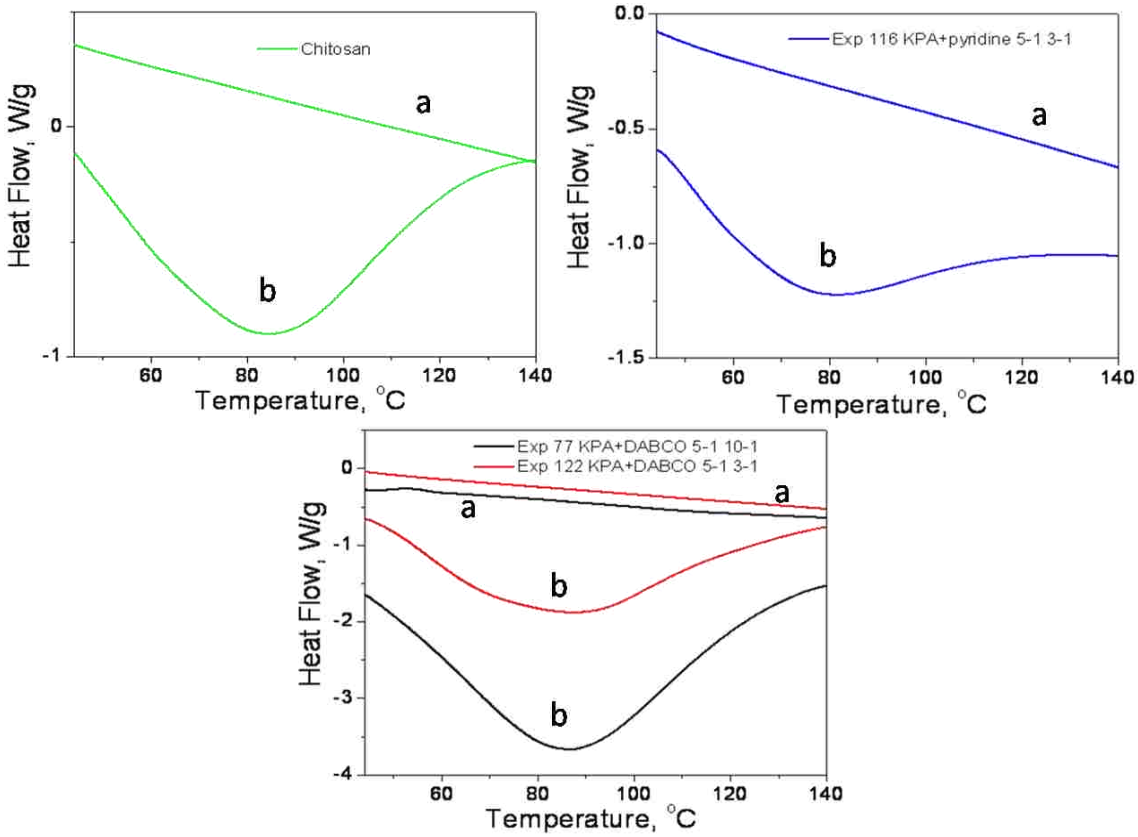

Figure 3.18 DSC thermograms of chitosan, chitosan reacted with PA (PA:AGU = 5:1) in the presence of: pyridine (pyridine:AGU = 3:1) or DABCO (DABCO:AGU = 3:1 and 10:1). Thermogram *a* corresponds to the first heating run to 150°C with an isothermal for 20 minutes, whereas thermogram *b* corresponds to the second heating scan to 150°C recorded immediately after the first run.

CHAPTER 4 . HOMOGENEOUS MODIFICATION OF CHITOSAN IN 1-BUTYL-3-METHYLIMIDAZOLIUM CHLORIDE

4.1 Objective of Study

Chitosan, a linear natural biopolymer, has been an attraction of scientists due to its wide application in chemical, biochemical and biomedical fields. Advantages of this polymer include availability, high biocompatibility, biodegradability, and nontoxicity. Chitosan is soluble in most solutions of organic acids when the pH of the solution is less than 6, in some dilute inorganic acids such as hydrochloric acid, perchloric acid, nitric acid, and in strong polar solvents such as N-dialkyl amides in presence of salts. There are some limitations in the above processing such as cost, toxicity, difficulty for the recovery of the solvent, or instability of the solvents over a wide range of temperature.(*81*) Some of chitosan's properties are: a chelating agent for harmful ions(*134*) such as copper, lead, mercury, and uranium from waste water; an excellent flocculant and a coagulating agent.(*135*) It is by itself hemostatic and chitosan bandages are prepared for wound protection and surgical treatment; it is used as a sustained release drug carrier.(*136-137*)

The present chapter focuses on the dissolution and functionalization of chitosan in homogeneous ionic liquid solutions. 1-butyl-3-methylimidazolium chloride (BMIMCl) (Figure 4.1) is the ionic liquid used to accomplish these goals. There is only one paper that mentions the dissolution of chitosan in 1-butyl-3-methylimidazolium chloride(*73*) but there are no papers describing the chitosan functionalization in this ionic liquid. On the other hand, several studies have reported the ionic liquids as a media for the functionalization of cellulose for producing products with desired properties, such as: acetylation,(*80-81*) esterification,(*82-83*) etherification,(*84*) and carboxymethylation.(*80*)

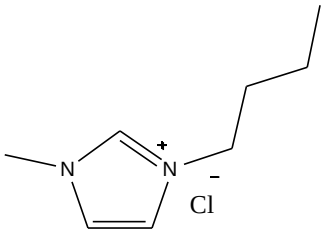

Figure 4.1 Chemical structure of 1-butyl-3-metrylimidazolium chloride (BMIMCl).

4.2 Overall Syntheses Performed in the Present Project

Chemical modification of chitosan was performed in 1-butyl-3-methylimidazolium chloride (BMIMCl) as solvent using phthalic anhydride, benzoyl chloride, and trityl chloride. Seafresh Chitosan powder (85% DAC-MW 227 000) was regenerated by dissolving it in a solution of 1% acetic acid. After the removal of the un-dissolved chitosan by centrifugation, the biopolymer was precipitated in methanol and ammonium hydroxide, filtrated and used without drying. BMIMCl was synthesized from 1-methyl imidazol and chlorobutane.(*138*) The regenerated chitosan was dissolved in BMIMCl at 110-120^{o}C under vacuum and agitation for about 4-5 hours. Toluene was used for the removal of the water present in the system by azeotropic distillation (Figure 4.2). A homogeneous chitosan solution could be obtained up to a concentration of 2wt %. The reaction of chitosan with phthalic anhydride was performed in the absence and in the presence of a base. The reaction of chitosan with benzoyl chloride or trityl chloride was carried out at elevated temperatures in the presence of a base to capture the hydrogen chloride released during the reaction. For all the reactions various molar ratios of the reagents and different temperatures were used.

4.3 Experimental

4.3.1 Materials

1-Butyl-3-methylimidazolium chloride (BMIMCl) was synthesized by addition of n-butyl chloride to N-methylimidizole in toluene.(*138*) Anhydrous toluene, benzoyl chloride, 1,4-diazobicyclo[2.2.2] octane and pyridine were obtained from Sigma Aldrich Chemical Company.

Seafresh chitosan powder with 85% DAC-MW 227 000 and manufactured by Seafresh Chitosan (Lab) Company was obtained from Bangkok, Thailand. Phthalic anhydride (PA) was acquired from Mallinckrodt and was ground to a fine powder before use.

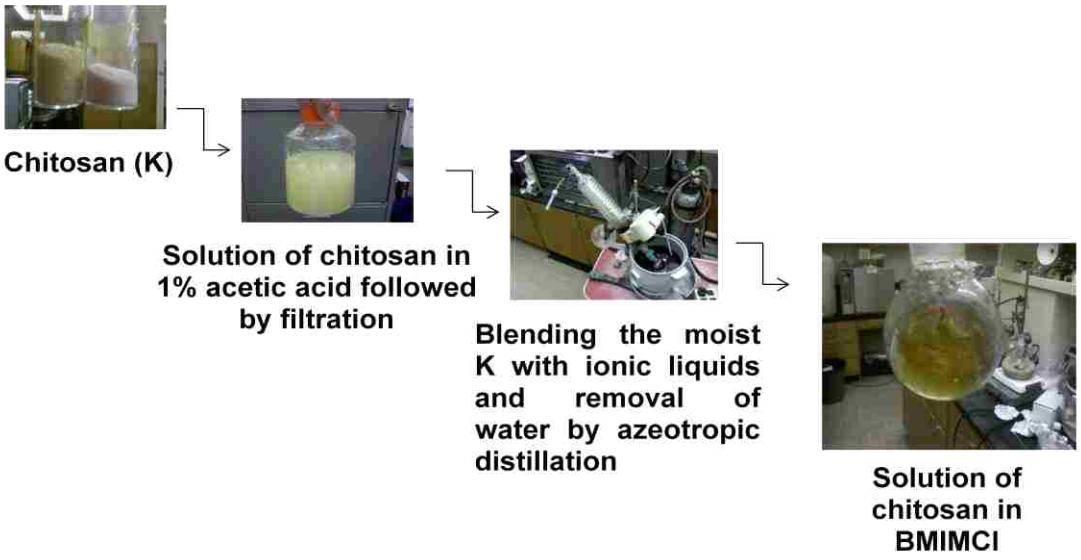

Figure 4.2 Dissolution of chitosan in BMIMCl.

4.3.2 Instrumentation

The ^{13}C NMR spectra were recorded on a VNMRS-700 spectrometer with an acquisition time of 0.21 sec and a relaxation delay of 2 sec. 256 scans were accumulated for each spectra.

FT-IR spectra were recorded on a ThermoNicolet 300 Fourier Transform Infrared spectrometer using a KBr disc containing 1% of very fine ground samples. Thirty two scans were taken for each sample in the range of 4000-400 cm^{-1} at a resolution of 4 cm^{-1} in the transmission mode.

DSC measurements were performed using a TA 2920 MDSC instrument. Samples of 2-5 mg were subjected to analysis using a heating rate of $10^{o}C$/min. Fresh and dried samples were used for a first heating run to $150^{o}C$ with an isothermal for 20 minutes followed by cooling to $25^{o}C$ and a second heating run to $150^{o}C$. The samples were placed in a covered aluminum sample holder while an empty pan was used as a reference. Dynamic thermogravimetric analysis was run in a nitrogen

atmosphere using a TA thermobalance (Model 2950). The experiments were conducted at a heating rate of 10^{o}C/min until 600^{o}C. Some of the experiments were first heated to 150^{o}C, held isothermally for 15 minutes, followed by cooling to room temperature and heating again to 600^{o}C. This procedure was used so that the water present in the systems would be completely eliminated in the first heating step. The thermogravimetric analysis was performed with 7-16 mg samples under nitrogen atmosphere. The integration and processing of the curves resulted from the DSC and TGA instruments were done by using TA Universal analysis software.

4.3.3 Syntheses

4.3.3.1 Representative Procedure for the Chemical Modification of Chitosan with Phthalic Anhydride (PA)

The regenerated chitosan (12.07 g wet chitosan that corresponds to 0.1833 g dry chitosan) was dissolved in BMIMCl (10 g) at 110-120^{o}C under vacuum and agitation for about 4-5 hours. Toluene (40 mL) was used for the removal of the water present in the system. The reaction of chitosan with phthalic anhydride was performed by adding the PA (0.505 g) at room temperature to the chitosan solution. The reaction was allowed to proceed for 2 hours at 80^{o}C. In a separate experiment the temperature was raised to 100^{o}C. The product was isolated by precipitation in 450 mL of methanol. The polymer was isolated by filtration and washed three times with 50 mL aliquots of methanol. The collected modified polymer was dried at 45^{o}C for 24 hours followed by a further drying under vacuum at 50^{o}C for 2 hours. The weight of the dry product was 0.2339 g with a computed % yield of 70% if the theoretical yield is calculated for a degree of substitution of 1.

4.3.3.2 Representative Procedure for the Chemical Modification of Chitosan with Phthalic Anhydride (PA) in the Presence of Pyridine or 1,4-Diazobicyclo[2.2.2] Octane (DABCO) as Base

Chitosan (0.064 g) was dissolved in BMIMCl (6.365 g) at 90-100^{o}C under magnetic stirring for 2 days. The reaction of chitosan with phthalic anhydride (0.294 g) in the presence of a base

(0.222 g) (pyridine or DABCO) was computed by adding the reagents to the chitosan solution and allowing the reaction to proceed at 100^{o}C for 4 hours. The product was isolated by precipitation in 450 mL of methanol. The polymer was isolated by filtration and washed three times with 50 mL aliquots of methanol. The collected modified polymer was dried at 45^{o}C for 24 hours followed by a further drying under vacuum at 50^{o}C for 2 hours. The weight of the dry product was 0.083 g with a computed % yield of 72% if the theoretical yield is calculated for a degree of substitution of 1.

4.3.3.3 Representative Procedure for the Chemical Modification of Chitosan with Benzoyl Chloride (BC)

The reaction of regenerated chitosan (16.968 g wet chitosan which corresponds to 0.4628 g dry chitosan) with BC was performed by adding first pyridine (1.4 mL) at room temperature to a chitosan solution in BMIMCl (1.1wt%) under continuous stirring. The solution was stirred for an additional 20 minutes. The temperature was then raised to 50^{o}C and BC (1.669 mL) was added in small amounts under agitation. Subsequently the reaction was allowed to proceed at 75-85^{o}C under vacuum for 2 hours. The product was isolated by precipitation in 450 mL of methanol. The polymer was isolated by filtration and washed three times with 50 mL aliquots of methanol. The collected modified polymer was dried at 45^{o}C for 24 hours followed by a further drying under vacuum at 50^{o}C for 2 hours. The weight of the dry product was 0.4984 g with a computed % yield of 65% if the theoretical yield is calculated for a degree of substitution of 1.

4.3.3.4 Representative Procedure for the Chemical Modification of Chitosan with Trityl Chloride (TC)

The reaction of chitosan (6.090 g wet chitosan which corresponds to 0.128 g dry chitosan) with TC was performed by adding pyridine (0.320 mL) and TC (0.664 g) to the chitosan solution in BMIMCl. The reaction was allowed to proceed at 80-90^{o}C under vacuum for 2 hours. The product was isolated by precipitation in 450 mL of methanol. The polymer was isolated by filtration and washed three times with 50 mL aliquots of methanol. The collected modified polymer was dried at

45°C for 24 hours followed by a further drying under vacuum at 50°C for 2 hours. The weight of the dry product was 0.147 g with a computed % yield of 46% if the theoretical yield is calculated for a degree of substitution of 1.

4.3.3.5 Representative Procedure for the Chemical Modification of Chitosan with Phthalic Anhydride (PA) and Trityl Chloride (TC)

A sequential reaction of PA and TC was performed by adding first the PA (3.963 g) at room temperature to the chitosan (1.437 g) solution in BMIMCl. The mixture was heated for 2 hours at 80-90°C; next the TC (7.457 g) dissolved in pyridine (3.62 mL) was added and heating continued for other 2 hours at 80-90°C. The product was isolated by precipitation in 450 mL of methanol. The polymer was isolated by filtration and washed three times with 50 mL aliquots of methanol. The collected modified polymer was dried at 45°C for 24 hours followed by a further drying under vacuum at 50°C for 2 hours. The weight of the dry product was 2.384 g.

4.3.3.6 Representative Procedure for the Chemical Modification of Chitosan with Trityl Chloride (TC) and Phthalic Anhydride (PA)

The sequential reaction with TC and PA was performed by adding first the TC (2.18 g) dissolved in pyridine (1.06 mL) at room temperature to 20 g of 2.85% chitosan solution in BMIMCl. The mixture was heated for 2 hours at 80-90°C; then the PA (1.16 g) was added and heating continued for other 2 hours at 80-90°C. The product was isolated by precipitation in 450 mL of methanol. The polymer was isolated by filtration and washed three times with 50 mL aliquots of methanol. The collected modified polymer was dried at 45°C for 24 hours followed by a further drying under vacuum at 50°C for 2 hours. The weight of the dry product was 0.563 g.

4.4 Results/Discussion

4.4.1 FT-IR Characterization of Phthaloylated Chitosan in BMIMCl Ionic Liquid

The reaction of PA with dissolved chitosan in BMIMCl (Scheme 4.1) resulted in products containing carboxylic, ester, amide, and imide groups. In the FT-IR spectra of the phthalated

chitosan the appearance of new peaks at 1772, 1713, 1648, and 1566 cm^{-1} (Figure 4.3) indicates that the reaction proceeded as described in Chapter 3.6.4. The band at 1713 cm^{-1} is evidence for the presence of carbonyl ester groups in anhydroglucose repeating units (AGU) of substituted chitosan. The absorption at 1648 cm^{-1} is attributed to an overlapping of carbonyl groups from carboxylic acid to the amide functions. The stretch of C=O in carboxylic acids appears at 1730-1700 cm^{-1}. However, due to the conjugation present in the system and intermolecular hydrogen bonding the carbonyl peak appears to a much lower frequency. The C=O stretch in amides is present in the spectra at approximately 1680-1630 cm^{-1}. In spectra of phthalated chitosan it is overlapped with the carboxyl absorption and consequently one peak can be seen at 1648 cm^{-1}. The band at 1566 cm^{-1} is indicative of N-H bending for secondary amides. The absorption at 1772 cm^{-1} corresponds to the imide carbonyl. The imide group is a result of the cyclization. None of the aromatic anhydride carbonyl bond absorptions (around 1850 cm^{-1} and 1790 cm^{-1}) were observed in spectra of the reaction products purified by washing with methanol, confirming thus that the products were free of unreacted phthalic anhydride.

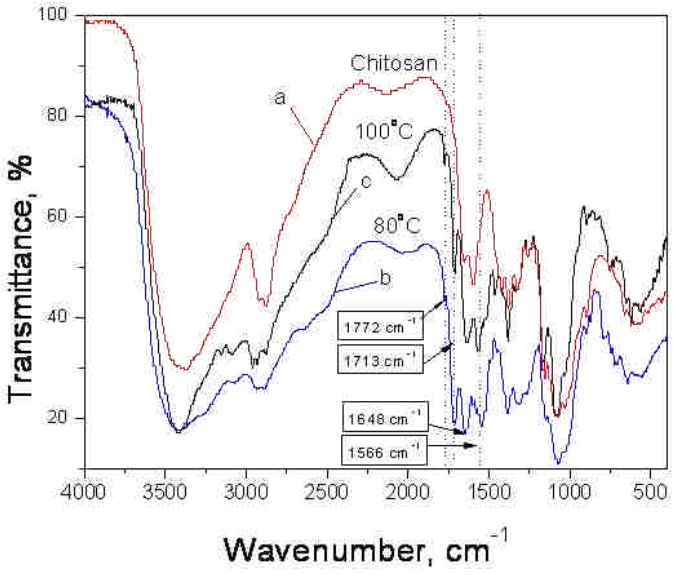

Figure 4.3 FT-IR Spectra of unmodified chitosan (spectrum a), chitosan reacted with PA at 80°C (spectrum b), and chitosan reacted with PA at 100°C (spectrum c); molar ratio phthalic anhydride/AGU 3:1.

Scheme 4.1 Reaction of phthalic anhydride with chitosan dissolved in BMIMCl.

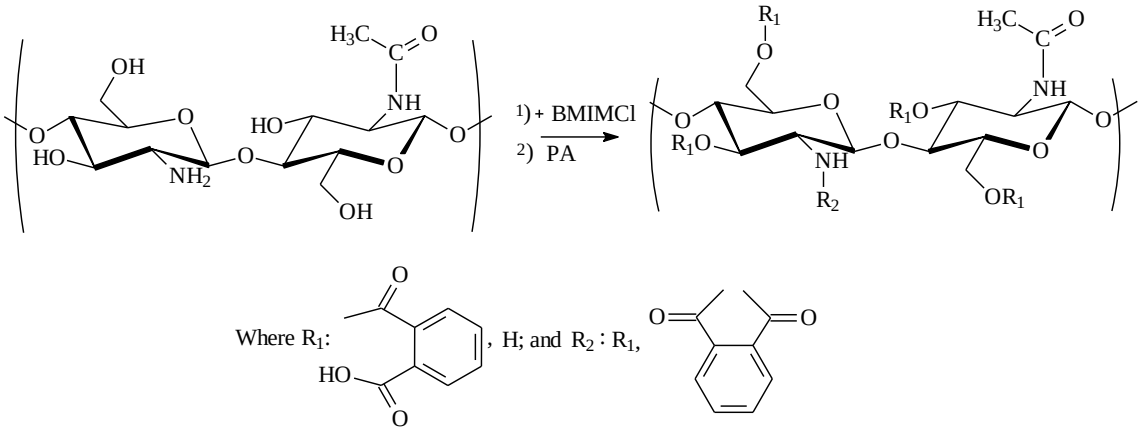

4.4.2 FT-IR Characterization of Benzoylated Chitosan in BMIMCl Ionic Liquid

Regarding the reaction of chitosan with BC (Scheme 4.2), the appearance of new peaks at 3091, 1629, 1517, 752, and 622 cm^{-1} are indicative of the presence of substituted AGU (Figure 4.4). The absorption peak at 3091 cm^{-1} is attributed to the sp^2 C-H stretch in the aromatic ring. The absorption bands at 1629 cm^{-1} and 1517 cm^{-1} are indicative of carbonyl stretch and N-H bending in amides, respectively. The peaks at 752 cm^{-1} and 622 cm^{-1} are evidence of the presence of monosubtituted aromatic rings. These new peaks confirm that only the $-NH_2$ groups from chitosan AGU reacted with BC. No ester peaks are present in the FT-IR spectra which confirm that the –OH groups of chitosan did not react. The absence of the carbonyl stretching at 1800 cm^{-1} confirms that the product was free of unreacted acid chloride.

Scheme 4.2 Reaction of benzoyl chloride with chitosan dissolved in BMIMCl.

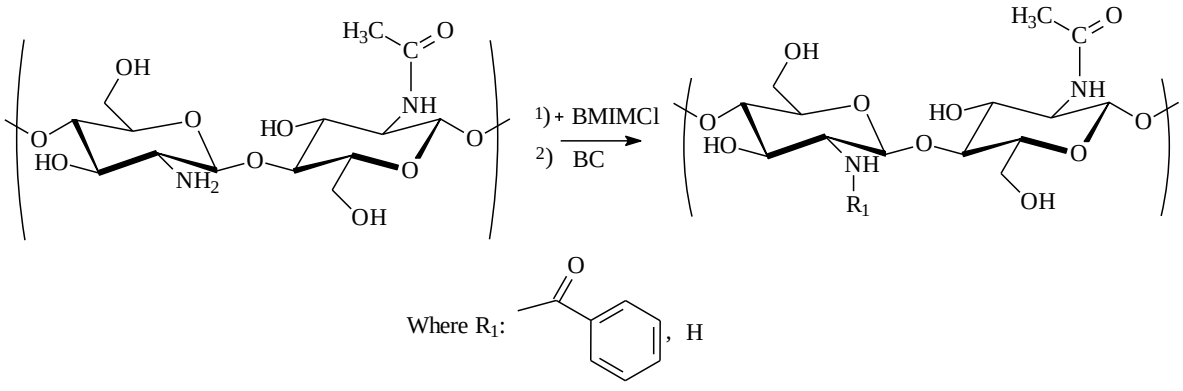

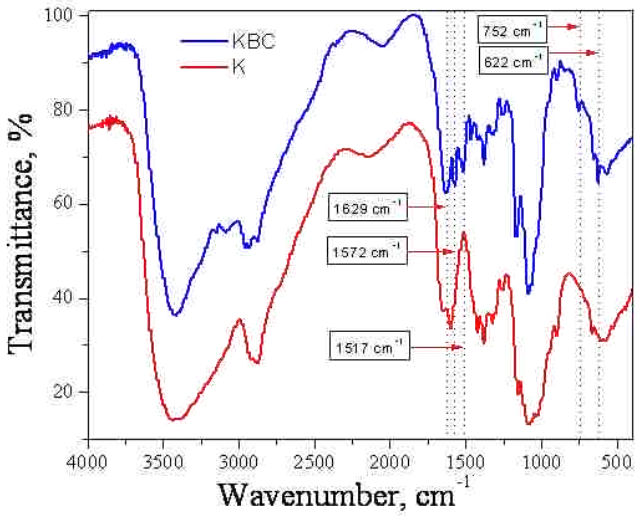

Figure 4.4 FT-IR Spectra of unmodified chitosan (red spectrum), chitosan reacted with benzoyl chloride (blue spectrum).

4.4.3 FT-IR Characterization of Tritylated Chitosan in BMIMCl Ionic Liquid

In the reaction of chitosan with TC (Scheme 4.3), the appearance of new peaks at 1625, 1512, 1164, 759, and 702 cm^{-1} are indicative of the presence of substituted AGU (Figure 4.5). The band at 1625 cm^{-1} is characteristic of the aromatic C=C stretch absorption. The peak at 1164 cm^{-1} is attributed to C-O-C stretching absorption. The absorption band at 1512 cm^{-1} corresponds to –NH bending in secondary amines. Characteristic to monosubstituted aromatic rings are the absorption bands at 759 cm^{-1} and 702 cm^{-1}. These new peaks confirm that the -NH_2 groups from chitosan AGU reacted with TC.

Scheme 4.3 Reaction of trityl chloride with chitosan dissolved in BMIMCl.

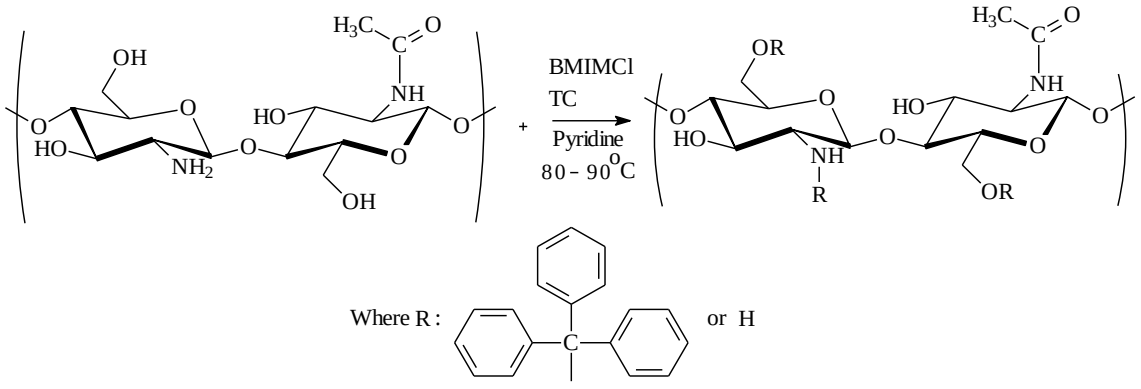

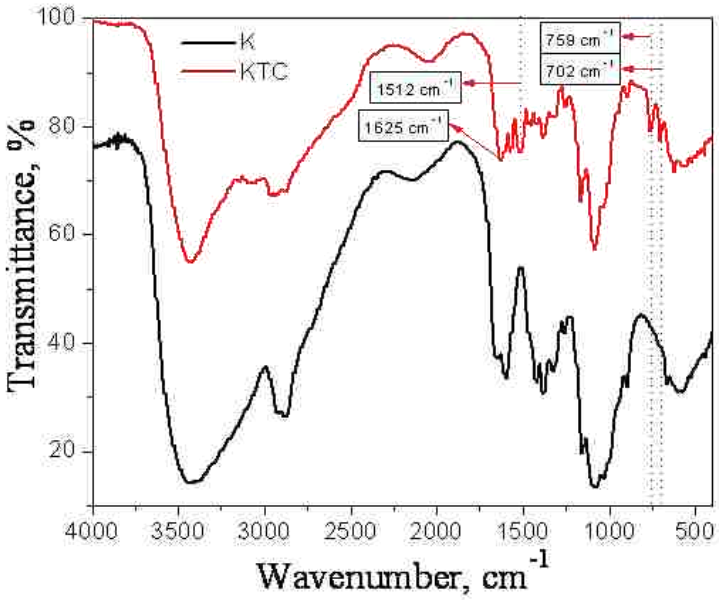

Figure 4.5 FT-IR Spectra of unmodified chitosan (black spectrum), chitosan reacted with trytil chloride (red spectrum).

4.4.4 FT-IR Characterization of Chitosan in BMIMCl Ionic Liquid Reacted Sequentially Either with Phthalic Anhydride and Trityl Chloride or with Trityl Chloride and Phthalic Anhydride

The reaction of chitosan with both PA and TC was performed to improve its organic solubility. The reaction with PA is ideal for protection as well for improving solubility while the reaction with TC is perfect for the regioselective ether protection of primary hydroxyl groups of chitosan or N-phthaloyl chitosan.

Figure 4.6 shows the spectra of chitosan reacted sequentially either with PA and TC [KPATC] or with TC then PA [KTCPA]. The absorption peaks at 1773 cm^{-1} and 1713 cm^{-1} are indicative of the presence of C=O stretch for imides and C=O stretch for esters, respectively. The formation of the ester groups is the result of the reaction of the –OH groups of chitosan with PA while the development of the imide groups is the result of the reaction of $-NH_2$ groups of chitosan with PA followed by cyclization. There are some differences between the two products, KPATC and KTCPA. When the KTCPA sequence is used, the absorption bands at 1773 cm^{-1} and 1713 cm^{-1} are not as intense as when the KPATC sequence is performed. This suggests that the TC reacted with

the $–NH_2$ groups and upon addition of PA, the availability of the $–NH_2$ groups has been decreased. This can be observed by a lower intensity to the corresponding absorption bands. The intensity of the absorption band at 1164 cm^{-1} is much higher in the case of KPATC. PA has reacted first with the $–NH_2$ groups and when the TC was added it has reacted mostly with the –OH groups resulting in a higher intensity for the C-O-C stretching absorption.

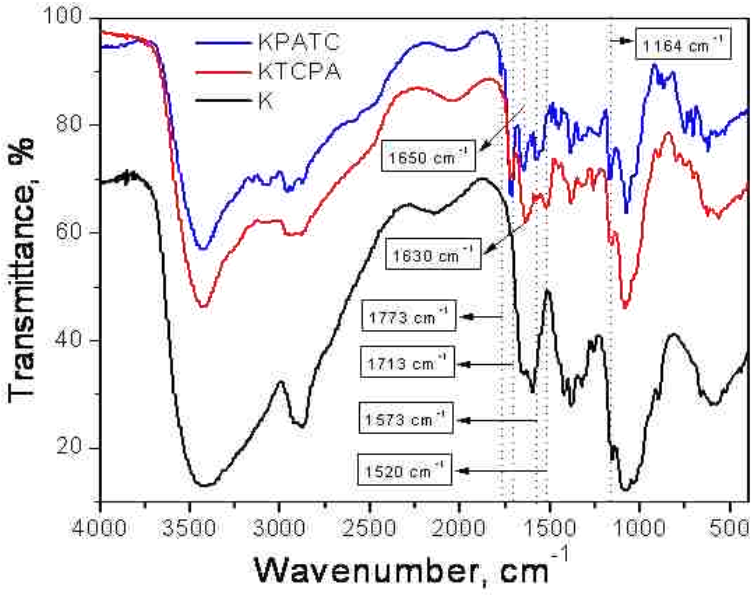

Figure 4.6 FT-IR Spectra of chitosan (black spectrum), chitosan reacted with phthalic anhydride and trityl chloride (blue spectrum), and chitosan reacted with trityl chloride and phthalic anhydride (red spectrum).

4.4.5 FT-IR Characterization of Chitosan in BMIMCl Ionic Liquid Reacted with Phthalic Anhydride in the Presence of a Base (DABCO or Pyridine)

The reaction of chitosan with PA in BMIMCl reported earlier(*139*) did not include a base. Although the reaction of chitosan with PA was confirmed by the FT-IR spectra, the intensities of the carbonyl bands between 1720 cm^{-1} and 1640 cm^{-1} were weak (Figure 4.7). On the other hand, the same reaction conducted in the presence of a base (pyridine) leads to products with stronger absorption bands (Figure 4.7). By increasing the amount of PA while keeping the molar ratio of chitosan to pyridine constant, an increase in the absorption intensities in the FT-IR spectra of the products is observed (Figure 4.7). However, when the amount of PA is kept constant and the molar

ratio of chitosan to pyridine is increased a significant change in the intensity of the peaks of the FT-IR spectra is not noticed (Table 4.1). By enhancing the temperature of reaction from 80°C to 100°C an increase of the intensity peaks of the products is observed (Table 4.3).

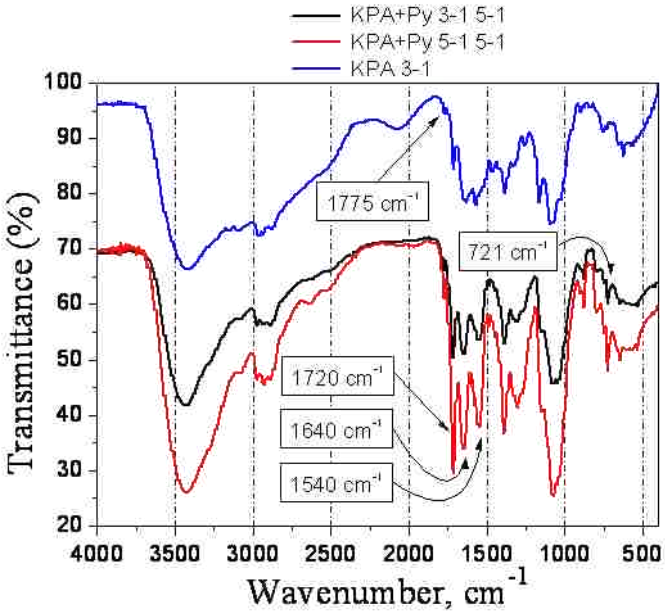

Figure 4.7 FT-IR Spectra of chitosan reacted with phthalic anhydride in a molar ratio of PA: AGU = 3:1 (blue spectrum); chitosan reacted with phthalic anhydride and pyridine in a molar ratio of: PA: AGU = 3:1 and Py: AGU = 5:1 (black spectrum); PA: AGU = 5:1 and Py: AGU = 5:1 (red spectrum).

The FT-IR spectra for the reactions of chitosan with PA in the presence of DABCO using BMIMCl as solvent are presented in Figure 4.8. It can be observed that in the presence of DABCO the absorption intensities are greater than those observed using pyridine. By increasing the amount of the base while keeping the molar ratio of chitosan to PA constant, an increase in the absorption intensities in the FT-IR spectra of the products has been observed (Table 4.2). This trend was not observed when the molar ratio of pyridine was varied while keeping constant the molar ratio of PA to chitosan (Table 4.1). When the films used for the collection of FT-IR spectra were heated to 200°C for 2 hours and spectra were again recorded, an increase in the intensity peaks corresponding to imide (1775 cm^{-1}) and ortho-disubstituted aromatic rings (722 cm^{-1}) and a decrease in the intensity

peaks for carbonyl stretch (1647 cm^{-1}) and N-H bending (1561 cm^{-1}) for amides is observed. This behavior is a result of cyclization with the formation of imide groups (Scheme 4.1).

The DS's of the reaction products calculated using the calibration curves from the previous chapter (Figure 3.12) are presented in Table 4.1 and Table 4.2. It can be observed that higher DS's are obtained in the presence of DABCO.

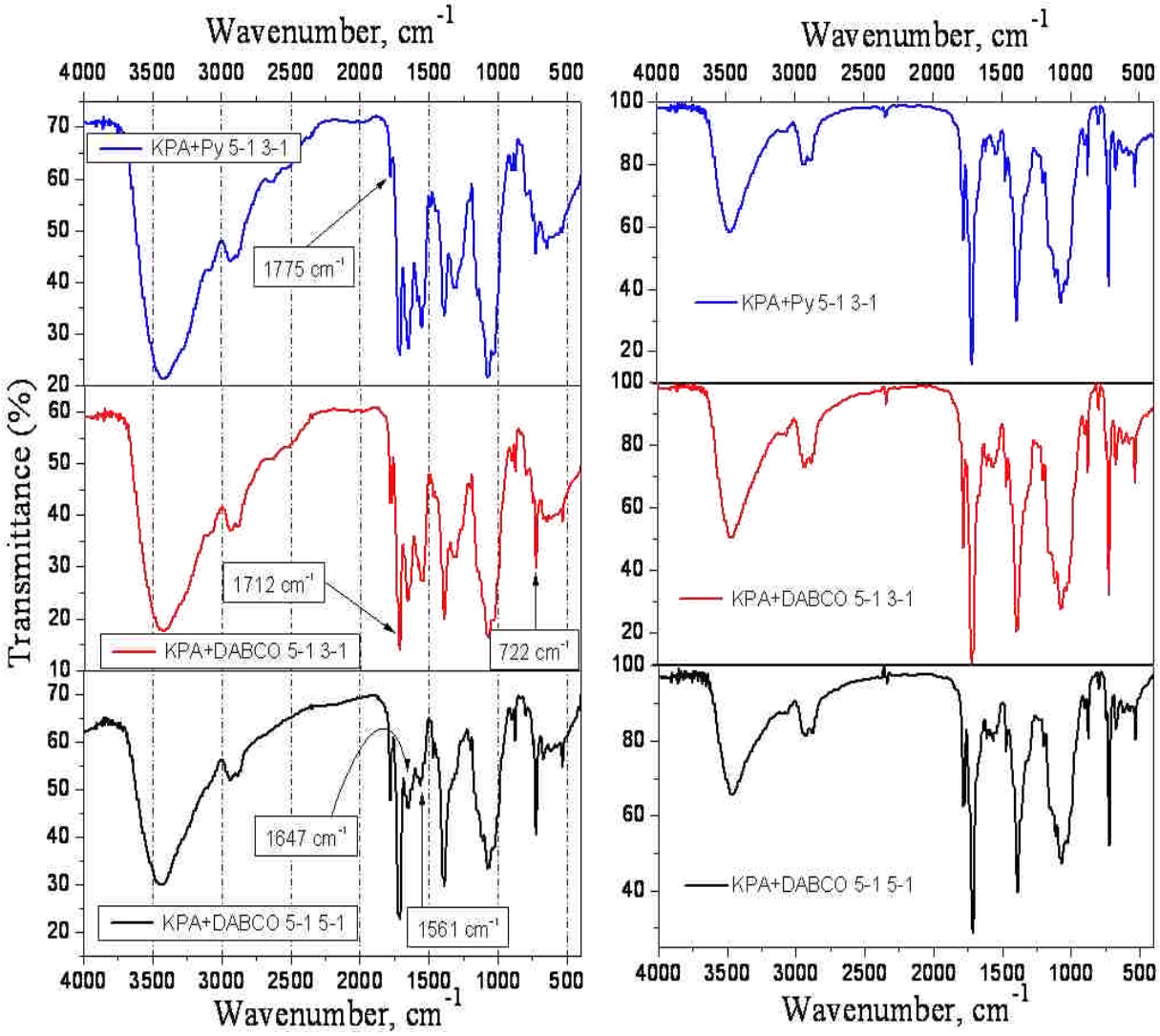

Figure 4.8 FT-IR Spectra of chitosan reacted with phthalic anhydride and pyridine in a molar ratio of PA: AGU = 5:1 and Py: AGU = 3:1(blue spectrum); chitosan reacted with phthalic anhydride and DABCO in a molar ratio of: PA: AGU = 5:1 and DABCO: AGU = 3:1 (red spectrum); PA: AGU = 5:1 and DABCO: AGU = 5:1 (black spectrum). The spectra on the right represent the samples heated at 200°C for 2 hours.

Table 4.1 Ratio of the newly formed absorption peaks in the phthalated K to the C-O-C bridge symmetric stretching (1076 cm^{-1}); the molar ratio of pyridine:K was 3:1, 5:1, and 10:1, respectively, while the molar ratio of PA:K was constant (5:1).

Experiment (4h at 100°C)	imide/CO	DS	Ester/CO	DS	carbox acid/CO	amideII/CO	1380/CO
Exp 120 KPA+Py 5:1 3:1, CL IL	0.15	0.04	0.85	0.26	0.8	0.69	0.63
Exp 91 KPA+Py 5:1 5:1, CL IL	0.16	0.05	0.88	0.27	0.74	0.62	0.65
Exp 121 KPA+Py 5:1 10:1, CL IL	0.2	0.06	0.88	0.28	0.8	0.7	0.7

Table 4.2 Ratio of the newly formed absorption peaks in the phthalated K to the C-O-C bridge symmetric stretching (1076 cm^{-1}); the molar ratio of DABCO:K was 3:1, 5:1, and 10:1, respectively, while the molar ratio of PA:K was constant (5:1).

Experiment (4h at 100°C)	imide/CO	DS	Ester/CO	DS	carbox acid/CO	amideII/CO	1380/CO
Exp 126KPA+DABCO 5:1 3:1, CL IL	0.29	0.09	1.15	0.42	0.75	0.62	0.86
Exp 127KPA+DABCO 5:1 5:1, CL IL	0.52	0.17	1.49	0.59	0.57	0.45	1.16
Exp 135 PA+DABCO 5:1 10:1, CL IL	0.44	0.14	1.29	0.49	0.62	0.59	1.12

Table 4.3 Ratio of the newly formed absorption peaks in the phthalated K to the C-O-C bridge symmetric stretching (1076 cm^{-1}); the molar ratio of both pyridine:K and PA:K was 5:1; temperatures of 80°C and 100°C were used for reactions.

Experiment 4h	imide/CO	ester/CO	carbox acid/CO	amideII/CO	1380/CO
Exp 138 KPA+Py 5:1 5:1, CL IL (80°C)	0.1	0.67	0.86	0.77	0.61
Exp 91 KPA+Py 5:1 5:1, CL IL (100°C)	0.16	0.88	0.74	0.62	0.65

4.4.6 Solid State ^{13}C NMR Measurements

The ^{13}C NMR (700 MHz; DMSO-d_6) resonances of the BMIMCl ionic liquid are: δ_C: 136.9 (N<u>C</u>HN), 123.3 (N<u>C</u>HCHNCH$_3$), 122.2 (CH$_3$N<u>C</u>HCHN), 48.1 (N<u>C</u>H$_2$(CH$_2$)$_2$CH$_3$), 35.6 (N<u>C</u>H$_3$), 31.4 (NCH$_2$<u>C</u>H$_2$CH$_2$CH$_3$), 18.5 (NCH$_2$CH$_2$<u>C</u>H$_2$CH$_3$), 12.8 (NCH$_2$CH$_2$CH$_2$<u>C</u>H$_3$). These results are in agreement with the data obtained from ACDLabs CNMR Predictor.

The solid state ^{13}C NMR spectrum of pure chitosan is presented in Figure 4.9. The chemical shifts between 50 ppm and 110 ppm are attributed to the 6 carbons of the glucosamine units of chitosan. The small peaks at 21.1 ppm and 171.5 ppm correspond to the methyl carbon and the carbonyl carbon of the amide functionality. These results are in agreement with those obtained by Paulino and Heux.(*140-141*) Because of the high degree of deacetylation of chitosan (82% calculated by NMR and 85% calculated by FT-IR) the resonances assigned to the N-acetyl-glucosamine (171.5 ppm) units could hardly be observed.

The solid-state ^{13}C NMR spectrum of chitosan reacted with trityl chloride, benzoyl chloride, phthalic anhydride, KTCPA, and KPATC are presented in Figure 4.10 - Figure 4.14. In all the spectra the presence of the four peaks at around 11 ppm, 17 ppm, 30 ppm, and 35 ppm indicates that traces of BMIMCl solvent are still present in the reaction products. The spectrum of chitosan reacted with trityl chloride (Figure 4.10) shows the presence of new peaks at 122.2 ppm and 134.8 ppm which are attributed to the carbons in aromatic rings. This indicates that the trytil chloride reacted with the chitosan. However, the small intensity of the aromatic peaks points out that a very low degree of substitution of chitosan was achieved. The solid-state ^{13}C NMR spectrum of chitosan reacted with benzoyl chloride (Figure 4.11) shows a similar pattern with the one for Figure 4.10 indicating that benzoyl chloride reacted with chitosan but not to a great extent. When chitosan is reacted with phthalic anhydride the solid-state ^{13}C NMR spectrum illustrates (Figure 4.12) the presence of more new peaks. The peak at 128.7 ppm corresponds to the aromatic ring carbons while the peak at 167.2 ppm corresponds to the carbonyl groups in acids, esters, and amides. It can be said that both the –OH and $-NH_2$ groups of chitosan have been reacted with phthalic anhydride due to the broad peak at 167.2 ppm which is attributed to an overlapping of ester, amide, and imide carbonyl and carboxyl groups. By looking at the intensity of the newly formed peaks and comparing to those corresponding to chitosan spectrum, it can be concluded that a much higher degree of substitution

took place in the reaction of chitosan with phthalic anhydride than in those with trityl chloride or benzoyl chloride.

The solid-state ^{13}C NMR spectrum of KTCPA shows a similar pattern with the one of KPATC exception being the intensity of the peaks (Figure 4.13 and Figure 4.14). The peaks at 128.6 ppm and 167.2 ppm (or 170.5 ppm) are indicative of the reaction of both functional groups of chitosan, $-NH_2$ and –OH, with the two reagents (trityl chloride and phthalic anhydride). However, the intensity peaks for the KTCPA are significantly lower than those for the KPATC. This can be explained by the fact that when chitosan is first reacted with trityl chloride (Figure 4.10) not a significant degree of substitution is being observed. When next it is time for the phthalic anhydride to react (Figure 4.13), its accessibility to the functional groups of chitosan is impeded to some extent due to the presence of the big molecules of trityl chloride existent in the system as well. In the case of KPATC (Figure 4.14), the phthalic anhydride molecules are not hindered anymore and a higher degree of substitution can occur and the solid-state ^{13}C NMR spectrum shows higher intensity peaks at 128.7 ppm and 167.2 ppm.

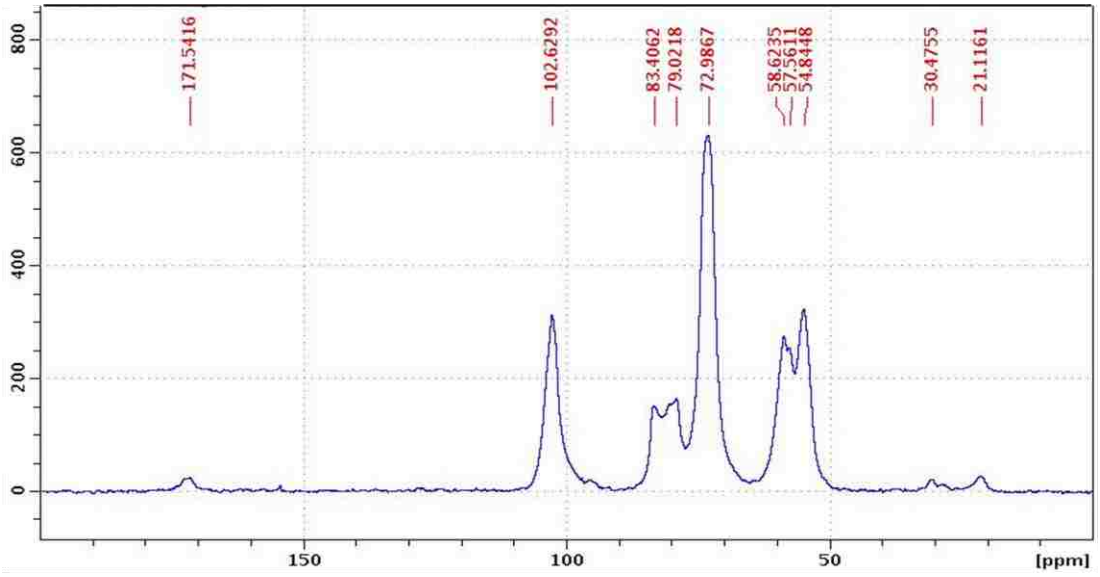

Figure 4.9 Solid-state ^{13}C NMR spectrum of chitosan powder.

The free hydroxyl groups at C-3 and C-6 and the free amino group at C-2 positions are the main reactive sites in chitosan. As shown in Figure 4.10 – Figure 4.14, the intensity of the signal at 54.8 ppm for C-2 decreased after the reaction with BC, PA, TC, KPATC, or KTCPA indicating that the reactions took place at the amino groups of chitosan. The intensity signal at 72.9 ppm for C-6 decreased as well indicating the reaction with the primary hydroxyl groups of chitosan.

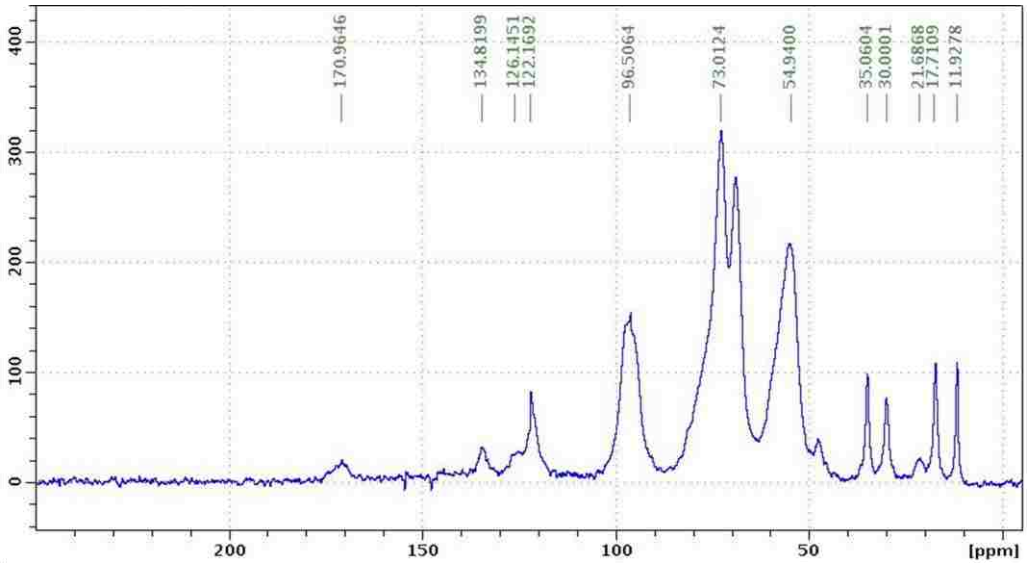

Figure 4.10 Solid-state ^{13}C NMR spectrum of chitosan reacted with trityl chloride.

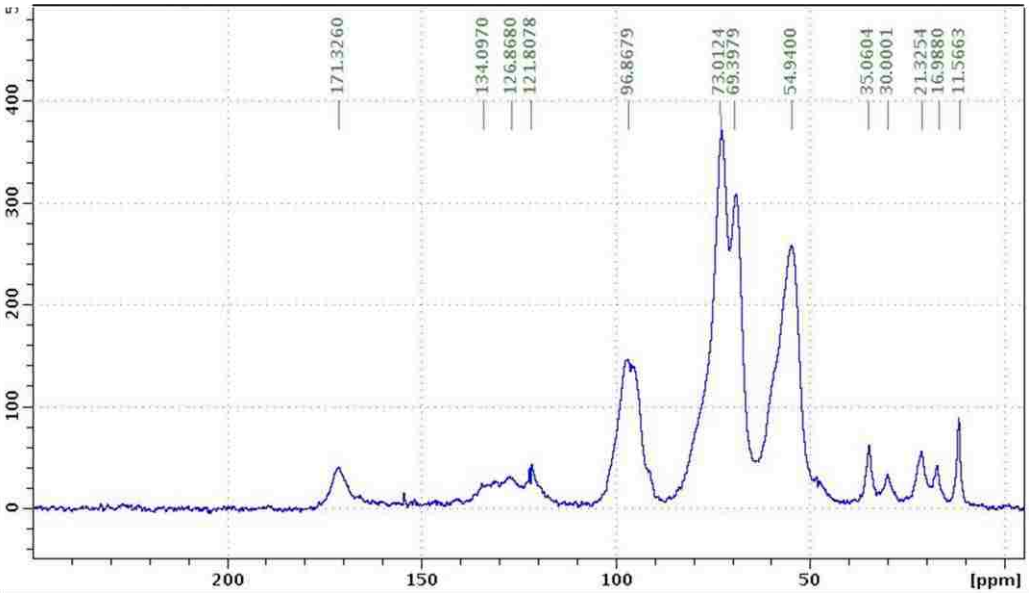

Figure 4.11 Solid-state ^{13}C NMR spectrum of chitosan reacted with benzoyl chloride.

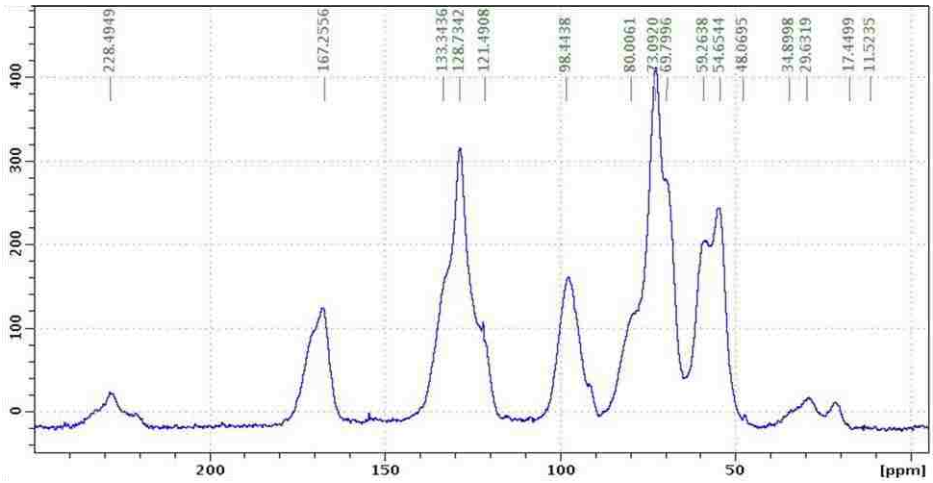

Figure 4.12 Solid-state ^{13}C NMR spectrum of chitosan reacted with phthalic anhydride.

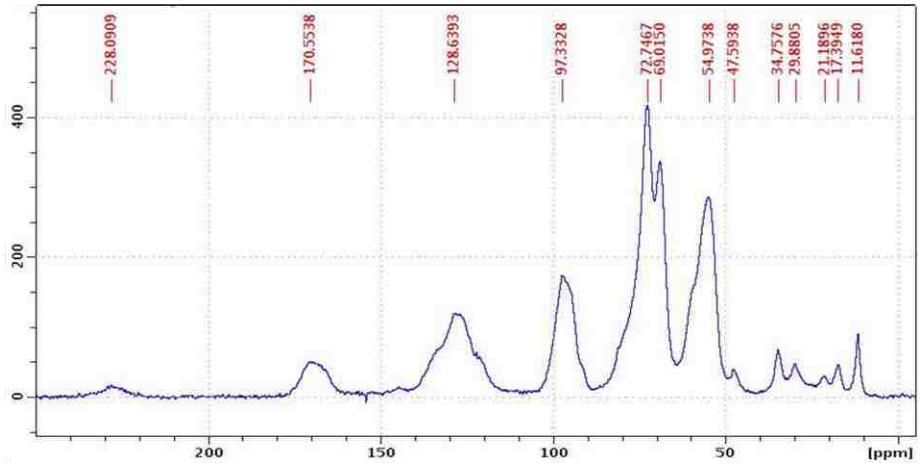

Figure 4.13 Solid-state ^{13}C NMR spectrum of chitosan reacted with trityl chloride and phthalic anhydride.

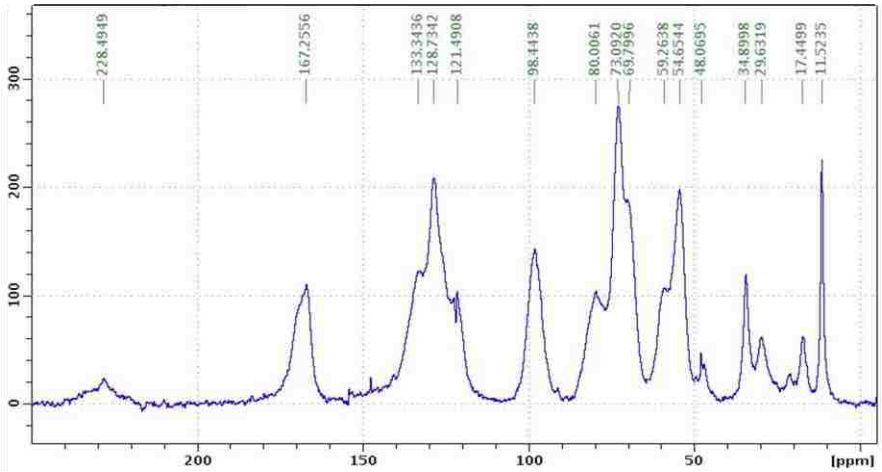

Figure 4.14 Solid-state ^{13}C NMR spectrum of chitosan reacted with phthalic anhydride and trityl chloride.

4.4.7 TGA/DSC Measurements

The thermal behavior of chitosan, K+BC, K+TC, K+PA, KTCPA, and KPATC were analyzed by TGA in N_2. Reaction of chitosan with both BC and PA reduced the thermal stability of reaction products. Phthalated chitosan degraded in two steps, clearly shown both by TG and DTG curves (Figure 4.15). The onset temperatures of degradation were 185^{o}C (chitosan reacted with BC), 191^{o}C and 225^{o}C (phthalated chitosan) and 264^{o}C for chitosan, with maximum rates (DTG) at 200^{o}C (chitosan reacted with BC), 207^{o}C and 234^{o}C (phthalated chitosan, showing perhaps degradation of amide and imide substituted species) and 289^{o}C (chitosan). The weight loss followed the same trend, viz., at 250^{o}C the reacted chitosan with BC lost already 46% of the initial weight and phthalated chitosan lost 30%, while chitosan was still 86% undegraded. However, as temperature increased, the amounts of residual fractions seemed to come closer, i.e., at 450^{o}C residual weights were 42%, 38% and 36% for chitosan, phthalated chitosan, and chitosan reacted with BC, respectively.

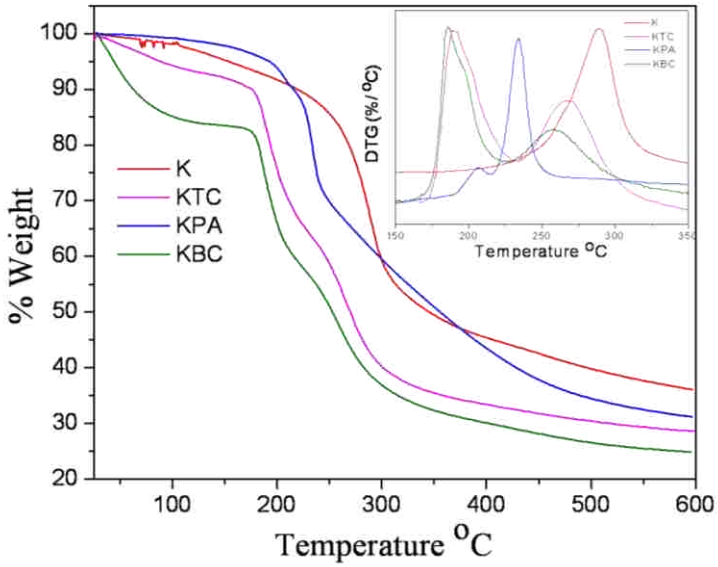

Figure 4.15 Thermogravimetric traces (TG) and corresponding derivatives for K, KPA, KBC, and KTC samples.

Thermogravimetric data for chitosan and for reaction products with TC and PA are compared in Table 4.4 and Figure 4.15 and Figure 4.16. Besides the nature of the reagent (TC or PA), the reaction

order with chitosan seems to have an equal influence on the thermal stability of the reaction products. According to data collected in Table 4.4, the first to decompose were the ether bonds formed by TC at a temperature as low as 175^{o}C (DTA peak at 190^{o}C), illustrated also by the first DTA peak occurring at 193^{o}C in Figure 4.15. The subsequent temperatures refer to decomposition of PA reacted products and unsubstituted chitosan fractions. If one compares the residual weights at 300^{o}C and 600^{o}C, the K+TC seems to be more stable than the K+PA product, with data close to that of unreacted chitosan (Table 4.4). However, when just the order of reaction is considered, the least stable was the KPATC sample, which exhibited the smallest residual weight at 300^{o}C and 600^{o}C, although up to 250^{o}C both KPATC and KTCPA samples experienced the same weight loss (- 42%, Figure 4.16).

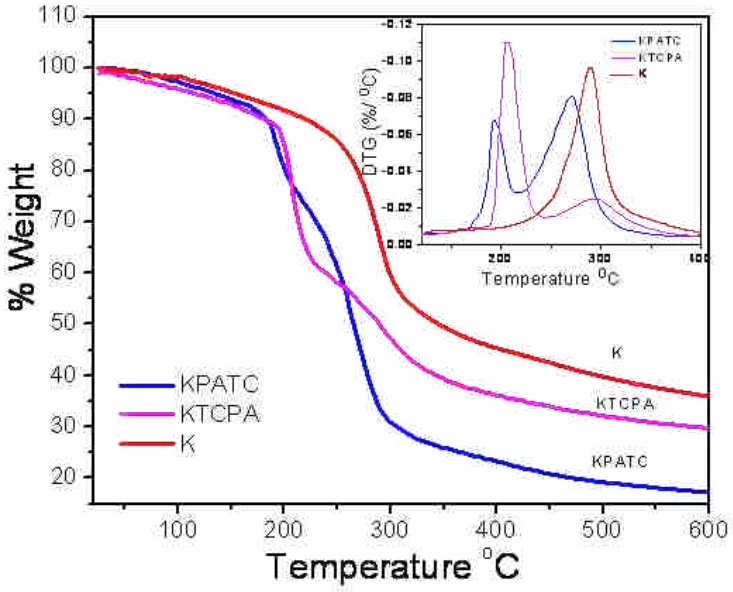

Figure 4.16 Thermogravimetric traces (TG) and corresponding derivatives for K, KPATC and KTCPA samples.

The reaction of chitosan with phthalic anhydride in the presence of either DABCO or pyridine improved the thermal stability of the corresponding products (Table 4.5 and Table 4.6). It can be observed that when chitosan is regenerated from the ionic liquid its thermal stability is considerably reduced. For example at 300^{o}C the pure chitosan lost 27.9% while at the same

temperature the regenerated chitosan already lost 44% of its initial weight. The higher amount of weight loss for the regenerated chitosan may be attributed to residual BMIMCl ionic liquid still present in the product. The lower onset temperature for regenerated chitosan when compared to that of pure chitosan is attributed to the degradation of the polymer during the dissolution process. All the reaction products presented in Table 4.5 and Table 4.6 showed an improved onset decomposition temperature and an increased thermal stability up until 350^{o}C when compared with both the regenerated chitosan and the pure chitosan.

Table 4.4 Thermogravimetric data for chitosan and for reaction products with TC and PA.

SAMPLE	Onset Decomposition Temperature(s), °C	DTA Peak(s) Temp, °C	Weight at 300°C (%)	Weight at 600°C (%)
K	264	289	60	36
K+TC	175, 249	190, 266	60	31
K+PA	191, 225	207, 234	40	29
KTCPA	196, 271	206, 294	48	34
KPATC	187, 248	193, 270	34	21

Table 4.5 Thermogravimetric data for chitosan, regenerated chitosan from BMIMCl ionic liquid, chitosan reacted with phthalic anhydride in the presence of DABCO when the molar ratio of PA:AGU was kept constant while varying the DABCO:AGU molar ratio from 3:1, 5:1, to 10:1.

Sample	Onset temperature °C	300°C Weight%	325°C Weight%	350°C Weight%	400°C Weight%
Chitosan	277.55	72.1	56.2	50.8	44.7
Regenerated chitosan	225.31	56	51.4	47.8	43.6
KPA+DABCO 5:1 3:1, CL IL	265.68 292.94	87.9	79.5	66.4	36.9
KPA+DABCO 5:1 5:1, CL IL	236.5 291.34	84.8	74.2	54.4	39.9
KPA+DABCO 5:1 10:1, CL IL	250.29 287.81	82.7	74.9	65.1	32.2

Table 4.6 Thermogravimetric data for chitosan, regenerated chitosan from BMIMCl ionic liquid, chitosan reacted with phthalic anhydride in the presence of pyridine when the molar ratio of PA:AGU was kept constant while varying the pyridine:AGU molar ratio from 3:1, 5:1, to 10:1.

Sample	Onset temperature ^{0}C	300^{0}C Weight%	325^{0}C Weight%	350^{0}C Weight%	400^{0}C Weight%
Chitosan	277.55	72.1	56.2	50.8	44.7
Regenerated chitosan	225.31	56	51.4	47.8	43.6
KPA+Py 5:1 3:1, CL IL	286.21	88.2	68	50	38.2
KPA+Py 5:1 5:1, CL IL	299.06	91	84.3	70.6	40.4
KPA+Py 5:1 10:1, CL IL	289.57	91.5	80	65.5	33.9

The weight loss up to 150^{o}C of the reaction products is attributed to the loss of water as a result of cyclization and formation of imide groups as confirmed by the FT-IR studies. Differential scanning calorimetry (DSC) measurements (Figure 4.17) were in agreement with this assumption. Fresh and dried samples were used for a first heating run to 150^{o}C followed by cooling to 25^{o}C and a second heating run to 150^{o}C. On the second heating run no endothermic peak was observed which suggests complete cyclization on the first heating run to 150^{o}C which showed an endothermic peak around 85^{o}C.

The onset temperature of degradation for chitosan is at 277.5^{o}C with maximum rates (DTG) at 90^{o}C and 300^{o}C. Even if the chitosan was dried at 80^{o}C for 48h before performing the TGA analysis, some water still exists in the chitosan structure. The polysaccharides have strong affinity for water due to their primary and supramolecular structures.(*142*) The high amount of hydroxyl and amino groups present in the chitosan structure are responsible for the strong water mediated hydrogen bonds, water which can not be completely removed simply by drying the sample at 80^{o}C

or in desiccators.(*143*) Going to temperatures above 100°C, the water is forced out from the polymer network. This is evidentiated by a decrease in weight loss (12%) of chitosan at 90°C. A second degradation step can be observed for chitosan at 277.5°C and is attributed to the decomposition of chitosan molecules.

The DSC thermograms of unmodified chitosan and phthalated chitosan have shown that even after successive cycles of heating and cooling, the hydrophilic groups in the amorphous regions of chitosan are associated with water (Figure 4.17).(*143*)

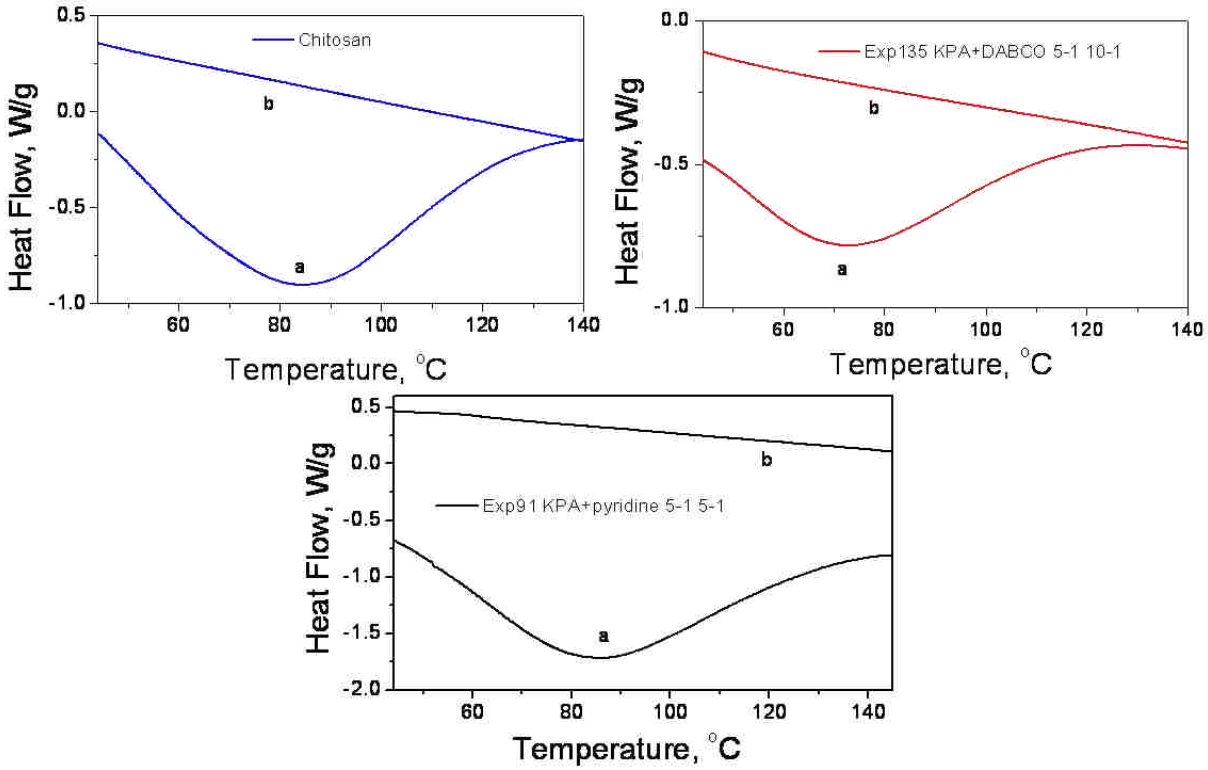

Figure 4.17 DSC thermograms of chitosan, chitosan reacted with phthalic anhydride (PA:AGU = 5:1) in the presence of pyridine (pyridine:AGU = 5:1) or DABCO (DABCO:AGU = 10:1). Thermogram *a* corresponds to the first heating run to 150°C with an isothermal for 20 minutes, whereas thermogram *b* corresponds to the second heating scan to 150°C recorded immediately after the first run.

CHAPTER 5 . BIOCOMPOSITE FILMS PREPARED FROM IONIC LIQUID SOLUTIONS OF CHITOSAN AND CELLULOSE

5.1 Objective of Study

Blending of polymers to improve their chemical and physical properties has been received a great attention in the past years.(*144-150*) When mixed in a common solvent, polymers may form a homogeneous solution. Fibers or films obtained from homogeneous solutions of two mixed polymers have reasonable physical properties as well as some other characteristics of both polymeric components.

Due to its chemical properties, chitosan is a widely investigated polymer but the physical properties of fabricated products are not satisfactory. Therefore incorporating chitosan into polymer blends is frequently used to obtain new materials with better mechanical and thermal stability. The thermal stability of the blends depends strongly on the compatibility of the polymers.(*151*)

The present investigation reports the formation of chitosan-cellulose blends in 1-butyl-3-methylimidazolium acetate (BMIMAc) ionic liquid and preparation of films from the polymeric solutions. Since the molecular structure of chitosan and cellulose are very similar, it is expected that the blend films to have high compatibility and miscibility. To the best of our knowledge, there are no reports regarding the simultaneous dissolution of both cellulose and chitosan polymers in the same ionic liquid.

5.2 Experimental

5.2.1 Materials

All chemicals were used as received from the vendors, without any further purification. 1-Butyl-3-methylimidazolium acetate (BMIMAc) and chitosan, with a Brookfield viscosity of 200K cps, were purchased from Sigma Aldrich Chemical Company. The cellulose used was a pulp powder

with a degree of polymerization of 670, and was a gift from Buckeye Tech. Inc. (Memphis, TN). Both chitosan and cellulose were dried over night at 90^{o}C and used without any further purification.

5.2.2 Instrumentation

Rheological measurements of the polymeric solutions were performed on a TA AR 1000 instrument (TA Instruments, Inc., New Castle, DE). A parallel-plate geometry with a diameter of 40 mm and a gap of 800 μm was used for all determinations. The instrument was equipped with an argon chamber to prevent hydroscopic absorption of atmospheric water leading to the precipitation of the polymers during the measurements. All rheological measurements were conducted using a temperature ramp step program and at a low shear rate (1/s).

A Labconco Freeze Dryer was used to freeze dry the wet polymeric films after they were previously frozen using liquid nitrogen. A high vacuum (0.010 mBar) and a temperature of -89^{o}C were employed during the drying process. The samples were allowed to rest at these conditions for 24 hours.

FT-IR spectra of the freeze-dried polymeric blends were recorded on a ThermoNicolet 300 Fourier Transform Infrared spectrometer using a KBr disc containing 1% of very fine ground samples. One hundred scans were taken for each sample in the range of 4000-400 cm^{-1} at a resolution of 4 cm^{-1} in the transmission mode.

Modulated thermogravimetric analyses (MTGA) of polymeric films were performed on a TA Instruments TGA 2950 thermobalance under nitrogen using the following program: 1) High resolution sensitivity 1; 2) Modulate +/- 5^{o}C every 200 seconds; and 3) Ramp 2.00^{o}C/min res 4 to 600^{o}C. This technique facilitates calculation of the activation energy of different processes involved in the degradation of a material from a single experiment. This is done by using an oscillatory temperature program to obtain kinetic parameters during a mass loss. Isothermal TGA of polymeric films was performed on ~2mg samples. The samples were heated under nitrogen from ambient

temperature to the isothermal temperature at a heating rate of $10^{o}C\ min^{-1}$ before being held in isothermal mode at T = $200^{o}C$ for 5 hours. The polymeric films were previously dried at $50^{o}C$ before performing the TGA analyses.

Scanning electron microscopy (SEM) measurements were made using a Hitachi S-3600N microscope with a voltage of 15 kV. Prior to SEM measurements the samples were freeze-fractured in order to expose the edge of the film and sputter-coated with a thin layer of gold.

The X-ray diffraction measurements of sample foams were made using a Siemens-Bruker D5000 X-ray diffractometer with a Cu K_{α} radiation of 1.54 Å. Diffraction patterns were collected from $2\theta = 2$ to 35^{o} with steps of 0.02^{o} and a scan time of 2 s per step. Samples were dried at $50^{o}C$ before each measurement. Powdered samples of cellulose and chitosan were examined as reference materials.

5.2.3 Preparation of Biocomposite Films

The dissolution of chitosan or cellulose in the 1-butyl-3-methylimidazolium acetate (BMIMAc) ionic liquid was performed by adding the material to a vial under argon followed by heating to 85^{o}-$95^{o}C$ and using an overhead mixer (Figure 5.1). The dissolution time varied with the percentage and the type of polymer added to the ionic liquid. The dissolution time allotted for chitosan was about 3 to 4 days while the time for the cellulose dissolution was 12 hours. Six distinct solutions were prepared using chitosan and/or cellulose with a total concentration of 6wt%. Two solutions were made of either neat chitosan or neat cellulose, while the other four solutions were blends of the neat solutions with chitosan-to-cellulose weight percent ratios of 5:95, 10:90, 25:75, and 50:50, respectively. The blends were obtained by mixing the cellulose and chitosan solutions in a glove box to prevent the exposure to moisture. Next, the blend solutions were mixed manually under argon with a spatula every 4-6 hours for 2 days. Between the mixing processes the vials were kept in an oven at $50^{o}C$. Homogeneous, transparent, and viscous solutions were obtained after the

complete dissolution of the polymers. Figure 5.3 displays pictures of the vials containing these polymeric solutions. It can be observed that all solutions, containing chitosan-cellulose blends, cellulose or chitosan are clear and transparent as opposed to the polymeric-BMIMAc slurries prior to dissolution (Figure 5.2). Films were prepared from each composition by manually spreading the solutions on a flat Teflon surface with a glass rod. The thickness of the spreading was kept constant at 1.5 mm. Following the spreading of solutions, the Teflon surface was dipped into a (50:50 by vol.) mixture of methanol and water to precipitate the films. The crude films (Figure 5.4) were washed several times with methanol and water and finally just with distilled water. In order to prevent the shrinkage of films, most of the absorbed water was removed by freeze drying under vacuum (Figure 5.5). Finally the films were stored in desiccators to remove the traces of water.

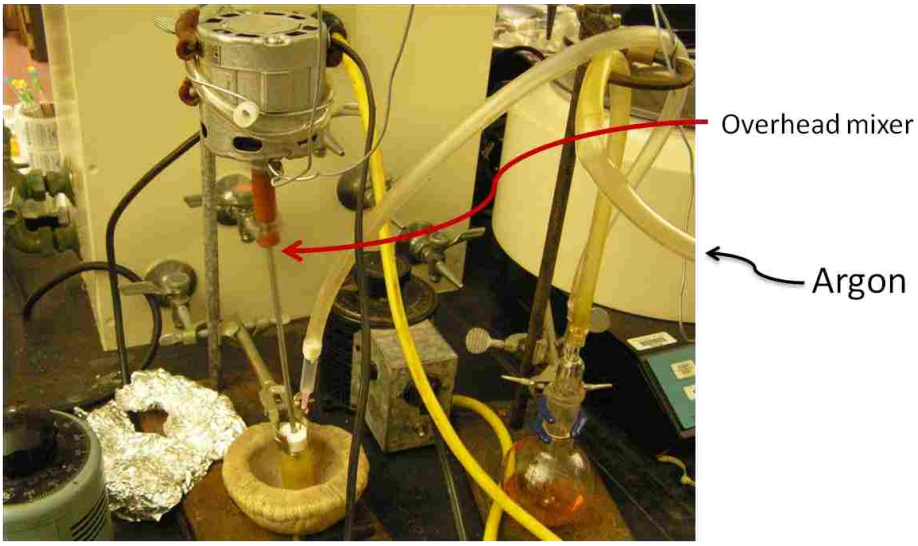

Figure 5.1 Dissolution of polymer (cellulose or chitosan) using an overhead mixer and heating to 85-95^{o}C.

Figure 5.2 Slurries of chitosan (187) and cellulose (188) in BMIMAc before dissolution.

Figure 5.3 Polymeric solutions containing chitosan and/or cellulose dissolved in BMIMAc.

Figure 5.4 Polymeric films before freeze drying (from left to right: cellulose film, chitosan film, chitosan 5 wt%-cellulose 95 wt% film, and chitosan 50 wt%-cellulose 50 wt% film).

Figure 5.5 Polymeric films containing chitosan and/or cellulose obtained by freeze drying technique.

5.3 Results/Discussion

5.3.1 Rheological Measurements of Polymeric Solutions

The relationship between shear viscosity (determined at a constant shear rate) and temperature for chitosan-cellulose blends and the pure components is illustrated in Figure 5.6. It can be observed that the viscosity of the solutions decreases as the temperature increases. At room temperature the molecules are tightly bound together by attractive intermolecular forces which are responsible for the viscosity of the solutions. When the temperature is increased, the thermal energy of the molecules is increased and the molecules become more flexible by overcoming the intermolecular forces within the liquid. As a result the viscosity of the solutions is decreased as the attractive binding energy is reduced.

The intermolecular forces within the 6 wt% chitosan solution seem to be the strongest ones as indicated by its high viscosity of 1037 Pa·s (at 31^{o}C) (Figure 5.6). The viscosity of the 6 wt% cellulose solution (472 Pa·s) at 31^{o}C is less than half of that of the chitosan solution. The solutions comprising both chitosan and cellulose with chitosan-to-cellulose weight percent ratios of 5:95, 10:90, 25:75, and 50:50, respectively showed a viscosity at 31^{o}C that is very close to that of the cellulose solution: 429, 424, 414, and 455 Pa·s, respectively. In the case of the solution containing 50:50 wt% chitosan: cellulose, one would expect a viscosity somewhere in between the viscosity of the chitosan and cellulose solutions. Instead, its viscosity is even lower than that of the cellulose solution. This behavior may be explained by the formation of a complex between the chitosan and cellulose molecules. The complex reduces the hydrodynamic radius leading to a solution with a much lower viscosity. As the temperature is increased, the viscosity of the solutions drops to a limiting value. For example, at 100^{o}C the viscosities of chitosan, cellulose, and 5:95, 10:90, 25:75, and 50:50 chitosan: cellulose blends were found to be 86, 11, 10, 10, 12, and 11 Pa·s, respectively.

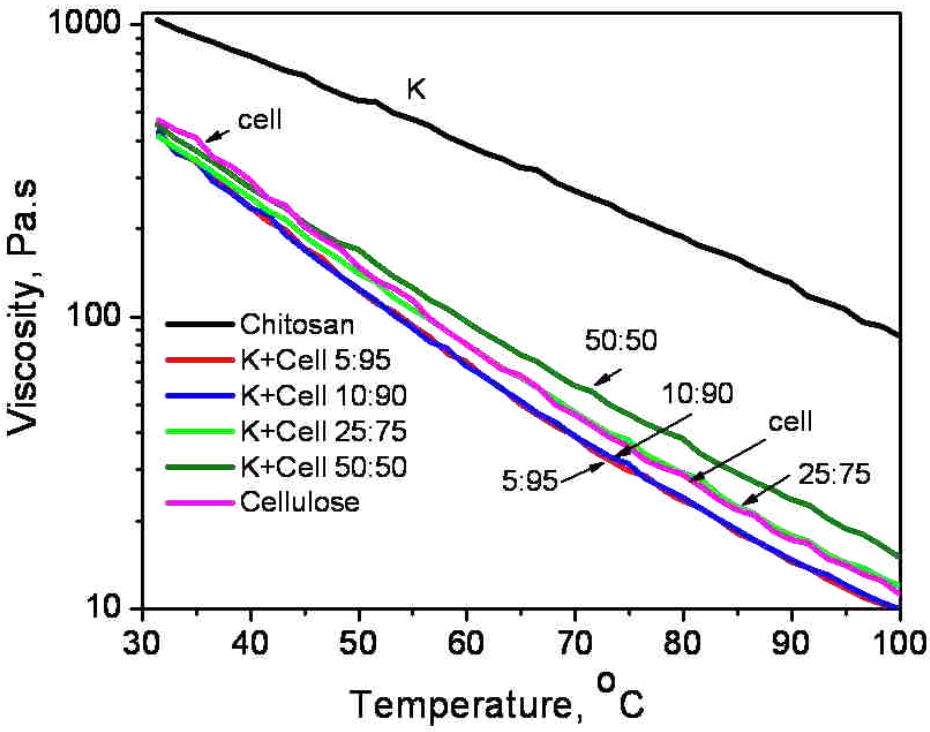

Figure 5.6 The relationship between the apparent viscosity and the temperature of the blended mixtures at a constant shear rate.

5.3.2 FT-IR Analysis of Polymeric Films

Formation of homogeneous chitosan and cellulose blends is a result of strong interactions via hydrogen bonds between the functional groups of the blend components. FT-IR spectroscopy was used to examine these interactions between chitosan and cellulose. The results of the FT-IR spectra of the chitosan-cellulose blends are presented in Table 5.1 and Figure 5.7. Table 5.1 shows that the characteristic bands of chitosan and cellulose are present in the spectra of their blends, and the intensities of the bands vary depending on their composition in the mixture. The spectrum of cellulose film shows similar bands to that of chitosan film except for the absorption band at 1597 cm^{-1} (Table 5.1). The absorption band of chitosan at 1659 cm^{-1} corresponds to carbonyl stretch in amides. The shifting of the carbonyl band to a lower frequency indicates that these groups are involved in H-bonding with cellulose functional groups. The presence of only one peak for the blends containing 5% and 10% chitosan with its value shifted to a lower frequency may indicate the

formation of a complex between the 2 polymers. The –NH bending in amide and amines is not observed anymore for these 2 polymeric films because the band was shifted to a higher frequency overlapping with the carbonyl stretch in amides. This shifting to a higher frequency indicate that the –NH groups of chitosan are involved in hydrogen bonding with the functional groups of cellulose, leading to a good miscible film. Xu and coworkers had reported a similar shift of the amino-group band of chitosan from 1578 cm^{-1} to 1584 cm^{-1} in the composite films with starch, a shift which the authors attributed to the interaction between the component polymers confirming their molecular miscibility.(*144*)

Table 5.1 FT-IR absorption of polymeric blends (chitosan-cellulose).

	Chitosan	5:95	10:90	25:75	50:50	Cellulose
A	3430	3434	3436	3427	3428	3430
B	2919	2920	2920	2920	2919	2919
C	1659	1637	1629	1636	1643	1637
D	1597	-	-	1565	1565	-
E	1422	1425	1425	1425	1422	1422
F	1378	1375	1377	1377	1378	1374
G	1154	1158	1159	1157	1156	1158
H	1072	1067	1067	1069	1069	1067

where:

A = -OH and –NH stretching

B = -CH stretching

C = C=O stretching (amide I), water in the amorphous region

D = -NH bending (amide II)

E = -CH and -NH vibrations

G = Anti-symmetric stretching of the C-O-C bridge

H = Skeletal vibrations involving the C-O stretching

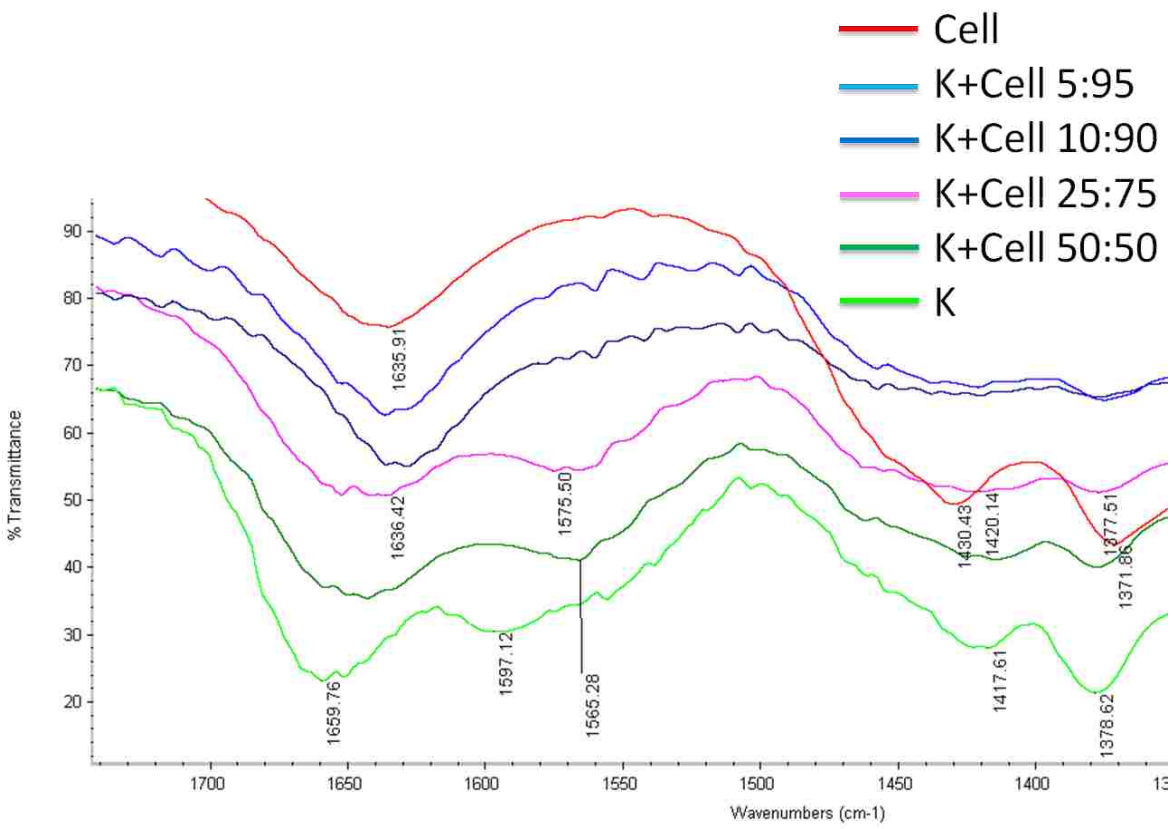

Figure 5.7 FT-IR spectra of chitosan-cellulose blends.

5.3.3 TGA Analysis of Polymeric Films

An investigation of the thermal behavior of the six polymeric films revealed weight loss values between 5–8 wt% up to 150^{o}C that were attributed to the loss of water (Figure 5.8 and Table 5.2). The thermal degradation of chitosan film consists of a thermal event that starts at 251^{o}C with the maximum rate at 268^{o}C and it is related to the depolymerisation of chitosan chains. The thermal event of cellulose is observed at 303^{o}C with a maximal rate at 328^{o}C. As indicated by derivative traces (DTG) plotted in Figure 5.9, the maximum decomposition rates were recorded at 268^{o}C for neat chitosan, 328^{o}C for neat cellulose, 324^{o}C for the samples made of chitosan-cellulose 5:95%

(w/w) and 10:90%, 273^{o}C and 322^{o}C for chitosan-cellulose 25:75%, and 270^{o}C and 316^{o}C for the sample made of chitosan-cellulose 50:50% (w/w). The DTG degradation profile of the films cast from the solutions containing chitosan-cellulose 5:95% and 10:90% (w/w) display only one peak that has an intermediate value between the peaks corresponding to chitosan and cellulose. The presence of only one maximum rate of degradation (mono-modal peak) for these blends, with the DTG peak shifted to a lower temperature as compared to the peak temperature of neat cellulose, may be indicative of interactions between the two polymers and could be considered as proof of their molecular miscibility. However, in the case of chitosan-cellulose 25:75% and 50:50% (w/w) films, two maximum rates of degradation took place. Neither of these values matches the temperatures of peak decomposition rates of neat polymers, being slightly shifted from the peak temperatures recorded for the pure polymers. This behavior may be explained by a partial miscibility of chitosan and cellulose. It is observed in Table 5.2 that the temperature of the blends where the decomposition starts (onset temperature) decreases with the content of chitosan present in the blends. TGA analyses for physical mixtures of the 2 polymers, chitosan and cellulose, were also performed (Figure 5.10). From the graph it can be seen that the 10:90% chitosan-cellulose physical mixture shows the presence of 2 maximum peaks of degradation as opposed to one peak of degradation for the 10:90% chitosan-cellulose film. This indicates that limited interactions are present between the polymers in the physical mixture.

The thermal stability of the chitosan-cellulose blends at 586^{o}C seems to be between those of chitosan and cellulose. It can be observed that the higher the content of chitosan it is, the higher the char yield of the blends (Figure 5.8). Thus, the addition of chitosan increases the thermal stability of cellulose, slowing down its thermal degradation. The obtained results confirm the presence of strong interaction between the two polymers. Interactions between the hydroxyl groups of cellulose and the

amino groups of chitosan that have been formed in the ionic liquid solution remain in films after the removal of solvent.

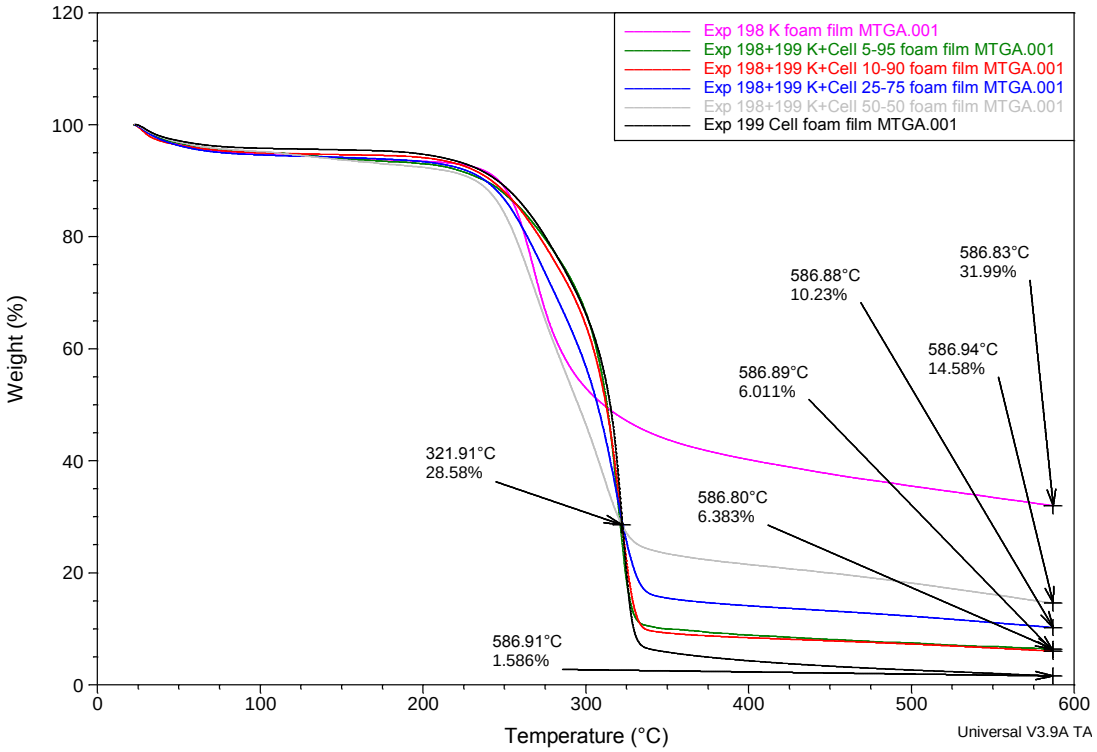

Figure 5.8 Thermogravimetric plot, TG, for chitosan (magenta line), cellulose (black line), and chitosan-cellulose films 5:95% (w/w) (green line), 10:90% (red line), 25:75% (blue line), and 50:50% (gray line).

Table 5.2 Thermogravimetric analysis of chitosan, cellulose, and chitosan-cellulose blends.

	Onset temp. °C	DTG °C	% wt. loss at 150°C	% wt. loss at 200°C
Chitosan	251	268	5.9	6.5
5:95	301	324	6.1	6.0
10:90	299	324	5.3	5.9
25:75	284	273 322	5.8	6.6
50:50	246	270 316	6.3	7.6
Cellulose	303	328	4.5	5.3

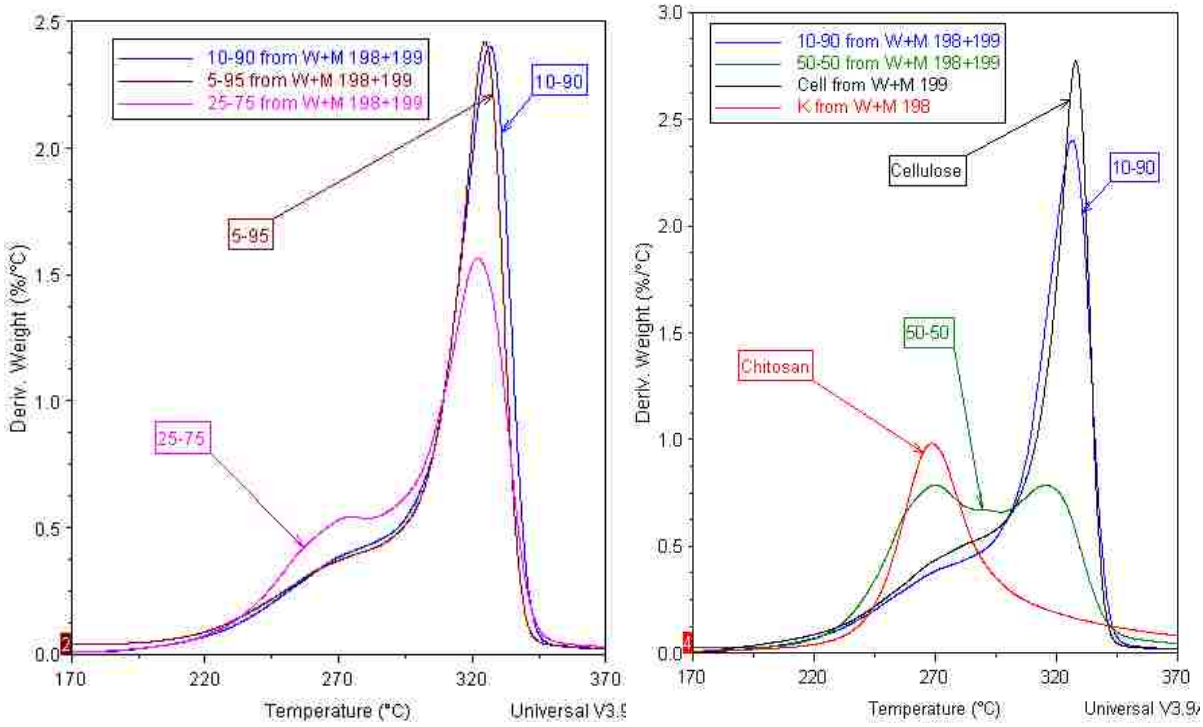

Figure 5.9 Derivative plots, DTG, for chitosan (red line), cellulose (black line), and chitosan/cellulose films 5:95% (w/w) (maroon line), 10:90% (blue line), 25:75% (magenta line), and 50:50% (green line).

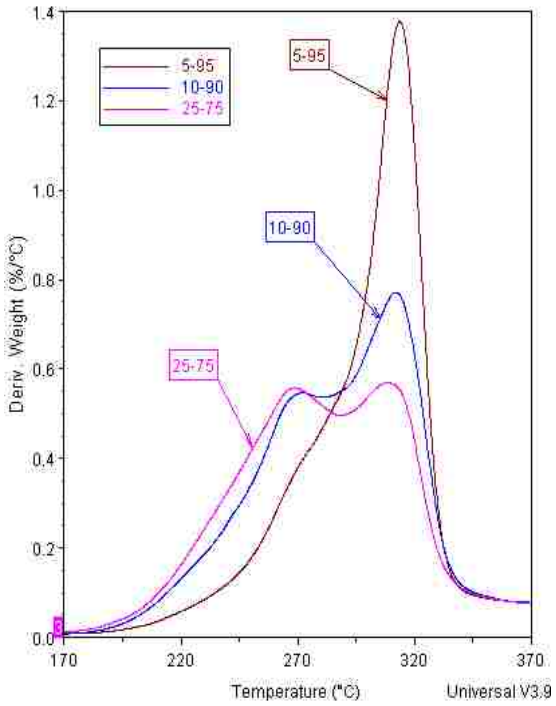

Figure 5.10 Derivative plots, DTG, for physical mixture of chitosan and cellulose films of different weight percent ratios: chitosan/cellulose films 5:95% (maroon line), 10:90% (blue line), and 25:75% (magenta line).

The activation energy (Ea) estimated by MTGA for the degradation of cellulose film (202.9 kJ/mol) correlates very well with the Ea ≈ 170-210 kJ/mol reported by LeVan and coworkers for the analysis of cellulose thermal decomposition in nitrogen atmosphere.(*152*)

The Ea distribution curves at the onset temperature for the polymeric blends obtained from MTGA are reproducible, showing very little variation between replicate runs (Table 5.3). Figure 5.12 illustrates that the Ea of the chitosan film (194.5 kJ/mol) is lower than the Ea of the cellulose film (202.9 kJ/mol). The calculated Ea of the polymeric blends (obtained using the weight averaged experimental Ea values of the neat polymers) (Figure 5.12 – blue dots) is expected to fall between the Ea of cellulose film and the Ea of chitosan film. Also the Ea of the blends is expected to decrease with the increase amount of chitosan. However, the experimental Ea of all the polymeric blends (Figure 5.12 – red squares) showed higher values than the Ea of both chitosan and cellulose films. These results are an indicative of the miscibility of the two polymers. The Ea of the 25:75 wt% chitosan/cellulose film exhibited the highest Ea among the polymeric films. The reason for the increased Ea for all the polymeric blends is attributed to the presence of strong interaction through hydrogen bonding between chitosan and cellulose which require higher Ea to be broken down.

Figure 5.11 shows the weight loss of cellulose, chitosan, and chitosan-cellulose blends versus time of degradation in nitrogen atmosphere at 200^{o}C. After 5 hours of degradation, the weight loss of cellulose film is the lowest and equal to 1.3%, in comparison with chitosan (3.4%) and chitosan-cellulose blends (2.7%, 3.2%, 4.3%, and 5.5% corresponding to 5:95%, 10:90%, 25:75%, and 50:50% blends, respectively). The weight loss of chitosan film is higher than the weight loss of the 5:95 and 10:90 wt% chitosan-cellulose blends but lower than the weight loss of the 25:75 and 50:50 wt% chitosan-cellulose films. This behavior may be explained by the formation of a complex between chitosan and cellulose through hydrogen bonding. The molecular forces existent in the complex of the polymeric blends are less stable than those existent in cellulose. The blends

containing 25 and 50 wt% chitosan are showing a higher weight loss than any of the other films because the complex formed between chitosan and cellulose is much easier to break which will result in a less thermal stability of the films. If no interaction is present between chitosan and cellulose, one will expect the weight loss at 200^{o}C for 5 hours for all the polymeric blends to be proportional to chitosan content; to be between the weight loss of chitosan and cellulose films. Since this not the case for the analyzed polymeric blends, the isothermal presented in Figure 5.11 is another proof of the compatibility of cellulose and chitosan where a complex between the two polymers is being formed.

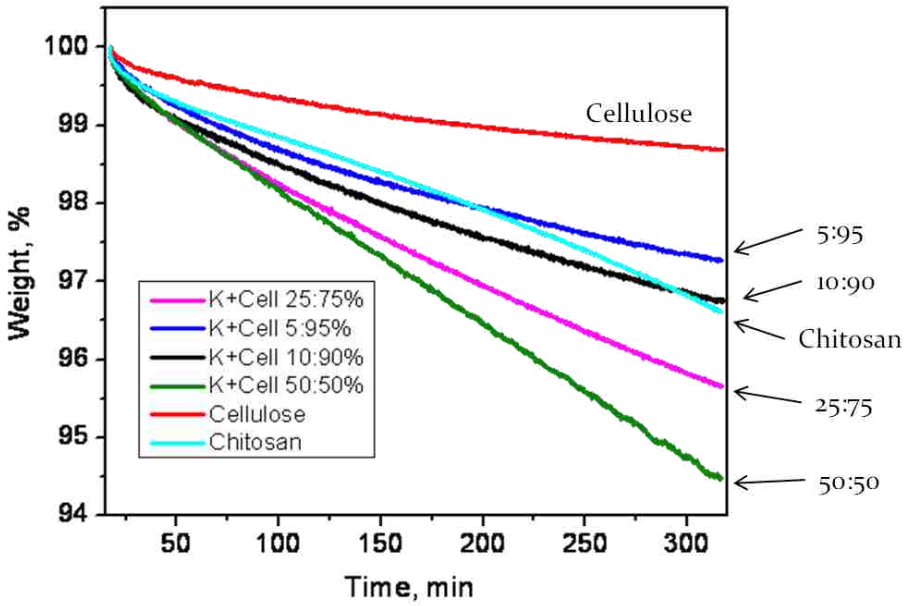

Figure 5.11 Isothermal TG at 200^{o}C for 5 hours for chitosan cyan line), cellulose (red line), and chitosan-cellulose films 5:95% (w/w) (blue line), 10:90% (black line), 25:75% (magenta line), and 50:50% (green line).

Table 5.3 Activation energy for 5:95 and 10:90 w/w% chitosan-cellulose films for replicate runs.

Chitosan/ Cellulose (w/w%) films	Ea, kJ/mol First run	Ea, kJ/mol Second run	Ea, kJ/mol Third run
5:95	228.6	225.9	249.0
10:90	253.7	251.3	234.0

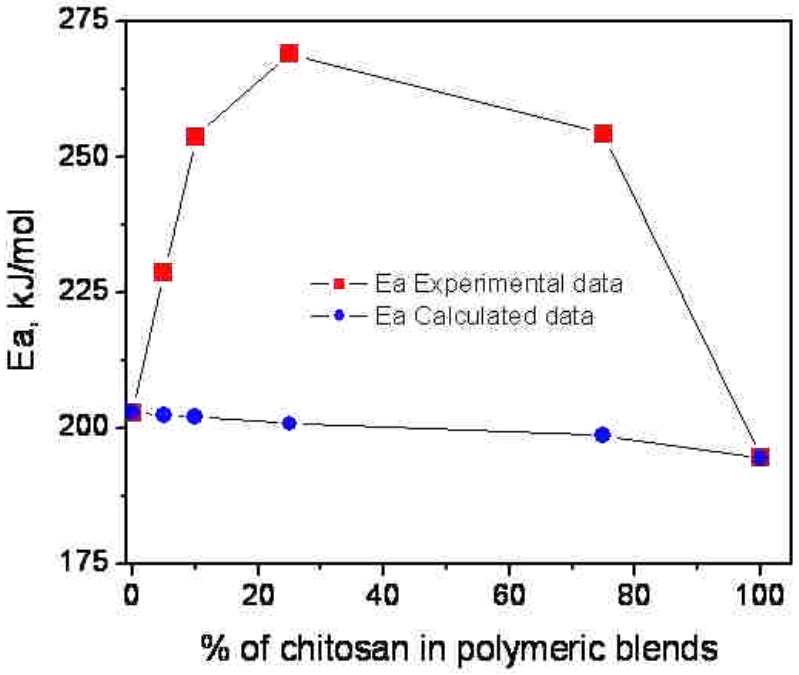

Figure 5.12 The activation energy of the polymeric films obtained from experimental data (red squares) and from calculation (blue dots).

5.3.4 X-Ray Diffraction of Polymeric Films

X-ray diffractograms of pure chitosan, pure cellulose, and chitosan and cellulose films prepared from ionic liquid solutions are presented in Figure 5.13. As observed, the chitosan powder was in a crystalline state because two main diffraction peaks (2θ = 10.7 and 19.8^{o}) were present in the X-ray diffraction pattern. These patterns, which are typical crystalline domains in this polysaccharide, were in agreement with the results reported by Nunthanid and coworkers.(*153*) After making the films by precipitating the polymer from ionic liquid solutions, two crystalline peaks (2θ = 10.9 and 20.1^{o}) still existed, but with smaller intensities. The XRD pattern of pure cellulose shows two diffraction peaks at 2θ = 14.9 and 23.1^{o}. The strongest peak originates from the cellulose crystalline plane 002.(*154*) The diffraction pattern of the cellulose film at 19.5^{o} indicates that the crystalline regions decreased significantly compared to that of pure cellulose.

When the two polymers were mixed at a chitosan to cellulose weight percent ratio of 5:95%, 10:90%, 25:75%, and 50:50%, only one diffraction peak with very low intensity was observed at

19.6, 19.7, 22.1, and 20.4°, respectively (Figure 5.14). The presence of only one peak for the polymeric blends indicates that the chitosan structure was influenced by the addition of cellulose. The crystalline peaks of chitosan and cellulose were suppressed for all the weight percent ratios of chitosan-cellulose blends leading to a significantly lower proportion of crystalline material. Blending the two polymers makes the resulting materials more amorphous, which explains the disappearance of sharp diffraction peaks. The chitosan-cellulose blends do not show any diffraction peaks at 2θ = 10.7 and 14.9°, which confirms good miscibility between the polymers.

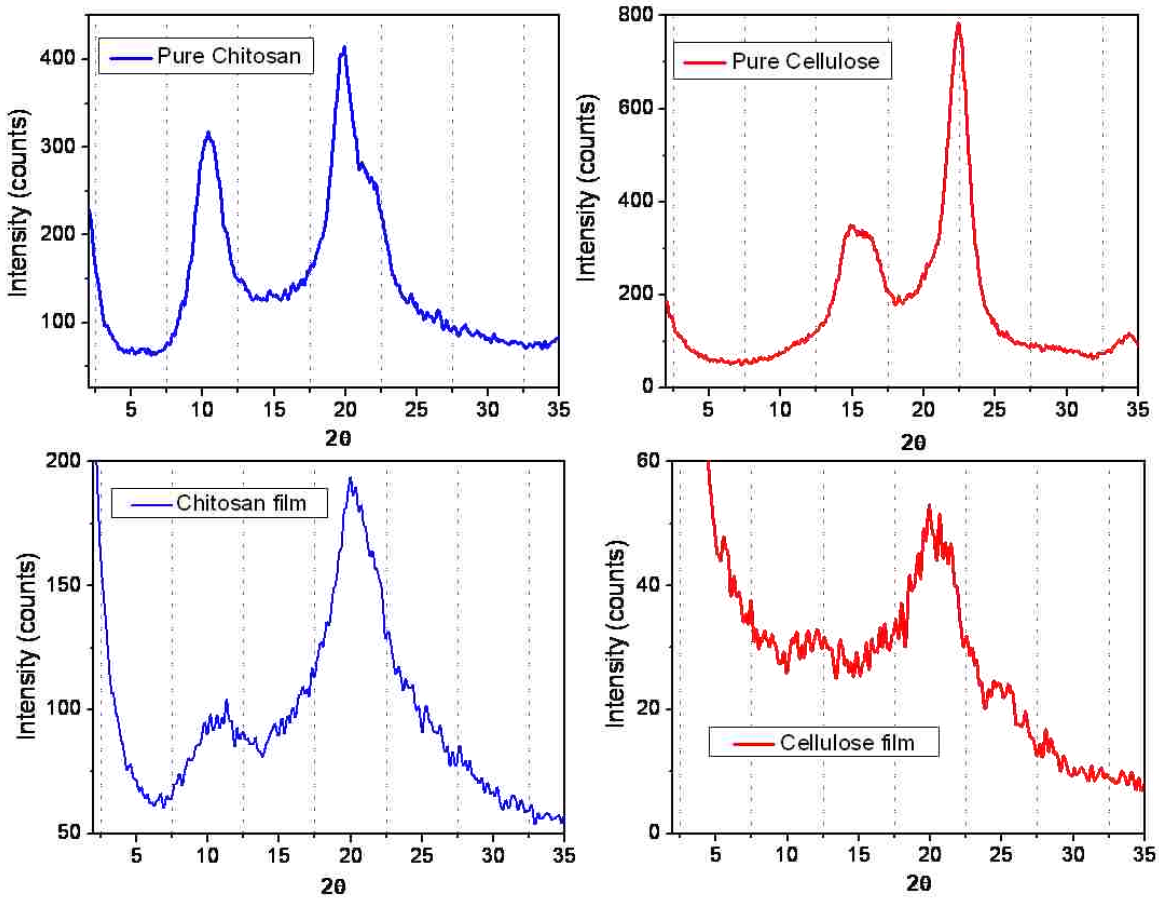

Figure 5.13 XRD patterns for pure chitosan, pure cellulose, and chitosan and cellulose films prepared from ionic liquid solutions.

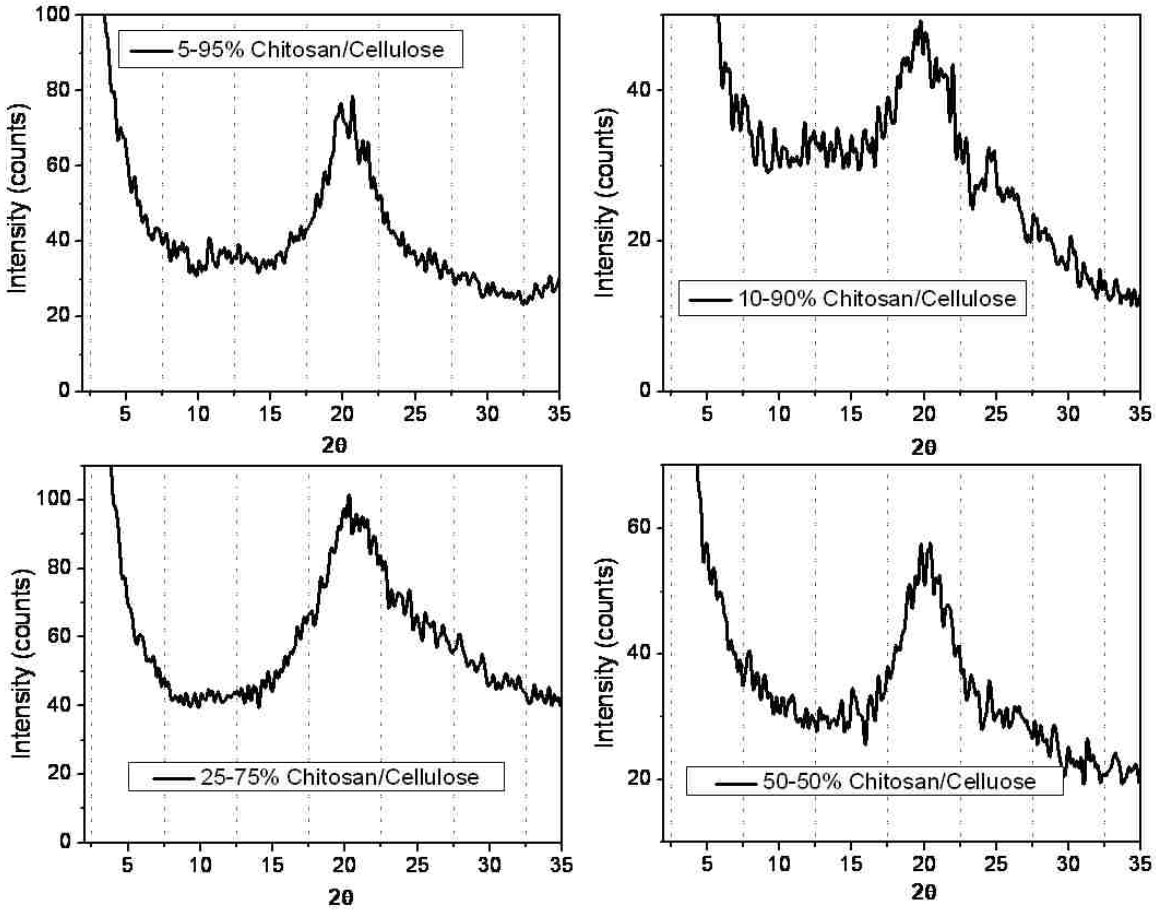

Figure 5.14 XRD patterns chitosan-cellulose (5:95%, 10:90%, 25:75%, and 50:50%) films prepared from ionic liquid solutions.

5.3.5 SEM Experiments of Polymeric Films

In Figure 5.15 through Figure 5.20 are presented the SEM micrographs at different magnifications that were obtained from freeze dried chitosan and/or cellulose films. The thickness of the films varied between 1 mm and 1.2 mm. The films were prepared by shear spreading a polymer-solution on a Teflon mold followed by polymer precipitation in methanol and water. Prior to SEM analysis the dried films were fractured following an axis perpendicular to the spreading direction. The fracture surface XY plane is defined in image ***a*** **(**Figure 5.15**)**. Image ***b*** represents a magnified version of the area delimited with a dashed line in image ***a***. Furthermore, image ***c*** represents a magnified version of the area delimited with a dashed line in image ***b*** (Figure 5.15).

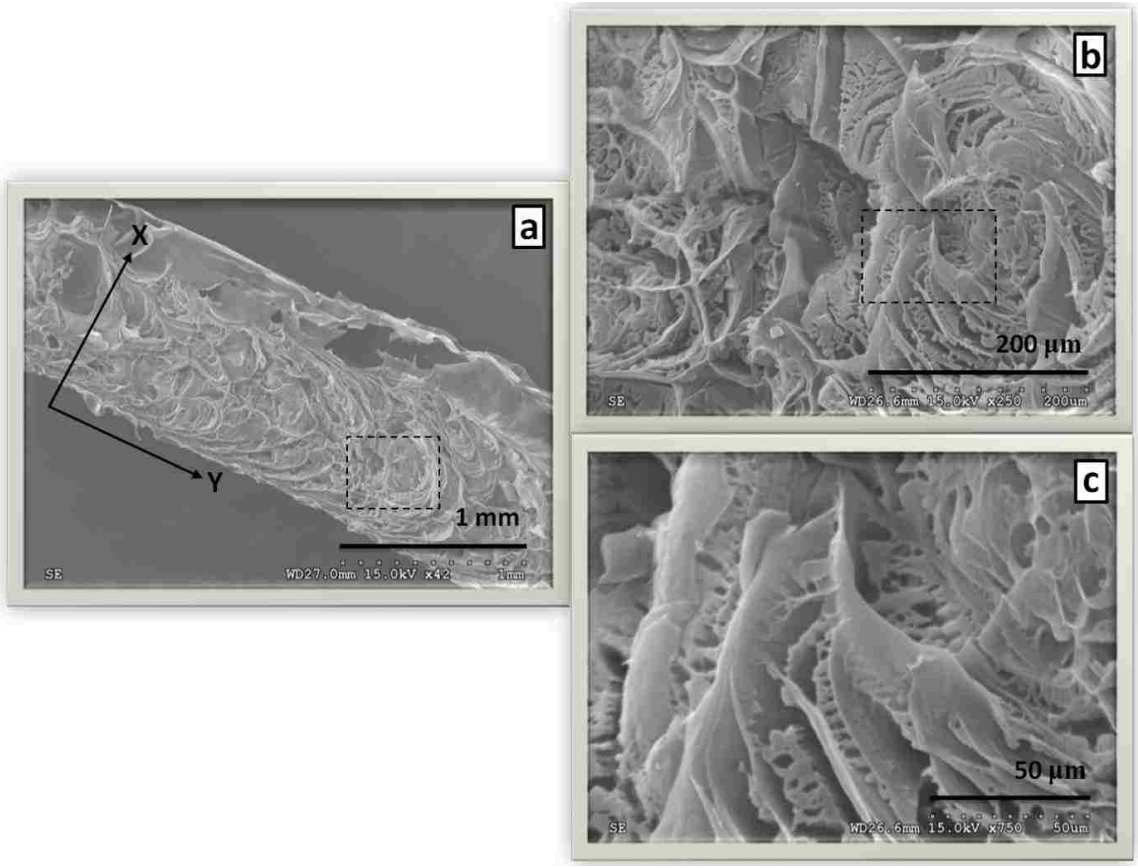

Figure 5.15 SEM micrographs of a freeze dried chitosan film prepared through shear spreading (cross-section).

From Figure 5.15 and Figure 5.16 it can be seen that the films of pure chitosan and pure cellulose have homogeneous morphology. In Figure 5.15 it can be easily observed that overall the precipitated chitosan film has a very porous and disorganized structure, in which the domains have no particular orientation. In image ***a*** it is apparent that the density of striations is higher towards the middle-bottom part of the film, along the thickness axis X, than at the top surface. An explanation could be related to the presence of solvent-rich and polymer-rich domains along the thickness of the film. If that was the case, the solvent-rich domains would be expected to induce a higher density of striations in the precipitated polymer, upon immersion in methanol and water. In images ***b*** and ***c*** it is apparent that the main structure of large striations that are visible in ***a***, is interpenetrated by a

secondary structure of smaller striations. Overall, it is hard to quantify the porosity of the film since various individual features exhibit different dimensions.

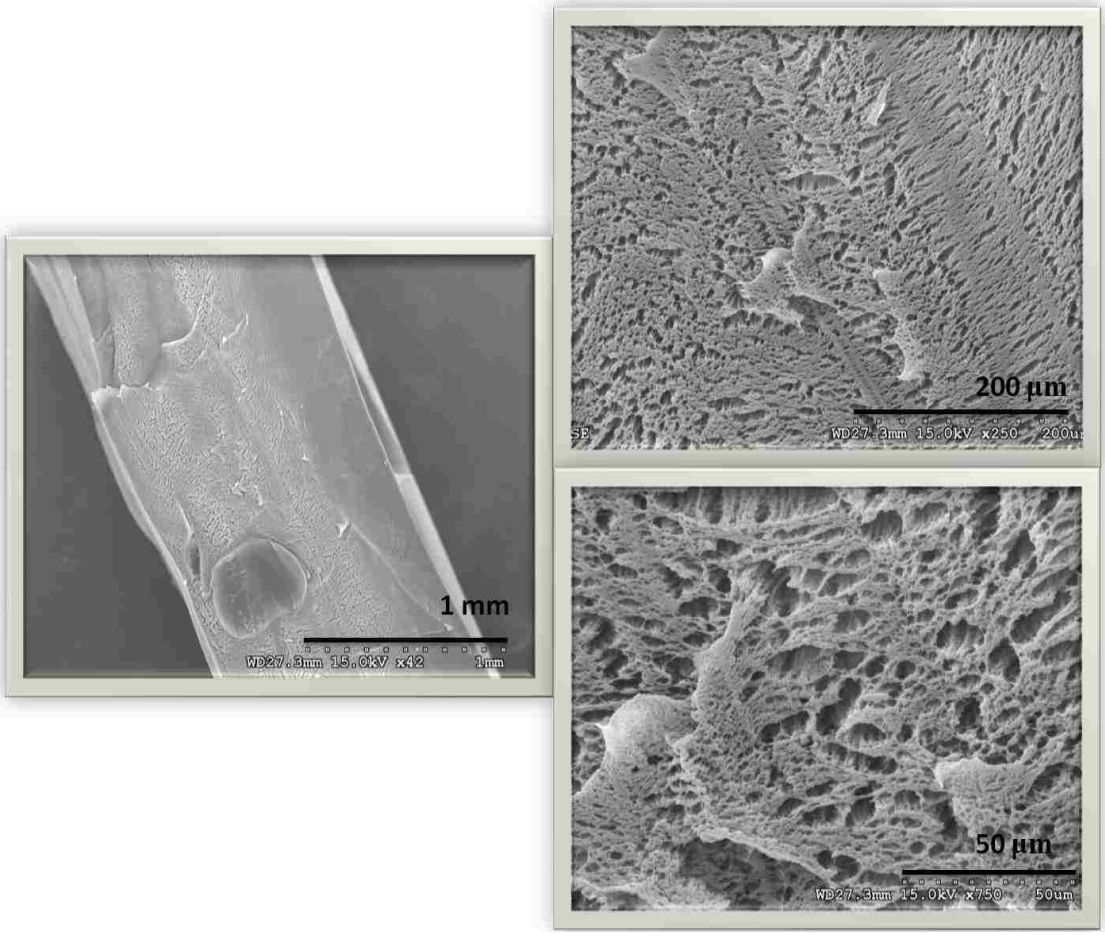

Figure 5.16 SEM micrographs of a freeze dried cellulose film prepared through shear spreading (cross-section).

In the case of cellulose film (Figure 5.16) a well-organized fiber-like network oriented along the spreading direction can be observed. The fibers seem to be parallel to each other but have a random distribution. Voids ranging from 1.9 µm to 13.5 µm are present throughout the fiber-like structure. These voids are the result of the extraction of the solvent from the cellulose ionic liquid solutions during the polymer precipitation process. The freeze-drying technique applied to the wet films was performed to prevent the collapsing of the polymeric films after the polymers were precipitated in water. Freeze drying involves the removal of water from the frozen polymeric films

by a process called sublimation. Sublimation takes place when the frozen water goes directly from the solid state to the gaseous state without passing through the liquid phase.

The morphology of the polymeric blends is quite different than that of pure chitosan and depends on the chitosan-cellulose weight percent ratio. For the samples with a 5:95% chitosan-cellulose, the cross-section structure resembles that of cellulose with a fiber-like network oriented along the spreading direction and voids varying from 1.9 μm to 10.4 μm (Figure 5.17). These voids may be looked at as "cracks" with no particular order. The same structure can be observed for the 10:90% chitosan-cellulose blend with an ordered fiber-like structure and uniformly distributed voids ranging from 1.9 μm to 10.4 μm (Figure 5.18). However, the fiber-like network seems to be more organized than in the case of cellulose or 5:95% chitosan-cellulose blend with the "cracks" being mostly parallel to each other. When the amount of chitosan in the polymeric blends is increased to 25 wt% (Figure 5.19), the cross-section of the corresponding film shows a more compact structure with fewer parallel voids than in the case of the blends with less than 25 wt% chitosan in their composition. The "cracks" are also smaller in size (8.33 μm). Figure 5.20 illustrates the SEM micrographs at different magnifications of the 50:50% chitosan-cellulose blends. The cross-section of the films looks more like a smooth surface with few "cracks" of about 4.16 μm. By looking and the voids it can be seen that the fiber-like network is present for this composition of blends (50:50%) as well. A homogeneous structure with no phase separation of the two polymers, cellulose and chitosan, was observed for all of the blends. Thus the SEM data serve as good evidence for complete miscibility between chitosan and cellulose in the solid state.

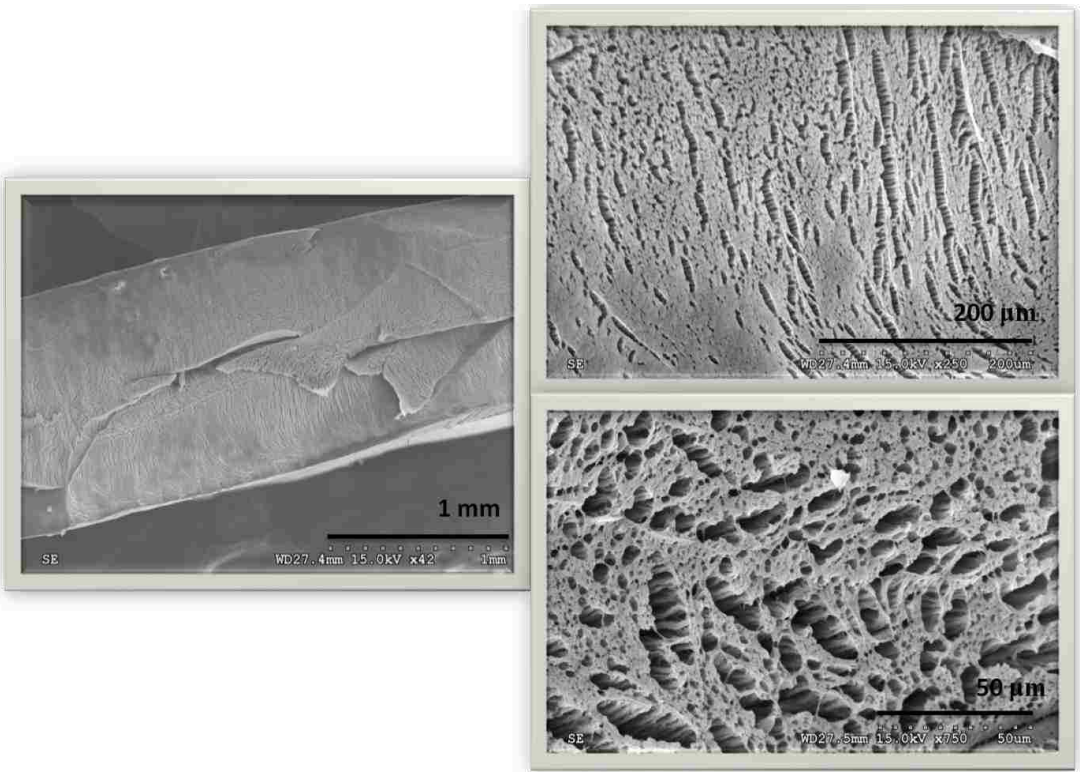

Figure 5.17 SEM micrographs of a freeze dried chitosan/cellulose (5:95%) blend prepared through shear spreading (cross-section).

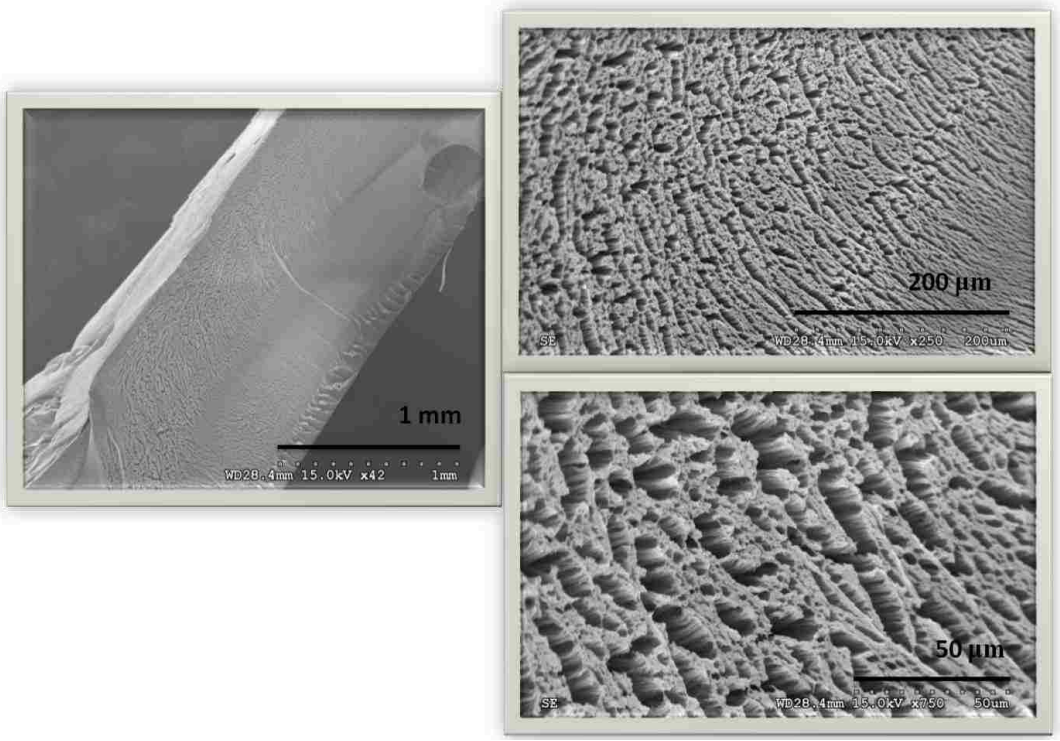

Figure 5.18 SEM micrographs of a freeze dried chitosan/cellulose (10:90%) blend prepared through shear spreading (cross-section).

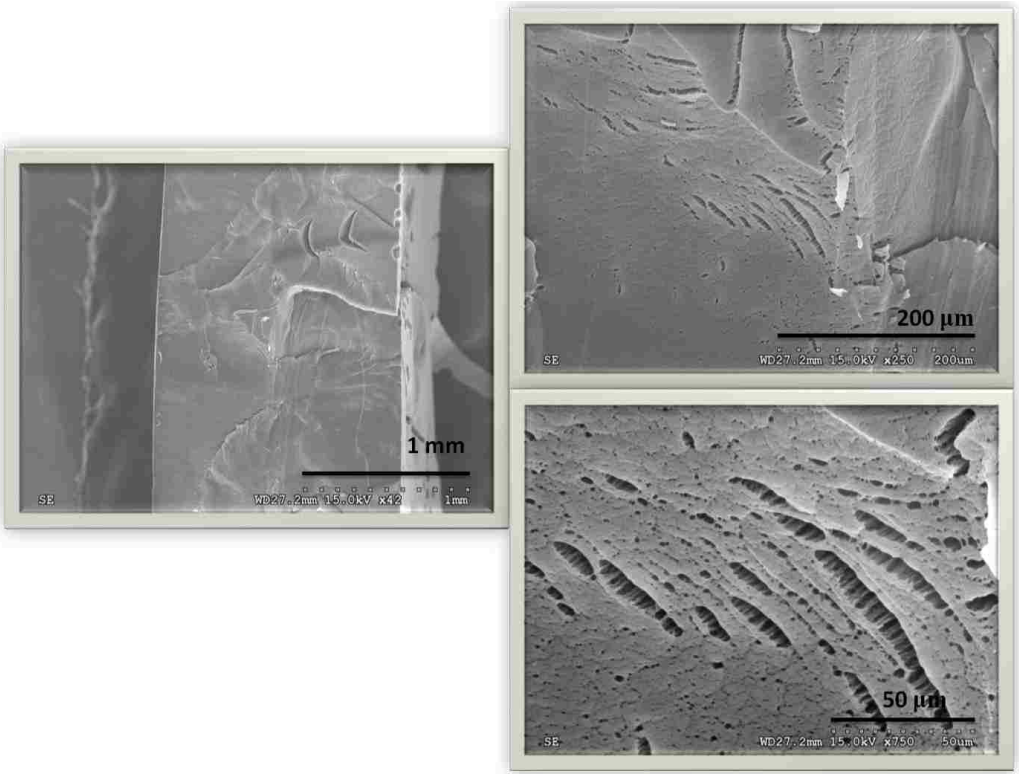

Figure 5.19 SEM micrographs of a freeze dried chitosan/cellulose (25:75%) blend prepared through shear spreading (cross-section).

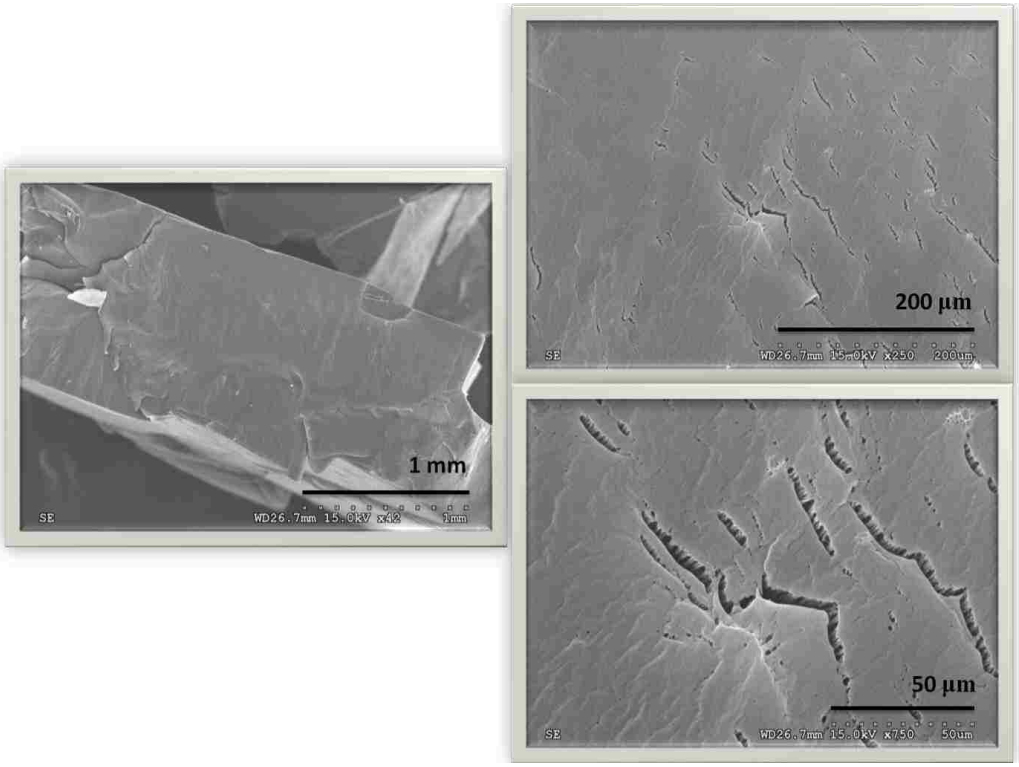

Figure 5.20 SEM micrographs of a freeze dried chitosan/cellulose (50:50%) blend prepared through shear spreading (cross-section).

CHAPTER 6 . CONCLUSIONS AND FUTURE WORK

6.1 Conclusions

The dissolution of chitosan in ionic liquids was successfully accomplished. It has been shown that 1-butyl-3-methylimidazolium acetate (BMIMAc) is a much better solvent than 1-butyl-3-methylimidazolium chloride (BMIMCl). Dissolution of chitosan in BMIMCl could not be realized without a prior regeneration of chitosan from 1% acetic acid solution. In the case of BMIMAc, both dried chitosan and regenerated chitosan from acetic acid solution have been dissolved in a relatively short amount of time. While concentrations only up to 1-2 wt% of chitosan in BMIMCl could be obtained, concentrations of 10 wt % of chitosan in BMIMAc were easily realized.

The homogeneous phthalation and benzoylation of chitosan were successfully achieved in these ionic liquids. According to FT-IR data the appearance of new peaks confirm that both the -OH and -NH_2 groups from chitosan AGU reacted with benzoyl chloride and phthalic anhydride, respectively. The reaction of chitosan with phthalic anhydride occurred in two steps: in the first step the amide has been formed and in the second step the imide cycles have been closed. Higher temperatures favored the imide group formation. Heating the isolated phthalated chitosan adducts to 150^{o}C leads to cyclization with the formation of imide groups and elimination of water. The FT-IR and DSC measurements supported this supposition.

The reaction of chitosan with phthalic anhydride in the presence of a base and using ionic liquids as a solvent media was also studied. The presence of a base into the system leads to an increase of the degree of substitution (DS = 0.41) of the functional groups of chitosan comparing with the reactions performed in the absence of a base (DS = 0.24). Chemical modification of chitosan using the chloride ionic liquid resulted in products with a higher thermal stability than adducts of chitosan prepared using the acetate ionic liquid as a solvent.

The reaction of chitosan with phthalic anhydride in the presence of *N*-Bromosuccinimide as catalyst using BMIMAc as an ionic liquid solvent was also investigated. The presence of a catalyst into the system resulted in an increase of the degree of substitution (DS = 0.85) of functional groups of chitosan as compared to that resulted from the reactions performed in the absence of a catalyst (0.24). The FT-IR data indicated that the hydroxyl groups of chitosan are being catalyzed to a greater extent than the amino groups. All the reactions products were soluble in dimethyl sulfoxide and dimethylformamide.

Blends of chitosan and cellulose were successfully accomplished using BMIMAc as solvent media. To the best of our knowledge, there are no reports regarding the simultaneous dissolution of both cellulose and chitosan polymers in the same ionic liquid. The rheological measurements of the polymeric solutions indicated the formation of a complex between chitosan and cellulose molecules. Films prepared from the polymeric solutions were investigated by means of FT-IR, TGA, X-ray diffraction and SEM measurements. The shifting of the band corresponding to –NH groups of chitosan from 1597 to 1565 cm^{-1} (FT-IR), the absence of the diffraction peaks at $2\theta = 10.7$ and 14.9^{o} (XRD), the increased Ea for all the polymeric blends (MTGA), and the presence of a homogeneous structure with no phase separation of the two polymers (SEM) serve as good evidence for the miscibility between chitosan and cellulose in the solid state.

6.2 Future Work

Future work will focus on enhancing the antimicrobial properties of chitosan by incorporating in it antibiotics with possible applications for local drug delivery systems. The goal is to deliver high levels of antibiotics to the site of wounds for a faster healing. This method will have the advantage of a lower overall concentration of drugs when compared to the oral or intravenous administration.

Chemical modification of chitosan and cellulose blends with antibiotics and spinning of fibers and casting of films for possible applications as wound dressing in biomedical field is another goal to be achieved. Our concepts of obtaining fibers and films from blends of chitosan and cellulose can be applied to skin tissue regeneration and accelerate healing of wounds effect created by the presence of chitosan that has distinctive biomedical properties when used as wound-dressing materials. The presence of cellulose is necessary so that the overall material obtained from the blends has better flexibility and increased mechanical properties.

REFERENCES

1. Solomons, T. W. G. (1992) *Organic Chemistry*, 5 ed., John Wiley & Sons, New York.

2. Methacanon, P., Prasitsilp, M., Pothsree, T., and Pattaraarchachai, J. (2003) Heterogeneous N-deacetylation of squid chitin in alkaline solution, *Carbohydrate Polymers 52*, 119-123.

3. Galed, G., Miralles, B., Paños, I., Santiago, A., and Heras, Á. (2005) N-Deacetylation and depolymerization reactions of chitin/chitosan: Influence of the source of chitin, *Carbohydrate Polymers 62*, 316-320.

4. Ravi Kumar, M. N. V. (2000) A review of chitin and chitosan applications, *Reactive and Functional Polymers 46*, 1-27.

5. Goosen, M. F. A. (1997) *Applications of Chitin and Chitosan*, CRC Press LLC.

6. Prudden, J. F., Migel, P., Hanson, P., Friedrich, L., and Balassa, L. (1970) The discovery of a potent pure chemical wound-healing accelerator, *Amer. J. Surg. 119*, 560-564.

7. Cho, Y.-W., Jang, J., Park, C. R., and Ko, S.-W. (2000) Preparation and solubility in acid and water of partially deacetylated chitins, *Biomacromolecules 1*, 609-614.

8. Poulicek, M., Voss-Foucart, M. F., and Jeuniaux, C. (1986) Chitinoproteic complexes and mineralization in Mollusk skeletal structures In *Chitin in Nature and Technology* (Muzzarelli, R. A. A., Jeuniaux, C., and Gooday, G. W., Eds.), pp 7-12, Plenum Press, New York.

9. Macossay, J., (Ed.) (1995) *Synthesis and characterization of water soluble chitosan derivatives*, Louisiana State University Libraries, Baton Rouge.

10. Wu, A. C. M., and Bough, W. A. (1978) A Study of Variables in the Chitosan Manufacturing Process in Relation to Molecular-Weight Distribution, Chemical Characteristics and Waste-Treatment Effectiveness., In *Proceedings of the First International Conference on Chitin/Chitosan* (Muzzarelli, R. A. A., and Pariser, E. R., Eds.), pp 88-102, Cambridge.

11. Jolles, P., and Muzzarelli, R. A. A. (1999) *Chitin and Chitinases*, Birkhauser Verlag, Basel.

12. Domard, A., and Ronaudo, M. (1983) Preparation and characterization of fully deacetylated chitosan, *International Journal of Biological Macromolecules 5*, 49-52.

13. Bough, W. A., Salter, W. L., Wu, A. C. M., and Perkins, B. E. (1978) Influence of manufacturing variables on the characteristics and effectiveness of chitosan products. I. Chemical composition, viscosity, and molecular-weight distribution of chitosan products, *Biotechnology and Bioengineering 20*, 1931-1943.

14. Muzzarelli, R. A. A. (1973) *Natural Chelating Polymers*, Pergamon of Canada Ltd., Toronto.

15. Kobayashi, T., Takiguchi, Y., Shimahara, K., and Sannan, T. (1988) Distribution of chitosan in Absidia strains and some properties of the chitosan isolated, , *Nippon Nogeikagaku Kaishi 62*, 1463-1469.

16. Solomons, T. W. G. (1989) *Organic chemistry*, 4 ed., John Wiley & Sons, New York.

17. Dai, H., Zhou, J., Huang, Y. R., and Zhang, Z. C. (2006) Carboxymethylation of chitosan and its application in retan of leather, *7th Asian International Conference of Leather Science and Technology Sect 1 and 2*, 389-394.

18. Raymond, L., Morin, F. G., and Marchessault, R. H. (1993) Degree of deacetylation of chitosan using conductometric titration and solid-state NMR, *Carbohydrate Research 246*, 331-336.

19. Ratajska, M., Struszczyk, M. H., Boryniec, S., Peter, M. G., and Loth, F. (1997) The degree of deacetylation of chitosan: optimization of the IR method, *Polimery 42*, 572-575.

20. Hirai, A., Odani, H., and Nakajima, A. (1991) Determination of degree of deacetylation of chitosan by H-1-NMR spectroscopy, *Polymer Bulletin 26*, 87-94.

21. dos Santos, Z. M., Caroni, A., Pereira, M. R., da Silva, D. R., and Fonseca, J. L. C. (2009) Determination of deacetylation degree of chitosan: a comparison between conductometric titration and CHN elemental analysis, *Carbohydrate Research 344*, 2591-2595.

22. Niola, F., Basora, N., Chornet, E., and Vidal, P. F. (1993) A rapid method for the determination of the degree of N-acetylation of chitin-chitosan samples by acid-hydrolysis and HPLC, *Carbohydrate Research 238*, 1-9.

23. Nanjo, F., Katsumi, R., and Sakai, K. (1991) Enzymatic method for determination of the degree of deacetylation of chitosan, *Analytical Biochemistry 193*, 164-167.

24. da Silva, R. M. P., Mano, J. F., and Reis, R. L. (2008) Straightforward determination of the degree of N-acetylation of chitosan by means of first-derivative UV spectrophotometry, *Macromolecular Chemistry and Physics 209*, 1463-1472.

25. Tan, S. C., Khor, E., Tan, T. K., and Wong, S. M. (1998) The degree of deacetylation of chitosan: advocating the first derivative UV-spectrophotometry method of determination, *Talanta 45*, 713-719.

26. Wu, T., and Zivanovic, S. (2008) Determination of the degree of acetylation (DA) of chitin and chitosan by an improved first derivative UV method, *Carbohydrate Polymers 73*, 248-253.

27. Muzzarelli, R. A. A. (1992) Modified chitosans carrying sulfonic-acid groups, *Carbohydrate Polymers 19*, 231-236.

28. Keisuke, K., Takanori, S., and Yoshio, I. (1979) Studies on chitin. VI. Binding of metal cations, *Journal of Applied Polymer Science 23*, 511-515.

29. Tsaih, M. L., and Chen, R. H. (1999) Molecular weight determination of 83% degree of decetylation chitosan with non-gaussian and wide range distribution by high-performance size exclusion chromatography and capillary viscometry, *Journal of Applied Polymer Science 71*, 1905-1913.

30. Nguyen, S., Winnik, F. M., and Buschmann, M. D. (2009) Improved reproducibility in the determination of the molecular weight of chitosan by analytical size exclusion chromatography, *Carbohydrate Polymers 75*, 528-533.

31. Muzzarelli, R. A. A. (1977) *Chitin*, Pergamon of Canada Ltd., Toronto.

32. Kurita, K., Sannan, T., and Iwakura, Y. (1977) Studies on chitin, 3. Preparation of pure chitin, poly(*N*-acetyl-D-glucosamine), from the water-soluble chitin *178*, 2595-2602.

33. Chen, X. G., and Park, H. J. (2003) Chemical characteristics of O-carboxymethyl chitosans related to the preparation conditions, *Carbohydrate Polymers 53*, 355-359.

34. Yang, H., Zhou, S. B., and Deng, X. M. (2004) Preparation and properties of hydrophilic-hydrophobic chitosan derivatives, *Journal of Applied Polymer Science 92*, 1625-1632.

35. Hirano, S., Senda, H., Yamamoto, Y., and Watanabe, A. (1984) In *Chitin, Chitosan and Related Enzymes* (Zikakis, J. P., Ed.), pp 77-95, Academic Press, Inc., Orlando.

36. Keisuke, K., Yoshiyuki, K., and Akihiko, T. (1986) Studies on chitin. IX. Crosslinking of water-soluble chitin and evaluation of the products as adsorbents for cupric ion, *Journal of Applied Polymer Science 31*, 1169-1176.

37. Kurita, K., Chikaoka, S., and Koyama, Y. (1988) Improvement of Adsorption Capacity for Copper (II) Ion by N-Nonanoylation of Chitosan, *Chemistry Letters 17*, 9-12.

38. Muzzarelli, R. A., Tanfani, F., and Scarpini, G. (1980) Chelating, film-forming, and coagulating ability of the chitosan-glucan complex from Aspergillus niger industrial wastes, *Biotechnology and Bioengineering 22*, 885-896.

39. Wu, A. C. M., Bough, W. A., Holmes, M. R., and Perkins, B. E. (1978) Influence of manufacturing variables on the characteristics and effectiveness of chitosan products. III. Coagulation of cheese whey solids, *Biotechnology and Bioengineering 20*, 1957-1966.

40. Holme, K. R., and Hall, L. D. (1990) Novel metal chelating chitosan derivative: attachment of iminodiacetate moieties via a hydrophilic spacer group, *Can. J. Chem. 69*, 585-589.

41. Nakajima, A., and Shinoda, K. (1977) Permeation properties of glycol chitosan-mucopolysaccharide complex membranes, *J. Appl. Pol. Sci. 21*, 1249-1255.

42. Rha, C., Rodriguez-Sanchez, D., and Kienzle-Sterzer, C. (1984) In *Biotechnology of marine polysaccharides* (Colwell, R. R., Pariser, E. R., and Sinskey, A. J., Eds.), pp 283-311, Hemisphere Publishing Corp., Washington.

43. Shigehiro, H., Kenji, T., Masahiro, H., and Noriaki, M. (1980) Permeability properties of gels and membranes derived from chitosan, *Journal of Biomedical Materials Research 14*, 477-485.

44. Uragami, T., and Tokura, S. (2006) *Material Science of chitin & chitosan*, Kodansha Ltd., Tokyo.

45. Uragami, T., and Tokura, S. (2006) *Material Science*, Kodansha Ltd., Tokyo.

46. Paoletti, M. G., Norberto, L., Damini, R., and Musumeci, S. (2007) Human Gastric Juice Contains Chitinase That Can Degrade Chitin, *Annals of Nutrition & Metabolism 51*, 244-251

47. Escott, G. M., and Adams, D. J. (1995) Chitinase activity in human serum and leukocytes, *Infection and Immunity 63* 4770–4773.

48. Renkema, G. H., Boot, R. G., Muijsers, A. O., Donker-Koopman, W. E., and Aerts, J. M. (1995) Purification and characterization of human chitotriosidase, a novel member of the chitinase family of proteins, *The Journal of Biological Chemistry 270*, 2198–2202.

49. Hakala, B. E., White, C., and Recklies, A. D. (1993) Human cartilage gp-39, a major secretory product of articular chondrocytes and synovial cells, is a mammalian member of a chitinase protein family, *The Journal of Biological Chemistry 268* 25803–25810.

50. Bierbaum, S., Nickel, R., Koch, A., Lau, S., Deichmann, K. A., Wahn, U., Superti-Furga, A., and Heinzmann, A. (2005) Polymorphisms and haplotypes of acid mammalian chitinase are associated with bronchial asthma, *American Journal of Respiratory and Critical Care Medicine 172*, 1505–1509.

51. Elias, J. A., Homer, R. J., Hamid, Q., and Lee, C. G. (2005) Chitinases and chitinase-like proteins in T(H)2 inflammation and asthma, *The Journal of Allergy and Clinical Immunology 116*, 497–500.

52. Zhao, J., Zhu, H., Wong, C. H., Leung, K. Y., and Wong, W. S. (2005) Increased lungkine and chitinase levels in allergic airway inflammation: a proteomics approach, *Proteomics 5*, 2799–2807.

53. Marsh, J. T., and Wood, F. C. (1945) *An Introduction to the Chemistry of Cellulose*, Vol. 3, Chapman And Hall Limited, London.

54. Lejeune, A., and Deprez, T. (2010) *Cellulose: Structure and Properties, Derivatives and Industrial Uses*, Nova Science Publishers Inc. , New York.

55. Zugenmaier, P. (2007) *Crystalline Cellulose and Derivatives: Characterization and Structures*, Springer, New York.

56. Woodings, C. (2001) *Regenerated cellulose fibers*, Woodhead Publishing Ltd, Boca Raton.

57. Stefanescu, E. A. (2009), Virginia Commonwealth University, Richmond, VA personal communication.

58. Rogers, R. D., and Seddon, K. R. (2003) CHEMISTRY: Ionic Liquids--Solvents of the Future?, *Science 302*, 792-793.

59. Davey, P., Earle, M., Newman, C., and Seddon, K. (1999) In *World Patent, WO9919288*.

60. Lok, C., Earle, M., Hamill, J., Roberts, G., Adams, C., and Seddon, K. (1998) In *World Patent, WO9807680*.

61. Thied, R. C., Seddon, K. R., Pitner, W. R., and Rooney, D. W. (1999) In *World Patent, WO9941752*.

62. Fields, M., Thied, R. C., Seddon, K. R., Pitner, W. R., and Rooney, D. W. (1999) In *World Patent, WO9914160*.

63. Greco, C., Sherif, F., and Shyu, L. (1998) In *U.S. Patent, US5824832*.

64. Keim, W., and Wasserscheid, P. (1997) In *World Patent, WO9847616*.

65. Kapustinskii, A. F. (1933) *Z. Phys. Chem. 22B*, 257.

66. Wypych, G. (2001) *Handbook of Solvents*, Vol. 2000, ChemTec Publishing, Toronto.

67. Carpio, R. A., Lowell, A. K., Lindstrom, R. E., Nardi, J. C., and Hussey, C. L. (1979) *J. Electrochem. Soc 126*, 1644-1650.

68. Bonhote, P., Dias, A., Papageorgiou, N., Kalyaanaasundaram, K., and Gratzel, M. (1996) Hydrophobic, highly conductive ambient-temperature molten salts, *Inorg. Chem. 35*, 1168-1178.

69. Swatloski, R. P., Spear, S. K., Holbrey, J. D., and Rogers, R. D. (2002) Dissolution of Cellose with Ionic Liquids, *J. Am. Chem. Soc. 124*, 4974-4975.

70. Zhu, S. D., Wu, Y. X., Chen, Q. M., Yu, Z. N., Wang, C. W., Jin, S. W., Ding, Y. G., and Wu, G. (2006) Dissolution of cellulose with ionic liquids and its application: a mini-review, *Green Chemistry 8*, 325-327.

71. Egorov, V. M., Smirnova, S. V., Formanovsky, A. A., Pletnev, I. V., and Zolotov, Y. A. (2007) *Analytical and Bioanalytical Chemistry 387*, 2263-2269.

72. Remsing, R. C., Swatloski, R. P., Rogers, R. D., and Moyna, G. (2006) Mechanism of cellulose dissolution in the ionic liquid 1-n-butyl-3-methylimidazolium chloride: a 13C and 35/37Cl NMR relaxation study on model systems, *Chemical Communications*, 1271-1273.

73. Xie, H. B., Zhang, S. B., and Li, S. H. (2006) Chitin and chitosan dissolved in ionic liquids as reversible sorbents of CO2, *Green Chemistry 8*, 630-633.

74. Stefanescu, C., Daly, W., and Negulescu, I. (2009) 1-Butyl-3-Methylimidazolium Acetate as a Solvent Media for Functionalization of Chitosan, *Polymer Preprints 50*, 143-144.

75. Stefanescu, C., Daly, W., and Negulescu, I. (2009) Nucleophilic Reactivity of Chitosan in Ionic Liquids Promoted by Tert-Amines, *Polymer Preprints 50*, 551-552.

76. Schlufter, K., Schmauder, H. P., Dorn, S., and Heinze, T. (2006) Efficient homogeneous chemical modification of bacterial cellulose in the ionic liquid 1-N-butyl-3-methylimidazolium chloride, *Macromolecular Rapid Communications 27*, 1670-1676.

77. El Seoud, O. A., and Heinze, T. (2005) Organic esters of cellulose: New perspectives for old polymers, In *Advances in Polymer Science*, pp 103-149, Springer Berlin / Heidelberg.

78. Moulthrop, J. S., Swatloski, R. P., Moyna, G., and Rogers, R. D. (2005) High-resolution 13C NMR studies of cellulose and cellulose oligomers in ionic liquid solutions, *Chemical Communications*, 1557-1559.

79. Lu, X., Hu, J., Yao, X., Wang, Z., and Li, J. (2006) Direct electron transfer of horseradish peroxidase and its biosensor based on chitosan and room temperature ionic liquid, *Electrochem. Commun. 8*, 874-878.

80. Heinze, T., Schwikal, K., and Barthel, S. (2005) Ionic liquids as reaction medium in cellulose functionalization, *Macromolecular Bioscience 5*, 520-525.

81. Wu, J., Zhang, J., Zhang, H., He, J., Ren, Q., and Guo, M. (2004) Homogeneous Acetylation of Cellulose in a New Ionic Liquid, *Biomacromolecules 5*, 266-268.

82. Liu, C. F., Sun, R. C., Zhang, A. P., Qin, M. H., Ren, J. L., and Wang, X. A. (2007) Preparation and characterization of phthalated cellulose derivatives in room-temperature ionic liquid without catalysts, *Journal of Agricultural and Food Chemistry 55*, 2399-2406.

83. Liu, C. F., Sun, R. C., Zhang, A. P., and Ren, J. L. (2007) Preparation of sugarcane bagasse cellulosic phthalate using an ionic liquid as reaction medium, *Carbohydrate Polymers 68*, 17-25.

84. Erdmenger, T., Haensch, C., Hoogenboom, R., and Schubert, U. S. (2007) Homogeneous Tritylation of Cellulose in 1-Butyl-3-methylimidazolium Chloride, *Macromolecular Bioscience 7*, 440-445.

85. White, P. (2001) Lyocell: The Production Process and Market Development, In *Regenerated Cellulose Fibres* (Woodings, C., Ed.), pp 62-87, Woodhead Publishing, Boca Raton.

86. Petrovan, S., Collier, J. R., and Negulescu, I. I. (2001) Rheology of Cellulosic N-Methylmorpholine Oxide Monohydrate Solutions of Different Degrees of Polymerization, *Journal of Applied Polymer Science 79*, 396-405.

87. Barthel, S., and Heinze, T. (2006) Acylation and carbanilation of cellulose in ionic liquids, *Green Chemistry 8*, 301-306.

88. Liu, C. F., Sun, R. C., Zhang, A. P., Ren, J. L., Wang, X. A., and Geng, Z. C. (2006) Structural and thermal characterization of sugarcane bagasse cellulose succinates prepared in ionic liquid, *Polymer Degradation and Stability 91*, 3040-3047.

89. Kohler, S., Liebert, T., Schobitz, M., Schaller, J., Meister, F., Gunther, W., and Heinze, T. (2007) Interactions of ionic liquids with polysaccharides-1: Unexpected acetylation of cellulose with 1-ethyl-3-methylimidazolium acetate, *Macromolecular Rapid Communications 28*, 2311-2317.

90. Silverstein, R. M., Bassler, G. C., and Morrill, T. C. (1999) *Spectrometric Identification of Organic Compounds*, 5 ed., John Wiley & Sons, Inc., New York.

91. Pavia, D. L., Lampman, G. M., and Kriz, G. S. (1996) *Introduction to Spectroscopy*, 2 ed., Saunders Golden Sunburst Series, Orlando.

92. Koenig, J. L. (1999) *Spectroscopy of Polymers*, Elsevier Science Inc., New York.

93. Silverstein, R. M., Webster, F. X., and Kiemle, D. J. (2005) *Spectrometric Identification of Organic Compounds*, 7 ed., John Wiley & Sons, Inc., New York.

94. Morrison, F. A. (2001) *Understanding Rheology*, Oxford University Press, Inc., New York, 10016.

95. Macosko, C. W. (1994) *Rheology: Principles, Measurements, and Applications* Wiley - VCH.

96. Larson, L. G. (1999) *The structure and rheology of complex fluids*, Oxford University Press, New York.

97. Stefanescu, E. A. (2008) Polymer-clay nanocomposites:impact of rheological properties of colloidal gels on the multilayered structure andthermo-mechanical properties of shear-applied thin films, pp 16-17, Louisiana State University, Baton Rouge.

98. Heal, G. R., Laye, P. G., Price, D. M., Warrington, S. B., and Wilson, R. J. (2002) *Principles of Thermal Analysis and Calorimetry*, The Royal Society of Chemistry, Cambridge, UK.

99. Benoist, L., Berghmans, H., Hemminger, W., Hohne, G. W. H., Jansen, J. A. J., Mathot, V. B. F., Richardson, M. J., Riesen, R., Schuijff, A., and Wingfield, M. (1994) *Calorimetry and Thermal Analysis of Polymers*, Hanser/Gardner Publications, Inc., Geleen, The Netherlands.

100. http://www.tainstruments.com/main.aspx?id=89&n=1&siteid=11.

101. Wunderlich, B. (1990) *Thermal Analysis*, Academic Press, Inc., San Diego, CA 92101, USA.

102. Flynn, J. H., and Wall, L. A. (1966) General Treatment of the Thermogravimetry of Polymers, *Journal of Research of the National Bureau of Standards-A, Physics and Chemistry 70A*, 487-523.

103. Flynn, J. H. (1969) Thermal Analysis, *Vol. 2, R. F. Schwenker, Jr. and P. D. Garn, Eds, Academic Press, New York and London*, 1111.

104. Cowie, J. M. G. (1991) *Polymers: Chemistry & Physics of Modern Materials*, 2nd ed., Nelson Thornes Ltd, Cheltenham, UK.

105. Odian, G. (1991) *Principles of Polymerization*, 3rd ed., Wiley - Interscience, New York, NY.

106. Young, R. J., and Lovell, P. A. (1991) *Introduction to Polymers*, 2nd ed., CRC Press LLC, Boca Raton, FL.

107. Sperling, L. H. (2006) *Introduction to Physical Polymer Science*, 4 ed., John Wiley and Sons, New Jersey.

108. Goldstein, J., Newbury, D., Joy, D., Lyman, C., Echlin, P., Lifshin, E., Sawyer, L., and Michael, J. (2003) *Scanning Electron Microscopy and X-Ray Microanalysis*, 3rd ed., Springer Science + Business Media, Inc., N.Y.10013, USA.

109. Echlin, P., Fiori, C. E., Goldstein, J., Joy, D. C., and Newbury, D. E. (1986) *Advanced Scanning Electron Microscopy and X-Ray Microanalysis* Plenum Press, New York.

110. Egerton, R. F. (2005) *Physical Principles of Electron Microscopy: An Introduction to TEM, SEM, and AEM*, Springer Science & Business Media, Inc., New York.

111. Stefanescu, E. A. (2009) Effect of solution concentration on the morphology of spray-dried ethylcellulose microspheres Virginia Commonwealth University, Richmond, VA, personal communication.

112. Warren, B. E. (1990) *X-Ray Diffraction*, Dover Publications, Inc., N.Y. 11501, USA.

113. Moore, D. M., and Reynolds, R. C., Jr (1997) *X-Ray Diffraction of Clay Minerals*, 2nd ed., Oxford University Press, Inc., N.Y. 10016, USA.

114. Cullity, B. D. (1978) *Elements of X-Ray Diffraction*, 2nd ed., Addison-Wesley Publishing Company, Inc., Massachusetts.

115. http://epswww.unm.edu/xrd/xrdbasics.pdf.

116. Egorov, V. M., Smirnova, S. V., Formanovsky, A. A., Pletnev, I. V., and Zolotov, Y. A. (2007) Dissolution of cellulose in ionic liquids as a way to obtain test materials for metal-ion detection, *Analytical and Bioanalytical Chemistry 387*, 2263-2269.

117. Remsing, R. C., Swatloski, R. P., Rogers, R. D., and Moyna, G. (2006) Mechanism of cellulose dissolution in the ionic liquid 1-n-butyl-3-methylimidazolium chloride: a C-13 and Cl-35/37 NMR relaxation study on model systems, *Chemical Communications*, 1271-1273.

118. Liu, L., Li, Y., Li, Y., and Fang, Y. E. (2004) Rapid N-phthaloylation of chitosan by microwave irradiation *Carbohydr. Polym. 57*, 97-100.

119. Nishimura, S.-I., Kohgo, O., Kurita, K., and Kuzuhara, H. (1991) Chemospecific manipulations of a rigid polysaccharide : syntheses of novel chitosan derivatives with excellent solubility in common organic solvents by regioselective chemical modifications, *Macromolecules 24*, 4745-4748.

120. Kurita, K., Ikeda, H., Yoshida, Y., Shimojoh, M., and Harata, M. (2002) Chemoselective Protection of the Amino Groups of Chitosan by Controlled Phthaloylation: Facile Preparation of a Precursor Useful for Chemical Modifications *Biomacromolecules 3*, 1-4.

121. Kurita, K., Ikeda, H., Shimojoh, M., and Yang, J. (2007) N-Phthaloylated Chitosan as an Essential Precursor for Controlled Chemical Modifications of Chitosan: Synthesis and Evaluation, *Polymer Journal 39*, 945-952.

122. Zhang, J., Yuan, Y., Shen, J., and Lin, S. (2003) Synthesis and characterization of chitosan grafted poly(N,N-dimethyl-N-methacryloxyethyl-N-(3-sulfopropyl) ammonium) initiated by ceric (IV) ion *European Polymer Journal 39*, 847-850.

123. Sajomsang, W., Tantayanon, S., Tangpasuthadol, V., and Daly, W. H. (2008) Synthesis of methylated chitosan containing aromatic moieties: Chemoselectivity and effect on molecular weight *Carbohydr. Polym. 72*, 740-750.

124. Miya, M., Iwamoto, R., Yoshikawa, S., and Mima, S. (1980) IR Spectroscopic determination of CONH content in highly deacylated chitosan, *Int. J. Biol. Macromol. 2*, 323-324.

125. Domard, A., Gey, C., Rinaudo, M., and Terrassin, C. (1987) 13C and 1H n.m.r. spectroscopy of chitosan and N-trimethyl chloride derivatives, *Int. J. Biol. Macromol. 9*, 233-237.

126. Rinaudo, M., Dung, P. L., Gey, C., and Milas, M. (1992) Substituent distribution on O, N-carboxymethylchitosans by 1H and 13C n.m.r, *Int. J. Biol. Macromol. 14*, 122-128.

127. Hirai, A., Odani, H., and Nakajima, A. (1991) Determination of degree of deacetylation of chitosan by 1H NMR spectroscopy, *Polymer Bulletin 26*, 87-94.

128. Satterthwait, A. C., and Jencks, W. P. (1974) Mechanism of the aminolysis of acetate esters, *J. Am. Chem. Soc. 96*, 7018-7031.

129. Sun, X. F., Sun, R. C., and Sun, J. X. (2004) Acetylation of sugarcane bagasse using NBS as a catalyst under mild reaction conditions for the production of oil sorption-active materials, *Bioresource Technology 95*, 343-350.

130. Liu, C. F., Zhang, A. P., Li, W. Y., Yue, F. X., and Sun, R. C. (2009) Homogeneous modification of cellulose in ionic liquid with succinic anhydride using *N*-bromosuccinimide as a catalyst, *J. Agric. Food Chem. 57*, 1814-1820.

131. Karimi, B., and Seradj, H. (2001) *N*-Bromosuccinimide (NBS), a novel and highly effective catalyst for acetylation of alcohols under mild reaction conditions, *Synlett 4*, 519-520.

132. Sun, X. F., Sun, R. C., Tomkinson, J., and Baird, M. S. (2003) Preparation of sugarcane bagasse hemicellulosic succinates using NBS as a catalyst, *Carbohydrate Polymers 53*, 483-495.

133. Wu, Y., Sasaki, T., Irie, S., and Sakurai, K. (2008) A novel biomass-ionic liquid platform for the utilization of native chitin, *Polymer 49*, 2321-2327.

134. Muzzarel.Ra, and Tubertin.O. (1969) Chitin and chitosan as chromatographic supports and adsorbents for collection of metal ions from organic and aqueous solutions and sea-water, *Talanta 16*, 1571-1577.

135. No, H. K., and Meyers, S. P. (1989) Crawfish chitosan as a coagulant in recovery of organic-compounds from seafood processing streams, *J. Agric. Food Chem. 37*, 580-583.

136. Oungbho, K., and Muller, B. W. (1997) Chitosan sponges as sustained release drug carriers, *Int. J. Pharm. 156*, 229-237.

137. Dhanikula, A. B., and Panchagnula, R. (2004) Development and characterization of biodegradable chitosan films for local delivery of paclitaxel, *Aaps Journal 6*, 12.

138. Dyson, P. J., Grossel, M. C., Srinivasan, N., Vine, T., Welton, T., Williams, D. J., White, A. J. P., and Zigras, T. (1997) Organometallic synthesis in ambient temperature chloroaluminate(III) ionic liquids. Ligand exchange reactions of ferrocene, *Journal of the Chemical Society-Dalton Transactions*, 3465-3469.

139. Martinas, C., Daly, W. H., and Negulescu, I. I. (2008) Reaction of Chitosan with Benzoyl Chloride and Phthalic Anhydride in Homogeneous Ionic Liquid Solutions, *Polymer Preprints 49*, 572-573.

140. Paulino, A. T., Simionato, J. I., Garcia, J. C., and Nozaki, J. (2006) Characterization of chitosan and chitin produced from silkworm crysalides, *Carbohydrate Polymers 64*, 98-103.

141. Heux, L., Brugnerotto, J., Desbrieres, J., Versali, M.-F., and Rinaudo, M. (2000) Solid state NMR for determination of degree of acetylation of chitin and chitosan, *Biomacromolecules 1*, 746-751.

142. Kacurakova, M., Belton, P. S., Wilson, R. H., Hirsch, J., and Ebringerova, A. (1998) Hydration properties of xylan-type structures: an FTIR study of xylooligosaccharides, *J. Sci. Food Agric. 77*, 38-44.

143. Kittur, F. S., Prashanth, K. V. H., Sankar, K. U., and Tharanathan, R. N. (2002) Characterization of chitin, chitosan and their carboxymethyl derivatives by differential scanning calorimetry, *Carbohydr. Polym. 49*, 185-193.

144. Xu, Y. X., Kim, K. M., Hanna, M. A., and Nag, D. (2005) Chitosan–starch composite film: preparation and characterization, *Industrial Crops and Products 21*, 185-192.

145. Flores-Ramirez, N., Elizalde-Pena, E. A., Vasquez-Garcia, S. R., Gonzalez-Hernandez, J., Martinez-Ruvalcaba, A. M., Sanchez, I. C., Luna-Barcenas, G., and Gupta, R. B. (2005) Characterization and degradation of functionalized chitosan with glycidyl methacrylate, *J. Biomater Sci Polym Ed. 16*, 473-488.

146. Zhao, Q., Yam, R. C. M., Zhang, B., Yang, Y., Cheng, X., and Li, R. K. Y. (2009) Novel all-cellulose ecocomposites prepared in ionic liquids, *Cellulose 16*, 217-226.

147. Luo, K., Yin, J., Khutoryanskaya, O. V., and Khutoryanskiy, V. V. (2008) Mucoadhesive and elastic films based on blends of chitosan and hydroxyethylcellulose, *Macromol. Biosci. 8*, 184-192.

148. Yin, J., Luo, K., Cheng, X., and Khutoryanskiy, V. V. (2006) Miscibility studies of the blends of chitosan with some cellulose ethers *Carbohydrate Polymers 63*, 238-244.

149. Wu, Y.-B., Yu, S.-H., Mi, F.-L., Wu, C.-W., Shyu, S.-S., Peng, C.-K., and Chao, A.-C. (2004) Preparation and characterization on mechanical and antibacterial properties of chitsoan/cellulose blends *Carbohydrate Polymers 57*, 435-440.

150. Pawlak, A., and Mucha, M. (2003) Thermogravimetric and FTIR studies of chitosan blends, *Thermochimica Acta 396*, 153-166.

151. Rao, V., and Johns, J. (2008) Thermal behavior of chitosan/natural rubber latex blends. TG and DSC analysus, *Journal of Thermal Analysis and Calorimetry 92*, 801-806.

152. LeVan, S. L. (1989) Thermal degradation, In *Concise Encyclopedia of Wood & Wood-Based Materials* (Schniewind, A. P., Ed.) 1 ed., Pergamon Press, New York.

153. Nunthanid, J., Puttipipatkhachorn, S., Yamamoto, K., and Peck, G. E. (2001) Physical properties and molecular behavior of chitosan films, *Dryg Dev. Ind. Pharm. 27*, 143-157.

154. Zhao, H., Kwak, J. H., Wang, Y., Franz, J. A., White, J. M., and Holladay, J. E. (2006) Effects of Crystallinity on Dilute Acid Hydrolysis of Cellulose by Cellulose Ball-Milling Study, *Energy & Fuels 20*, 807-811.

VITA

Cristina Stefanescu was born in 1980 in Roman, Romania, to the proud parents of Mr. and Mrs. Gheorghe Martinas. After graduating from a public high school, she enrolled in the fall of 1999 at the Industrial Chemistry Department of the Technical University of Iasi, Romania. During the last of the five years spent there, Cristina prepared her thesis work with the help and guidance of Professor Spiridon Oprea. In the summer of 2004 she obtained a Bachelor of Science from the Industrial Chemistry Department of the Technical University of Iasi.

In August 2006 Cristina moved to the United States to pursue a Doctor of Philosophy in the Chemistry Department of Louisiana State University. She joined the research group of Professors William H. Daly and Ioan I. Negulescu in January 2007. Under their guidance Cristina's research focuses on the dissolution and functionalization of chitosan in ionic liquid solutions and also on incorporating chitosan into polymer blends to obtain new materials with better mechanical properties. During her graduate training, she became a member of the American Chemical Society (ACS), American Physical Society (APS) and the Macromolecular Studies Graduate Student Association (MSGSA) at LSU where she served as Vice-President for the 2009-2010 academic year. Cristina has had the opportunity to present her research several times at the ACS national conference. She has received honorable awards including the 2009 and 2010 Coates Travel Award, the 2010 Excellence in Graduate Polymer Research Award, the 2010 Dow Macromolecular Scholar Award, and the 2010 Teaching Award in Organic Chemistry 2364. At the December 2010 Commencement, Cristina Stefanescu will receive the degree of Doctor of Philosophy in chemistry.